J. Fluid Mech. (2006), *vol.* 560, *pp.* 159–227.
doi:10.1017/S0022112006000450 Printed in the United Kingdom

Infinite-Prandtl-number convection. Part 2. A singular limit of upper bound theory

By G. R. IERLEY[1], R. R. KERSWELL[2] AND S. C. PLASTING[3]

[1]Cecil H. and Ida M. Green Institute of Geophysics and Planetary Physics, University of California, San Diego, La Jolla, CA 92093-0225, USA

[2]Department of Mathematics, University of Bristol, Bristol BS8 1TW, UK

[3]Scripps Institution of Oceanography, University of California, La Jolla, CA 92093-0230, USA

(Received 24 May 2005 and in revised form 9 January 2006)

An upper bound on the heat flux for infinite-Prandtl-number convection between two parallel plates is determined for the cases of no-slip and free-slip boundary conditions. For no-slip the large-Rayleigh-number (Ra) scaling for the Nusselt number is consistent with $Nu < c\,Ra^{1/3}$, as predicted by Chan (1971). However, his commonly accepted picture of an infinite hierarchy of multiple boundary layer solutions smoothly approaching this scaling is incorrect. Instead, we find a novel terminating sequence in which the optimal asymptotic scaling is achieved with a three-boundary-layer solution. In the case of free-slip, we find an asymptotic scaling of $Nu < c\,Ra^{5/12}$, corroborating the conservative estimate obtained in Plasting & Ierley (2005). Here the infinite hierarchy of multiple-boundary-layer solutions obtains, albeit with anomalous features not previously encountered. Thus for neither boundary condition does the optimal solution conform to the well-established models of finite-Prandtl-number convection (Busse 1969*b*), plane Couette flow, and plane or circular Poiseuille flow (Busse 1970). We reconcile these findings with a suitable continuation from no-slip to free-slip, discovering that the key distinction – finite versus geometric saturation – is entirely determined by the singularity, or not, of the initial, single-boundary-layer, solution. It is proposed that this selection principle applies to all upper bound problems.

1. Introduction

Significantly, for the upper bound problem of Rayleigh–Bénard convection at infinite Prandtl number, the momentum equation is employed as a pointwise constraint. This differs fundamentally from the upper bound problem for arbitrary Prandtl number, not merely because a lower scaling exponent is achieved by virtue of the added constraint, but because the physics that underlies the turbulence in this instance could be claimed to be the simplest, hence severest, test of the success of upper bound theory; it is in that sense a *canonical* problem of upper bound theory as well as the one (for no-slip) long regarded as most rigorously established in a formal asymptotic sense. It turns out also to be a physics whose variational bound (based anyway on energy integrals) exposes a remarkable range of novel features, the description and elucidation of which is here significantly advanced, if not completed.

The first blossoming of upper bound theory (hereafter denoted as MHB, ordered historically after the three principals Malkus, Howard, and Busse) was inspired by laboratory experiments on convection (Malkus 1954*a*, *b*), in which Malkus noted

a series of sharp transitions in the slope of the $Nu(Ra)$ relation, coincident with discrete changes in the spatiotemporal complexity of the observed flow. These led him in the direction of a theory of turbulence (Malkus 1956), one element of which was a maximum of the heat flux. Aiming at a clearer mathematical formulation, Howard (1963) focused exclusively on the associated formal bound and was able to establish that $Nu < c\,Ra^{1/2}$. These ideas were later extended in a remarkable series of papers by Busse (Busse 1969*a*, *b*, 1970), who developed the 'multi-α' solution as a useful extension of Howard's work and applied this asymptotic expansion to both convection and shear flow.

The second flowering of upper bound theory (further references to which are denoted by CDH) stems from a formalism first developed by Hopf (1941), but only recently exploited to great effect in a seminal series of papers (Doering & Constantin 1992, 1994; Constantin & Doering 1995; Doering & Constantin 1996). These have formed the foundation upon which many more works have subsequently built. A critical supplement in tightening such bounds was provided with the introduction of the 'balance parameter' in Nicodemus, Grossmann & Holthaus (1997*a*), an element we utilize extensively in this study.

These complementary approaches to the problem of bounding turbulent transport have previously been shown by Kerswell (1997, 2001) to constitute dual variational principles for convection at finite Prandtl number, a complementarity now imagined to hold more generally. A similar result is established in Plasting & Ierley (2005) (hereafter referred to as Part 1) for the specific limit of infinite Prandtl number: the maximization of heat flux is a problem with a saddle point, with the MHB formulation approaching the bound from below and the CDH from above. This defining property of the latter accounts for much of the renewed interest in upper bounds, since one can often obtain conservative bounds using simple trial fields, with more elaborate variational forms serving only further to refine the leading constant.

For the present problem, however, conservative bounds prove unusually difficult to extract. As commented in Part 1, we found it necessary to go to $Ra = 10^{30-35}$ to convincingly clinch the value of the exponent from computation. The need for hyperprecision (up to 96 digits) to avoid fatal roundoff error is the practical reflection of a cancellation intrinsic to the variational solution, and which cancellation precluded successful analytic derivation of the result, even by machine-assisted algebra.

Moreover, the Part 1 conservative no-slip bound of $Nu < c\,Ra^{7/20}$ – itself an improvement on the one-parameter test function estimate of $Ra^{2/5}$ (Otero 2002) – falls short of the leading-order behaviour of the best possible MHB bound reported in Chan (1971), namely $Nu < 0.152\,Ra^{1/3}$. While the gap between these estimates does not present a contradiction, as the MHB and CDH problems treat the same saddle, the question remains of what essential aspect of the optimal solution, if not a residual interior temperature gradient, needs be incorporated in the conservative test function to close the gap.

But perhaps the yet more striking feature of no-slip boundaries is the glaring discrepancy between the elegant, but technically formidable, result by Chan and the recent, wholly rigorous, bounds due to Constantin & Doering (1999), Yan (2004), and Doering, Otto & Reznikoff (2005). While each of these makes use of more information in the form of harmonic estimates to obtain bounds on chosen derivatives of the temperature and velocity fields, counter perhaps to intuition all nonetheless yield higher bounds than Chan; $Nu < c\,Ra^{1/3}(\log Ra)^{2/3}$, $Nu < 1.26\,Ra^{4/11}$ and $Nu < 0.644\,Ra^{1/3}(\log Ra)^{1/3}$ respectively. Further, while the first and last of these furnish transparently tighter asymptotic bounds than that found by the conservative

method exploited in Part 1, less apparent is that even the last result does not actually improve upon Part 1 until $Ra > 1.8 \times 10^{86}$, a value well beyond any that could be realized in nature.

The case of free-slip (and also mixed boundaries) has received generally less attention. In his thesis Chan (1970) considered the free-slip problem but he never published the result. His conclusion was that a 1-α solution would obtain as the upper bound for all Ra, a suggestion gaining later numerical support based on computations appearing in Straus (1976*a*). More recent works include Vitanov (1998) and Vitanov (2000*a*, *b*). For the purpose of this study, the first of these (concerned exclusively with computation of the 1-α solution) is the most relevant. It was precisely Chan's intriguing conjecture that motivated us to explore the free-slip case as an afterthought. As we shall see, the difficulties attending numerical solution for the free-slip conservative bound have an intimate relation with the character of the optimal solution reported here.

1.1. *Outline*

In § 2 we give a brief recapitulation of the dual problem statements of CDH and MHB from Part 1. Next we present a representation suitable for solution of the governing Euler–Lagrange equations. A scalar 'balance parameter' plays a key conceptual role in elucidating the nature of the variational problem but also serves as a useful tool for diagnosis of numerical results, as we observe in the conclusion to § 3. So far as we are aware, the latter is novel to this work, hence we illustrate its later application with care.

Our approach in characterizing the optimal bound is a mixture of numerical and analytic methods. A complete summary of the numerical findings is presented in tabular form in § 4, accompanied by brief supplemental remarks. Next we present an extensive diagnostic treatment of numerical results for no-slip (§ 5) and free-slip (§ 6) solutions for the Euler–Lagrange equations posed in the CDH formulation.

The great majority of the analytic discussion is confined to the appendices in order that the main body of the paper be reasonably accessible to the reader. This is not, however, to say that the appendices in this work are in any way derivative of, or secondary to, the principal themes: every significant argument advanced in the main body rests heavily upon original analysis developed in the appendices. Owing to the striking novelty of the initial bifurcation for free-slip, we have chosen to develop the more elementary portion of that expansion in § 7 to give the reader at least an initial exposure to the analysis.

In § 8 we turn to a unification of the free-slip and no-slip results by means of a mixed boundary condition. This generalization clarifies the singular nature of the no-slip condition, indicating that the first bifurcation in any upper bound problem immediately fixes the entire sequence as either an infinite geometric progression or, as here for no-slip, a finite, terminating, sequence.

Particularly where fractional exponents, and, in the especial case of multi-α solutions, *small differences* of fractional exponents are expected, it is self-evident that numerical limitations on the accessible range of Rayleigh number mean that computations alone can never be fully definitive in discriminating among nearly adjacent scalings. Even more so is this the case where, based on Chan's earlier analysis for no-slip, one expects the appearance of fractional powers of the logarithm of Ra. Both for that reason, and with a view to more fully substantiating the novel finite saturation of lowest wavenumber introduced by free-slip boundary conditions, Appendices A–C present a comprehensive treatment of the 1-α boundary-layer

problem for both free-slip and no-slip boundary conditions. The treatment of each gains lucidity by comparison with the other, as there are subtle differences as well as the more obvious similarities. In Appendix D we continue the development of § 7 by deriving the solution for two wavenumbers. Together, this pair of solutions differs fundamentally from the conventional model for multi-α solutions.

Lastly, numerical solution of the governing Euler–Lagrange equations requires extreme boundary layer resolution, for which purpose we use a stable spectral scheme based in the most general case on the less commonly used Jacobi polynomials. The governing numerical considerations, along with details on the practical implementation, are briefly sketched in Appendix E. We also note an unexpected bifurcation encountered with both boundary conditions, one that, in other problems, could greatly complicate the process of determining a global upper bound.

Readers seeking an abbreviated path through the paper may wish to concentrate primarily on §§ 2, 4 and 8.

2. Formulation of the upper bound problem

The established model of fluid convection within the Boussinesq approximation is the Rayleigh–Bénard equations

$$\left.\begin{aligned} \frac{1}{\sigma}\left(\frac{\partial \boldsymbol{u}}{\partial t}+\boldsymbol{u}\cdot\nabla\boldsymbol{u}\right)+\nabla p &= \nabla^2\boldsymbol{u}+Ra\,T\,\widehat{\boldsymbol{z}},\\ \frac{\partial T}{\partial t}+\boldsymbol{u}\cdot\nabla T &= \nabla^2 T,\\ \nabla\cdot\boldsymbol{u} &= 0. \end{aligned}\right\} \tag{2.1}$$

The dimensionless parameters σ and Ra are, respectively, the Prandtl number and the Rayleigh number, with

$$\sigma=\frac{\nu}{\kappa},\qquad Ra=\frac{\alpha g\Delta T d^3}{\kappa\nu},$$

the material parameters as defined in Part 1, and the temperature contrast from bottom to top, ΔT, is positive. We study the case of infinite Prandtl number ($\sigma=\infty$), a rigorous justification of which limit has recently been given in Wang (2004).

From Part 1, the momentum equation reduces to a dynamical constraint on the vertical velocity, w, in terms of simply the temperature field, T, and the Rayleigh number

$$\nabla^4 w+Ra\nabla_H^2 T=0, \tag{2.2}$$

where the horizontal Laplacian is $\nabla_H^2=\partial_x^2+\partial_y^2$ and the dynamical fields satisfy either no-slip

$$w=w_z=0 \quad \text{at} \quad z=0 \text{ and } 1, \tag{2.3}$$

or free-slip boundary conditions

$$w=w_{zz}=0 \quad \text{at} \quad z=0 \text{ and } 1. \tag{2.4}$$

The associated dimensionless boundary conditions on T are $T(0)=1$ and $T(1)=0$.

The Nusselt number of the flow is defined as the ratio of the time-averaged total heat flux to the conductive heat flux between the plates. This can be written either as

$$Nu=1+\langle wT\rangle \tag{2.5}$$

or, based on the global entropy flux balance,

$$Nu=\|\nabla T\|^2. \tag{2.6}$$

Regarding notation, we use $\overline{(\cdot)}$, $\langle\cdot\rangle$, and $\|\cdot\|^2$ as horizontal, volume, and L_2 averages respectively, that is

$$\overline{(\cdot)} = \lim_{L_{x,y}\to\infty} \frac{1}{4L_xL_y}\int_{-L_x}^{+L_x} \mathrm{d}x \int_{-L_y}^{+L_y} \mathrm{d}y(\cdot),$$

$$\langle\cdot\rangle = \int_{-1/2}^{1/2} \overline{(\cdot)}\,\mathrm{d}z, \qquad \|f\|^2 = \langle|f|^2\rangle.$$

In Part 1, equations (2.5), (2.6), and the momentum constraint (2.2) were used to formulate two variational problems.

2.1. *Recapitulation of two variational statements*

For the CDH theory we decompose the temperature field into *background* and *fluctuation* parts

$$T(\boldsymbol{x}, t) = \tau(z) + \theta(\boldsymbol{x}, t), \tag{2.7}$$

where the background field takes on the temperature boundary conditions $\tau(0) = 1$ and $\tau(1) = 0$, and θ satisfies Dirichlet boundary conditions. We further decompose

$$\theta = \widehat{\theta} + \overline{\theta},$$

thus $\widehat{\theta}$ is a zero-mean field.

As derived in Part 1, the CDH theory reduces to minimization of

$$Nu - 1 \leqslant \frac{\lambda^2}{4(\lambda-1)}(\|\tau'\|^2 - 1), \tag{2.8}$$

subject to the spectral constraint (hereafter denoted SC)

$$\mathcal{G}(w, \widehat{\theta}) = \|\nabla\widehat{\theta}\|^2 + \lambda\langle w\widehat{\theta}\tau'\rangle \geqslant 0 \tag{2.9}$$

for all zero-mean fields $(w, \widehat{\theta})$ that satisfy equation (2.2) and the specific boundary conditions. We have used the substitution $\lambda = b/(b-1)$ to simplify notation.

The derivation following Part 1 (2.14) shows that $b > 1$ in order that the variational problem have a solution. This in turn implies that $\lambda > 1$. □

The MHB theory proceeds from the assumption of statistical stationarity of all horizontal averages. In contrast to the CDH formulation, we decompose the temperature field into *mean* and *zero-mean* components

$$T(\boldsymbol{x}, t) = \overline{T}(z) + \widehat{\theta}(\boldsymbol{x}, t).$$

For arbitrary Prandtl number the homogeneous functional to be maximized is

$$F = \frac{\langle w\widehat{\theta}\rangle^2 - \langle w\widehat{\theta}\rangle\|\nabla\widehat{\theta}\|^2}{\|w\widehat{\theta} - \langle w\widehat{\theta}\rangle\|^2}, \tag{2.10}$$

subject to the power constraint

$$\|\nabla\widehat{\theta}\|^2 + \|w\widehat{\theta} - \langle w\widehat{\theta}\rangle\|^2 = \langle w\widehat{\theta}\rangle, \tag{2.11}$$

and appropriate boundary conditions. For the particular case of $\sigma = \infty$, the optimization of F is further subject to the momentum constraint (2.2) and provides an upper bound on the Nusselt number, $Nu - 1 \leqslant \sup F$. The Euler–Lagrange equations that result are stated in Part 1. □

In § 3 we derive the optimal equations for the CDH formulation. These are the basis for the numerical solutions that follow. The corresponding equations for the MHB approach are used for the development of our analytical results for both no-slip and free-slip boundary conditions. Remember that, owing to the proof given in Part 1 of the equivalence of these formulations, the bounds that result are independent of which set of equations is used. The choice is a matter of convenience. The CDH approach enjoys the advantage, for numerical purposes, of unambiguously signalling the emergence of multi-α structure via the spectral constraint. By contrast, when the purpose is to develop an asymptotic expansion of a particular solution branch, the spectral constraint is irrelevant, and the MHB formulation particularly convenient.

3. Solution technique

Following the CDH method, we now present the programme for solving the optimal problem. The functional to be optimized is

$$\check{N}u - 1 = \frac{\lambda^2}{4(\lambda - 1)}(\|\tau'\|^2 - 1) - \mathscr{G}(w, \widehat{\theta}) - \big\langle q(\boldsymbol{x})\big(\nabla^4 w + Ra\nabla_H^2\widehat{\theta}\big)\big\rangle, \tag{3.1}$$

where $q(\boldsymbol{x})$ is a Lagrange multiplier enforcing the momentum constraint and satisfying 'natural' boundary conditions (cf. Courant & Hilbert 1953), which turn out to be those of w.

3.1. *Euler–Lagrange equations*

As noted in Part 1, there is no preferred horizontal direction in the optimal solution since the Euler–Lagrange equations have horizontal derivatives of even order only. Hence without loss of generality we can represent a single-mode solution in the form

$$w = w(z)\cos\alpha x, \qquad q = q(z)\cos\alpha x, \qquad \widehat{\theta} = \widehat{\theta}(z)\cos\alpha x.$$

After suitable manipulation, the w, $\widehat{\theta}$ and q variations are found to be

$$2(\mathrm{D}^2 - \alpha^2)\widehat{\theta} - \lambda w\tau' + Ra\,\alpha^2 q = 0, \tag{3.2}$$

$$(\mathrm{D}^2 - \alpha^2)^2 q + \lambda\widehat{\theta}\tau' = 0, \tag{3.3}$$

$$(\mathrm{D}^2 - \alpha^2)^2 w - Ra\,\alpha^2\widehat{\theta} = 0. \tag{3.4}$$

This set is supplemented by the derivative of (3.1) with respect to α,

$$\langle\widehat{\theta}^2\rangle - 2\langle q(\mathrm{D}^2 - \alpha^2)w\rangle - Ra\langle q\widehat{\theta}\rangle = 0. \tag{3.5}$$

The equation for the optimal background field is

$$\lambda(\tau' + 1) = w\widehat{\theta} - \langle w\widehat{\theta}\rangle, \tag{3.6}$$

while the optimal balance parameter, λ, satisfies

$$\lambda = 2 - \frac{\langle(\mathrm{D}\widehat{\theta})^2 + (\alpha\widehat{\theta})^2\rangle}{\langle w\widehat{\theta}\rangle}. \tag{3.7}$$

3.2. *Spectral constraint*

In the CDH formulation the competitor fields are those background fields satisfying the spectral constraint (2.9). We use the terminology that a background field is 'SC-stable' if it satisfies the spectral constraint and 'SC-neutral' for the particular case that it marginally satisfies the constraint, i.e. lies on the boundary of the admissible

set. By embedding in the appropriate (L_2) infinite-dimensional generalization of a Euclidean space, it can be shown that the geometry of the spectral constraint implies that there is a unique SC-neutral solution to the Euler–Lagrange equations.

A solution to the CDH Euler–Lagrange equations constitutes an upper bound on the heat transport if and only if the background field is SC-stable. At the point where a solution branch loses SC-stability an additional wavenumber enters into the solution, and a non-smooth branching in the optimal solution curve occurs. (In principle, more than one wavenumber can enter the solution simultaneously but this was never found to happen.) The spectral constraint becomes

$$\mathscr{G} = \langle (\mathrm{D}\widehat{\theta})^2 + (\alpha\widehat{\theta})^2 \rangle + \lambda \langle w\widehat{\theta}\tau' \rangle \geqslant 0, \tag{3.8}$$

which must be satisfied for each single-mode pair $(w, \widehat{\theta})$ that satisfies equation (3.4) and the governing boundary conditions.

This condition can be posed as an eigenvalue problem: the background field τ and associated balance parameter λ are SC-stable if the eigenvalues of the following system are non-positive ($\mu \leqslant 0$) for all wavenumbers α:

$$\left.\begin{aligned} 2(\mathrm{D}^2 - \alpha^2)\widehat{\theta} - \lambda w\tau' + Ra\,\alpha^2 q &= \mu\widehat{\theta}, \\ (\mathrm{D}^2 - \alpha^2)^2 q + \lambda\widehat{\theta}\tau' &= 0, \\ (\mathrm{D}^2 - \alpha^2)^2 w - Ra\,\alpha^2\widehat{\theta} &= 0, \end{aligned}\right\} \tag{3.9}$$

for w, q, and $\widehat{\theta}$ eigenfunctions of z, which satisfy the specific boundary conditions. Comparison with the optimal equations (3.2)–(3.4) shows that the optimal background field must be SC-neutral. In this paper the spectral constraint is checked carefully using standard numerical eigenvalue software. An approach to the optimal bound would seem unavoidably to require such an element of numerical verification and to that degree must always fall short of constituting a mathematical proof.

3.3. *Multi-α solutions*

The single-mode solution branch begins at the energy stability point Ra_c, at which the conduction state ($w = \widehat{\theta} = 0$ and $\tau = 1 - z$ for all $z \in [0, 1]$) is unstable to single-wavenumber rolls. The critical Rayleigh number and wavenumber for free-slip boundary conditions are, respectively,

$$Ra_c = \frac{27\pi^4}{4} \approx 657, \qquad \alpha_c = \frac{\pi}{2}, \tag{3.10}$$

and for no-slip boundary conditions

$$Ra_c = 1707.76177710, \qquad \alpha_c = 3.11632355. \tag{3.11}$$

When $\lambda = 1$ the spectral constraint makes contact with the energy stability problem. Therefore, the optimal solution bifurcates from the conduction state onto the single-mode branch at $Ra = Ra_c$. Continuation in Ra can be made along the single-mode branch while SC-neutrality is preserved. As is generally observed with these bounding problems, the single-mode solution gives way to a two-mode solution, which later (in Ra) loses SC-stability to a three-mode solution, and so on. We denote by N_j, for $j = 1, 2, \ldots$, the value of the functional for a j-mode solution of the optimal equations. When $N_j = N_{j+1}$ the j-mode solution loses SC-stability to the $(j+1)$-mode solution branch. The optimal upper bound on the Nusselt number will be denoted by

$$Nu = \max_j N_j, \tag{3.12}$$

where the maximizing subscript is invariably a monotone increasing function of Ra.

Therefore, at any particular Ra, the maximum will be achieved by the M-mode solution branch and the generic nature of the optimal fields is

$$\widehat{\theta} = \sum_{m=1}^{M} \widehat{\theta}^{(m)}(z)\cos\alpha_m x, \quad w = \sum_{m=1}^{M} w^{(m)}(z)\cos\alpha_m x, \quad q = \sum_{m=1}^{M} q^{(m)}(z)\cos\alpha_m x, \tag{3.13}$$

where each subfield $(\alpha_m, w^{(m)}, q^{(m)}, \widehat{\theta}^{(m)})$ must individually satisfy the four equations (3.2)–(3.5), while collectively they determine the background field and optimal balance parameter

$$\lambda(\tau'+1) = \sum_{m=1}^{M} \left(w^{(m)}\widehat{\theta}^{(m)} - \langle w^{(m)}\widehat{\theta}^{(m)}\rangle\right), \tag{3.14}$$

$$\lambda = 2 - \frac{\displaystyle\sum_{m=1}^{M} \langle \left(\mathrm{D}\widehat{\theta}^{(m)}\right)^2 + \left(\alpha_m\widehat{\theta}^{(m)}\right)^2\rangle}{\displaystyle\sum_{m=1}^{M} \langle w^{(m)}\widehat{\theta}^{(m)}\rangle}. \tag{3.15}$$

3.4. *Balance parameters and scaling laws*

In common with nearly all problems governed by a large or small parameter, here too we seek, from numerical data computed over a finite range in Ra, to estimate power-law exponents that hold asymptotically. While it often suffices for that purpose to make a log–log plot of the quantity in question, we are seeking slight differences in successive exponents. In addition, while local estimates of the exponent do give plausible graphical evidence of tending to a limit, in only a few instances can the computations be carried sufficiently far in Ra to make that limit self-evident. In all remaining cases, a reliable estimate of the limit requires that we model one, or more, of the transients as well, each governed by its own characteristic exponent(s). We develop this idea through a formal expansion of the intuitive power-law estimate based on the logarithmic derivative but also, and less obviously, by appeal to the balance parameter defined by (3.15). We expand on the latter's relation to the upper bound on Nu, deriving a specific relation for three model forms chosen to reflect the range of asymptotic behaviours reported in succeeding sections. From this relation follows a second, more stable, independent estimator for the desired exponent. (For added background on the balance parameter and related considerations in the case of plane Couette flow see Plasting 2004.)

Recall the Lagrangian, here slightly rewritten as

$$\check{N}u - 1 = \frac{\lambda^2}{4(\lambda-1)}(\|\tau'\|^2 - 1) - \mathscr{G}(w,\widehat{\theta}), \tag{3.16}$$

where $\mathscr{G}(w,\widehat{\theta}) = \|\nabla\widehat{\theta}\|^2 + \lambda\langle w\widehat{\theta}\tau'\rangle$. The spectral constraint $\mathscr{G}(w,\widehat{\theta}) \geqslant 0$ must be fulfilled by all single-mode fields $(w,\widehat{\theta})$ satisfying both the pointwise constraint $\nabla^4 w + Ra\nabla_H^2\widehat{\theta} = 0$ and appropriate boundary conditions.

If we let $w \to Ra^{1/2}w$ and $\theta \to Ra^{-1/2}\theta$ then the parametric dependence on Ra is confined to the spectral constraint

$$\widetilde{\mathscr{G}} = \|\nabla\widehat{\theta}\|^2 + R\langle w\widehat{\theta}\tau'\rangle \geqslant 0 \quad \text{for all suitable } (w,\widehat{\theta}), \tag{3.17}$$

where we define an auxiliary variable $R = \lambda Ra$. For a candidate function τ there exists a critical point $R = R_c$ below which the spectral constraint is satisfied, while for $R > R_c$ the spectral constraint does not hold. This critical point implicitly defines a family of SC-neutral functions, $\tau(R)$, (dropping the subscript) that marginally satisfy the spectral constraint, and without explicit reference to the balance parameter.

Restricting ourselves to that family, the bound reduces to subsidiary scalar optimization of the function

$$\widetilde{D} = \frac{\lambda^2}{4(\lambda - 1)}(\|\tau'(R)\|^2 - 1) \tag{3.18}$$

over λ noting that, if we fix the external parameter Ra, then R has to be regarded as a function of λ and in particular $\mathrm{d}R/\mathrm{d}\lambda = R/\lambda$. Setting $\mathrm{d}\widetilde{D}/\mathrm{d}\lambda = 0$ provides the optimal value of λ. In application to a specific assumption of the asymptotic form for $\|\tau'(R)\|^2$, the result of this optimization, substituted back into (3.18), gives the desired bound on $Nu - 1$. In all cases, the optimal λ must lie in the interval $[1, \infty)$.

For the optimal profiles addressed here, the balance parameter computed from the explicit form (3.7) must of course satisfy the relation $\mathrm{d}\widetilde{D}/\mathrm{d}\lambda = 0$. While these considerations apply equally to functions like the two-parameter piecewise linear profiles considered in Part 1, in that paper, because the scaling exponent is independent of λ, for computational simplicity we set $\lambda = 2$.

The first paper to exploit a balance parameter was Nicodemus *et al.* (1997*a*), on bounds for the friction factor in plane Couette flow, where the same form arises for $\widetilde{D}$. Where previously λ had simply been set equal to 2 (giving a prefactor, as in (3.18), of unity), the authors showed that, for the simplest one-parameter test functions, the optimal choice of balance parameter is $\lambda = 3/2$ for $Re \to \infty$. Nicodemus *et al.* (1997*b*) calculated a tighter bound by using two-parameter, piecewise-quadratic, profiles with a numerical treatment of the spectral constraint but found the same asymptotic limit for λ. Lastly Plasting & Kerswell (2003) also recover the same limit of λ in a numerical study that, as here, exhausts the bounding potential over all one-dimensional background fields. In fact, this limit for λ holds for any family of test functions for plane Couette flow that captures the correct power of Re.

The reason that the optimal λ tends to the same value for all test functions that achieve the same scaling exponent is more easily seen if we consider, not the balance parameter itself, but the exponent estimate that derives from it, namely

$$\mu_1 = \frac{2 - \lambda}{\lambda - 1} \tag{3.19}$$

(cf. Plasting 2004). As noted in the introduction to this section, a second quantity, more commonly computed for the same purpose, is

$$\mu_2 = \frac{\mathrm{d}(\log Nu)}{\mathrm{d}(\log Ra)}.$$

The latter is typically noisier, as it requires numerical differentiation, whereas the former is computed from integrals of the solution. As detailed below, each of these has a natural expansion in a small parameter, $Ra^{-\mu}$ (possibly augmented by factors of $\log Ra$), for some $\mu > 0$. Generally each is a rational function of its argument but, for sufficiently large Ra, that rational function can itself be expanded in a series. Differences in the resulting series for μ_1 and μ_2 can aid in eliciting the correct asymptotic form for Nu; hence μ_2, though possibly more troublesome to compute, is a helpful supplement.

The implicit algebra that defines λ and $\mu_{1,2}$ above can be made explicit by use of suitable asymptotic expansions of all quantities, given a particular form for Nu. Looking first at a comparatively simple expansion for Nu (developed to this order for the free-slip 1-α solution in Appendix C.1),†

$$Nu \sim c_1 Ra^{1/3} + c_2 + (c_3 \log Ra + c_4) Ra^{-1/3}, \tag{3.20}$$

this exercise generates the following:‡

$$\lambda \sim \frac{7}{4} + \frac{3(c_2-1)}{16 c_1 Ra^{1/3}} + \frac{3c_3}{8c_1}\frac{\log Ra}{Ra^{2/3}} - \frac{3\left(3c_2^2 - 6c_2 + 3 + 12c_3c_1 - 8c_4c_1\right)}{64 c_1^2 Ra^{2/3}}, \tag{3.21}$$

$$\mu_1 \sim \frac{1}{3} - \frac{c_2-1}{3c_1\, Ra^{1/3}} - \frac{2c_3}{3c_1}\frac{\log Ra}{Ra^{2/3}} + \left(\frac{(c_2-1)^2}{3c_1^2} + \frac{c_3}{c_1} - \frac{2c_4}{3c_1}\right) Ra^{-2/3}, \tag{3.22}$$

$$\mu_2 \sim \frac{1}{3} - \frac{c_2}{3c_1\, Ra^{1/3}} - \frac{2c_3}{3c_1}\frac{\log Ra}{Ra^{2/3}} + \left(\frac{c_2^2}{3c_1^2} + \frac{c_3}{c_1} - \frac{2c_4}{3c_1}\right) Ra^{-2/3}, \tag{3.23}$$

from which one sees that the relation of μ_1 to μ_2 results from the transformation of c_2 to $c_2 - 1$, that is to say,

$$\mu_1 \sim \frac{\mathrm{d}(\log(Nu-1))}{\mathrm{d}(\log Ra)}. \tag{3.24}$$

(In cases other than an algebraic controlling factor, both this relation and (3.19) must be modified appropriately.) In figure 1, we plot $\log(\mu_1 - \mu_2)$ for a case to be discussed later and compare it with the logarithm of the first non-vanishing term predicted by the difference between (3.22) and (3.23). As the needed constant c_1 is known analytically, the comparison is free of arbitrary parameters and the agreement is thus seen to confirm the expansions above, the assumption that (3.20) is the appropriate form for Nu in the case considered, and the accompanying theory that provides the requisite value of c_1.

Similarly for

$$Nu \sim c_1 Ra^{2/5} + c_2 Ra^{1/5} + c_3, \tag{3.25}$$

the elementary form of which for the 2-α free-slip solution follows from the analysis in Appendix D.2, there results

$$\lambda \sim \frac{12}{7} + \frac{5}{49}\frac{c_2}{c_1\, Ra^{1/5}} + \frac{10}{343}\frac{7(c_3-1)c_1 - 3c_2^2}{Ra^{2/5} c_1^2}, \tag{3.26}$$

$$\mu_1 \sim \frac{2}{5} - \frac{c_2}{5c_1 Ra^{1/5}} + \left(\frac{c_2^2}{5c_1^2} - \frac{2(c_3-1)}{5c_1}\right)\frac{1}{Ra^{2/5}}, \tag{3.27}$$

$$\mu_2 \sim \frac{2}{5} - \frac{c_2}{5c_1 Ra^{1/5}} + \left(\frac{c_2^2}{5c_1^2} - \frac{2c_3}{5c_1}\right)\frac{1}{Ra^{2/5}}, \tag{3.28}$$

† Hereafter, although we are speaking of bounds on heat flux, we use an asymptotic symbol in relations such as (3.20). It is to be understood that the form on the right is, in each case, a *bound* on (strictly) $Nu - 1$. The notation is intended to emphasise the asymptotic nature of these estimates. Little confusion should result.

‡ The expansion for λ is somewhat tedious to derive directly. One introduces an expansion for λ and also one for $\|\tau'(R)\|^2$ in (3.18) substantially of the form assumed for Nu, but with unknown coefficients. The derivative condition couples the two expansions, and enforcing those relations in the subsequent expansion of (3.18), when equated to $Nu - 1$, closes the set. It proves easier, based on the general result (3.24), to find μ_1 given μ_2, and solve for λ from (3.19).

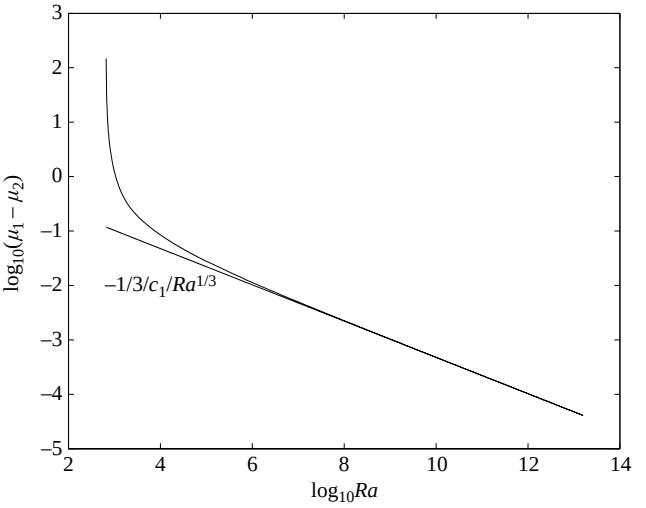

FIGURE 1. This example, showing the expected difference between two estimates of the leading-order algebraic exponent, is taken from § 6, on free-slip computations.

and c_3, the constant term in the asymptotic form for Nu, plays the same role as above. Finally, for the general relation

$$Nu \sim c_1 Ra^{\mu}(\log Ra)^{\nu} + c_2, \tag{3.29}$$

the associated expansions take the form

$$\lambda \sim \frac{2+\mu}{1+\mu} - \frac{\nu}{(1+\mu)^2 \log Ra} + \frac{\mu(c_2-1)}{(1+\mu)^2 Ra^{\mu}(\log Ra)^{\nu}}, \tag{3.30}$$

$$\mu_1 \sim \mu + \frac{\nu}{\log Ra} - \frac{\mu(c_2-1)}{c_1 Ra^{\mu}(\log Ra)^{\nu}}, \tag{3.31}$$

$$\mu_2 \sim \mu + \frac{\nu}{\log Ra} - \frac{\mu c_2}{c_1 Ra^{\mu}(\log Ra)^{\nu}}. \tag{3.32}$$

Although one cannot prove $\nu \geqslant 0$ for every conceivable upper bound problem, this appears always to be the case. Consequently, a log term in the leading-order dependence means that both μ_1 and μ_2 will approach their common limit from above. By contrast, the constant term in the algebraic forms for Nu, e.g. (3.20), is not expected to exhibit a sign preference, hence the limit may be approached from either side, and even for μ_1 and μ_2 to approach the limit one from above and the other from below in the case of (3.20) (and its generalization) for $0 < c_2 < 1$.

The results for the balance parameter are asymptotic with the normal limitations that implies for finite Ra. In particular, the balance parameter λ must pass smoothly to $\lambda = 1$ at the energy stability point, $Ra = Ra_c$, a feature unlikely to be captured by these expansions.

In closing, we comment that, for more complex bounding problems, the spectral constraint cannot generally be parameterized by a single variable (here $R = \lambda Ra$), although there may for particular problems be a simple two- or three-dimensional equivalent factorization into constraint space and optimizing space.

	Free-slip	No-slip
1-α	$Nu \sim 0.32498941162098\, Ra^{1/3}$ $\alpha_1 \sim 5.5377856128012329 + c_1\, Ra^{-1/3}$	$Nu \sim 0.14816941588087\, Ra^{3/10}(\log Ra)^{1/5}$ $\alpha_1 \sim (Ra/13)^{1/4}$
2-α	$Nu \sim 0.1017 Ra^{2/5}$ $\alpha_{2,1} \sim 1.9662$ $\alpha_{2,2} \sim 0.6519 Ra^{1/5}$	$Nu \sim 0.128693\, Ra^{0.33175}\,(\log Ra)^{0.0325}$ $\alpha_{2,1} \sim c\, Ra^{1/4}$ $\alpha_{2,2} \sim c\, Ra^{0.33175}\,(\log Ra)^{0.0325}$
3-α	$Nu \sim 0.068197\, Ra^{31/75}$ $\alpha_{3,1} \sim c$ $\alpha_{3,3} \sim c_3 Ra^{6/25}$	$Nu \sim 0.1380 Ra^{1/3}$ $\alpha_{3,k} \sim c_k Ra^{1/3}$ $c_k = \{0.002925, 0.02850, 0.1328\}$
N-α	$Nu \sim c_N Ra^{5/12(1-5^{-N})}$ $\alpha_{N,1} \sim c \quad \alpha_{N,N} \sim c Ra^{1/4(1-5^{1-N})}$	$Nu \sim c_N Ra^{1/3}$ $\alpha_{N,k} \sim c_k Ra^{1/3}\ \forall k$

TABLE 1. Compilation of all numerical results from solution of the CDH form of the Euler–Lagrange equations.

4. An overview

Asymptotic analysis of multi-α solutions rests in the first instance on a firm grounding for the solution with a single horizontal mode. And, although the 1-α branch remains a valid upper bounding solution only while the spectral constraint is satisfied, we compute both free-slip and no-slip solutions well beyond this point. We do the same for all successive bifurcating branches as well, although numerical limitations generally prevent us from following each of these as far as one would like.

If limited only to the segments of the α branches prior to bifurcation, the available range of data is simply so far from asymptotic that extrapolation for the leading-order behaviour is pointless. Even using the unrestricted branch, a persuasive case requires that one fit the transient terms as well. When, as for the 1-α solutions, there is a complete analytic theory at hand, those transients are easily determined. In those cases where analytic guidance is lacking, arguments have inevitably to be in the nature of a 'bootstrap'.

Table 1 gives a summary overview of the results established in this work. We support Chan's 1-α solution but disagree with his scalings for all other branches. Confirmation of the 1-α result rests partly on numerical findings and partly on extensive supplemental analysis presented in Appendices B and C. Conclusions regarding the higher branches for the no-slip problem rest on numerical evidence alone. We agree with a part of Vitanov's previous work (Vitanov 1998) on the 1-α solution for the free-slip problem but find significant differences. A complete analysis of this case is presented, with the leading-order balance in the main body of the paper, and additional details on matching given in Appendices B and C, the latter points paralleling similar considerations for no-slip. Analysis and numerical results are in complete accord for this case. We present the leading-order analysis, which consists of the determination of a certain set of indicial exponents, for a novel balance arising from the 2-α branch for free-slip. All of these features are supported by the numerical evidence. A supplemental analytic discussion on closing the set of equations in the midlayers is given in Appendix D. A portion of this analysis is fairly accessible to comparison with, and shown to be supported by, numerical results. Finally we

propose that free-slip higher branches generate a geometric series of relations for Nu that approaches a limit of $Ra^{5/12}$.

Where needed for clarity, we shall use a subscript to denote a solution with k wavenumbers, e.g. λ_k for the associated balance parameter. A second subscript is used to enumerate the boundary layers; hence the wavenumber, for example, is indicated by $\alpha_{k,j}$ where $1 \leqslant j \leqslant k$ and $j = 1$ corresponds to the smallest wavenumber. (We omit the second subscript in the case that $k = 1$.)

5. No-slip numerical results

5.1. 1-α *results*

All the arguments in Appendices A and B support the leading-order 1-α result for Nu, given in equation (118a) of Chan, that

$$Nu_C \sim \left(\frac{6}{I}\right)^{6/5} \frac{Ra^{3/10}(\log Ra)^{1/5}}{(13)^{13/10}(20)^{1/5}} = 0.14816941588087 Ra^{3/10}(\log Ra)^{1/5} \tag{5.1}$$

as $Ra \to \infty$. (The integral I is defined and evaluated in Appendix A.) The implicit coupled relations that arise on maximizing F generate higher-order terms than are stated by Chan. While these added terms are incomplete in that a full accounting of higher coefficients requires subsidiary expansions not completed in this paper, it is nonetheless helpful here to note the general form for Nu that emerges, i.e.

$$Nu \sim \left(\frac{6}{I}\right)^{6/5} \frac{Ra^{3/10}(\log Ra)^{1/5}}{(13)^{13/10}(20)^{1/5}} \left[1 + \frac{1}{5}\frac{4\log\log Ra - 4\log(10I/3) - \log 13}{\log Ra} + \dots\right]. \tag{5.2}$$

Thus the dependence on $\log\log Ra/\log Ra$, for example, will persist in the computed results, but with additions to the above coefficient of 4/5. The fundamental origin of these terms can be traced to (B 4), the singular solution for w in the intermediate layer.

On this ordering of terms, purely algebraic corrections remain subdominant, and hence undetermined, but we can allow for such a correction in an empirical fit. Our numerical results carried past $Ra = 10^{17}$ are consistent with

$$Nu \sim \left(\frac{6}{I}\right)^{6/5} \frac{Ra^{3/10}(\log Ra)^{1/5}}{(13)^{13/10}(20)^{1/5}} \left[1 + \frac{0.1391\log\log Ra - 2.6575}{\log Ra} + \frac{1.3054}{Ra^{3/10}}\right]. \tag{5.3}$$

The magnitude of the apparent corrections seems unexceptionable, e.g. 4/5 above now becomes 0.1377. Subsidiary issues, such as appropriate fitting algorithms for coefficients of asymptotic expansions in the presence of systematic errors in the data, and intrinsic ill-conditioning of higher-order fits for logarithmic expansions, notwithstanding, the coincidence of curves in figure 2, where we have plotted Nu/Nu_C against the fitted value of the same ratio, gives the appearance of a correct asymptotic characterization.† As the only coefficients fitted are those stated in decimal form, *a fortiori* every component of the leading-order prediction (5.1) is verified. Given Chan's prediction of 3/10 for the algebraic dependence of Nu on Ra, there is a further consequence: the interior slope of $\overline{T}$ remains $-1/13$ as $Ra \to \infty$, which implies that the slope of τ is positive in the interior, $\tau' = 1/23$.

† The slight gap appearing for $Ra > 10^{16}$ indicates a growing loss of precision. For an expansion in polynomials up to degree 1800, the spectral fall-off for $\widehat{\theta}$ is only about 0.007.

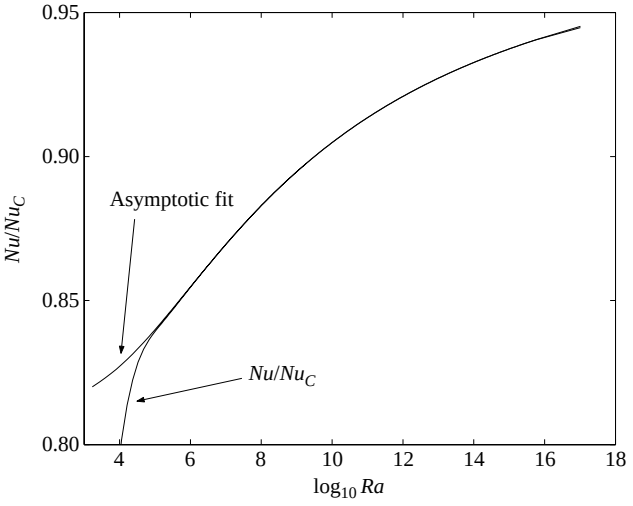

FIGURE 2. The Nusselt number, Nu, divided by the leading-order result, Nu_C, and an empirical asymptotic fit.

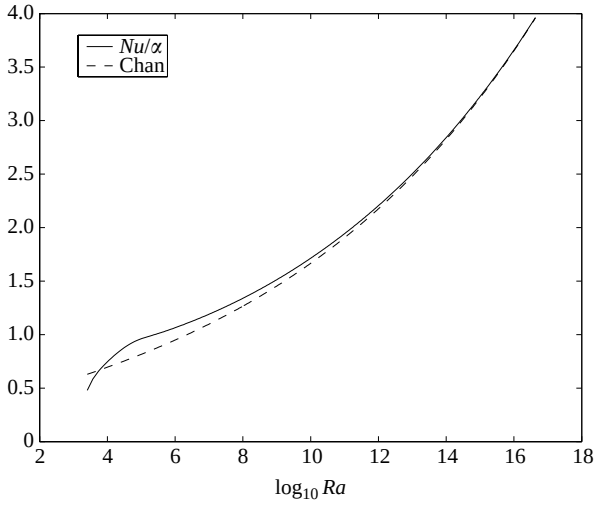

FIGURE 3. Direct confirmation of Chan's 1-α prediction.

A second test of Chan's analysis is the wavenumber prediction

$$\alpha_1 \sim \left(\frac{Ra}{13}\right)^{1/4} \qquad \text{as} \qquad Ra \to \infty \tag{5.4}$$

(equation (54) in Chan 1971). This is readily confirmed as above by using a fit with suitable logarithmic corrections but, to make the case more sparely without recourse to freely fitted terms, we compare the computed ratio Nu/α_1 to the leading-order prediction derived from Chan, namely

$$Nu/\alpha_1 \sim 0.28134837224762\, Ra^{1/20} (\log Ra)^{1/5}. \tag{5.5}$$

The rapid confluence of the curves in figure 3, in spite of the weak dependence predicted, is a convincing demonstration of the validity of Chan's expansion. That

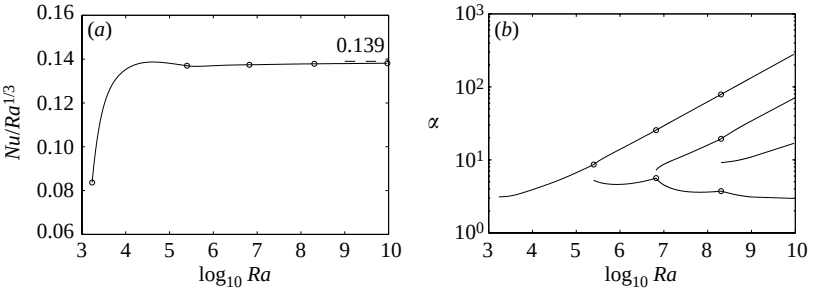

FIGURE 4. (*a*) The no-slip Nusselt bound scaled by $Ra^{1/3}$. Here and henceforth circles indicate bifurcation from k to $k+1$ wavenumber solutions. (*b*) Bifurcation of the no-slip horizontal wavenumbers $\alpha_{k,j}$ for the optimal solution.

(5.5), without any empirically fitted corrections, so closely matches the computed result has to be attributed to a serendipitous degree of cancellation between numerator and denominator since the explicit estimates of the numerator available from (5.3) show that asymptotic correction terms of order $\log\log Ra/\log Ra$ remain significant over the accessible range of computation. For comparison, a plot of the asymptotic expansion for the balance parameter by (3.30) with $\mu = 3/10$ and $\nu = 1/5$ shows only crude agreement with direct numerical computation, precisely owing to the need of such corrections.

There are several delicate points raised in Chan's expansion of the leading-order solution. The full series (B 4), of which only the first term is given by Stewartson (1966), is asymptotically similar to a generalized hypergeometric function, (B 10). The series contains only one free parameter, which enters at second order, and yet matching to the interior would normally dictate that there be two parameters. Even a determination of that single parameter is tricky, with the result, shown in figure 23, turning on a comparison of the optimal asymptotic truncation of (B 4) with a numerical solution of the integral equation (B 12). Analysis of matching of the outer limit of the wall layer in (C 28) and the inner limit of the intermediate layer in (B 5) shows both the need for a subsidiary expansion of the latter and that care must be taken in consistently defining the amplitude of the wall layer as given in (C 29) (with the consequences apparent in (5.2)). All of these points are developed in detail in the appendices in order fully to support the case that the 1-α solution is correct. By contrast, we see in § 5.2 that the elaborate multi-α scenario envisioned by Chan is wholly incorrect. The failure of his arguments can be initially understood by reference to a crucial modification of the intermediate layer solution.

5.2. *Multi-α results*

The optimal solution was followed up to, and including, four wavenumbers. The bifurcation to five wavenumbers was fixed at Ra approximately equal to 9.398×10^9. In figure 4, approach to an asymptotic limit of $Ra^{1/3}$ is reasonably evident. We estimate a limiting prefactor of 0.139, which lies about 9% below Chan's asymptotic prediction of $0.152Ra^{1/3}$.† Circles represent bifurcations from mode j to $j+1$, the points at which SC-neutrality switches to solutions with a greater number of nested boundary

† The value quoted comes directly from Chan (1971, equation (119)) but, on substitution of his stated numerical values for I and β (we have confirmed both) into his preceding analytic form, (95), we compute a prefactor 0.163345, with our result then a reduction of 15% instead.

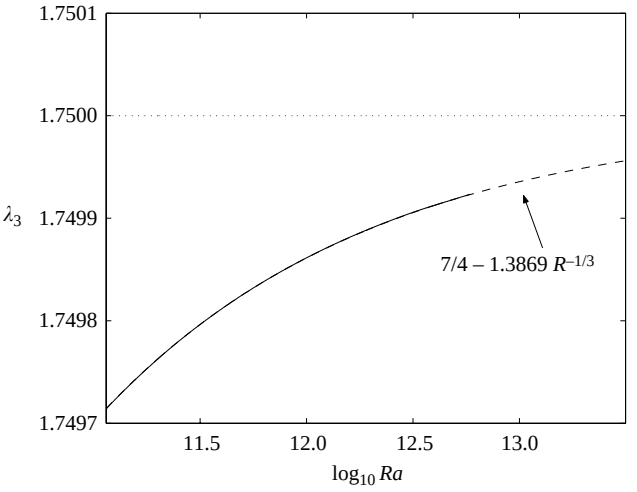

FIGURE 5. The balance parameter λ_3 with a two-term prediction for the no-slip 3-α solution.

layers. Bifurcations in the horizontal wavenumbers of the optimal solution are shown in figure 4(*b*). Chan estimated that the first bifurcation occurs at $Ra = 10^{10}$ and that the number of wavenumbers included in the optimal solution grows as $O(\log\log Ra)$. Straus (1976*b*) gave apparent support for this, reporting that no bifurcation is seen for $Ra \leqslant 10^6$. However, we find that the first bifurcation takes place at $Ra = 2.4968 \times 10^5$.

For the 3-α branch, λ tends far more quickly to its limit than does λ for the 1-α branch. On the revised assumption that Nu takes the form (3.20), the balance parameter has the asymptotic expansion given in (3.21). As the data for Nu do not permit an accurate determination of c_2 or higher constants, we appeal to (3.21) to justify the use of an empirical one-parameter fit, namely

$$\lambda_3 = 7/4 + \tilde{c}_1 Ra^{-1/3}. \tag{5.6}$$

The result, shown in figure 5 with $\tilde{c}_1 = -1.3869$, patently confirms that (5.6) is the appropriate form and thus λ_3 tends to the limit stated. The 3-α solution immediately attains the saturated dependence, $Ra^{1/3}$; there is no leading-order logarithmic contribution at all.

The addition of figure 6 makes the point clear beyond doubt. Five curves are plotted – $\alpha_{3,k}$ ($k = 1, 2, 3$), Nu, and $Ra^{1/3}$ – with a free vertical offset of four of the five in order to bring the set into transparent coincidence. (Nu is held fixed.) It should be clear at once what this means: there is no asymptotic scale separation of successive wavenumbers. We have instead a scenario somewhat reminiscent of the analytical scheme originally proposed by Busse for shear flow (where successive scales differed by a factor of four, albeit in that case only asymptotically and, strictly speaking, formal scale separation was still obtained between successive layers). Here $\alpha_{3,k} = c_k Ra^{1/3}$ with the values of the c_k given by

$$c_1 = 0.1328673, \quad c_2 = 0.0285047, \quad c_3 = 0.0029252.$$

The coupled equations for this case follow immediately but analysis of this set is obviously hampered by the lack of scale separation. Rather, one can utilize only the numerical separation of the c_k.

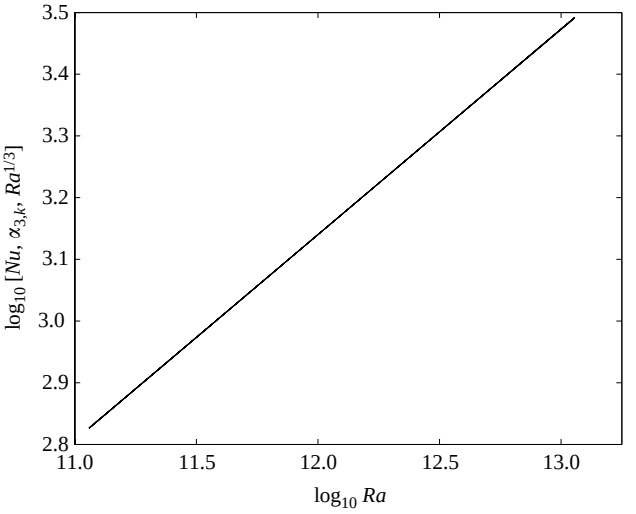

FIGURE 6. A superposition of the $\alpha_{3,k}$ and Nu demonstrating that the 3-α solution attains the limiting form of $Ra^{1/3}$ and with no scale separation of the wavenumbers.

The reader will naturally wonder at this point about the 2-α branch. This turns out to be a delicate transitional solution; neither of the precise algebraic–logarithmic form proposed by Chan, nor quite of the saturated form found above. While we have not pursued the details of the 3-α expansion, in a broad sense there is not much more for such an exploration to reveal; the contours of the solution are perfectly clear. This is far from the case for the 2-α solution, where we do not see the means yet to advance beyond an empirical determination of the scaling.

The single most striking and reliably established characteristic of the 2-α solution is that, in common with the pattern of the 3- and 4-α solutions, and in sharp contrast with Chan's prediction, the ratio $Nu/\alpha_{2,2}$ tends rapidly to a constant, slightly larger than unity. This immediately and decisively undermines the envisioned nesting of sublayers as given in Chan but it is considerably more challenging to determine the leading-order dependence of Nu itself than simply to observe its relation to $\alpha_{2,2}$.

The most useful diagnostics are the numerical estimates for the controlling factor, μ_1 and μ_2. If μ_1 or μ_2 alone is plotted, a determination of μ relies on judging the horizontal asymptote. In the case of an elementary exponent, such as $1/3$, this presents no difficulty. But when, as here, the leading exponent need not take an elementary value, one requires a fitting algorithm. If Nu is assumed to vary as $c_1 Ra^{\mu} + c_2$, then $\mu_1 = \mu + cRa^{-\mu}$ while taking $Nu \sim c_1 Ra^{\mu} + c_2 Ra^{\nu}$ necessitates a three-parameter fit, $\mu_1 = \mu + cRa^{\nu-\mu}$. In such an ambiguous circumstance it is more useful to plot $\log|\mu_1 - \mu_2|$, where the desired exponent for either form of Nu is simply read off as the slope or, to be sure, the limiting value of that slope.

A plot of $\log|\mu_1 - \mu_2|$ for the 2-α solution does seem to show algebraic decay with an apparent value of $\mu = 0.3387$. While limitations in the accuracy of the data (primarily μ_2) leave an unacceptably large uncertainty in the estimate of μ – confined by the 3-α results, μ cannot in any case exceed $1/3$ – it is crudely in the range expected. But unlike the case of the balance parameter in (5.6), the individual curves for μ_1 and μ_2 tend to a limit much more slowly than $Ra^{-\mu}$ and they approach that limit from above. Each of $\mu_{1,2}$, that is, has a more slowly decaying transient and the transients are identical in their dependence on Ra (at least to $O(1)$). While this

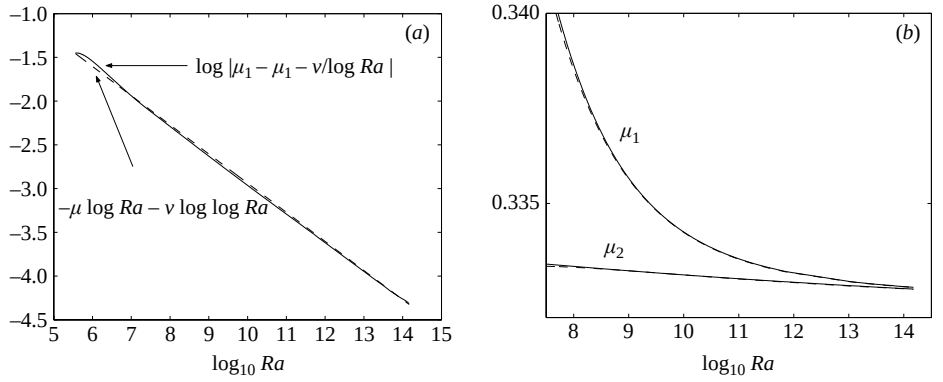

FIGURE 7. Evidence for the asymptotic scale of Nu on the 2-α branch. (a) A self-consistent fit of μ_1 in order to determine the parameters μ and ν. (b) Computed (solid) and predicted (dashed) values for μ_1 and μ_2.

qualitative description certainly implies a purely algebraic asymptotic form, such as (3.25), conditioned principally by the form of the 1-α scaling, it is natural to consider (3.29) and, in the end, it provides the more persuasive fit. This may seem too general a form as a basis for stable estimates, as it is frequently observed that fitting coefficients and exponents simultaneously is a numerical procedure to be avoided, but various cross-checks are helpful in this regard.

The values for μ and ν must be such that

$$\mu + \nu(\log Ra)^{-1}, \tag{5.7}$$

when subtracted from μ_1 and μ_2, leaves a transient which itself decays with the seeming algebraic decay noted above. For (3.29), that residual transient is not $Ra^{-\mu}$ but rather $Ra^{-\mu}(\log Ra)^{-\nu}$. However, as the difference plot of $\log|\mu_1 - \mu_2|$ was observed to be nearly a straight line, we can anticipate that ν must be small in magnitude.

This determination of μ and ν is more stably computed from μ_1, particularly the latter parameter. The results of this analysis are shown in figure 7, with panel (a) vindicating the choice of μ and ν. (The logarithmic correction term is included in the dashed line though its influence is negligible over the range plotted.) Figure 7(b) shows two dashed lines, given by (3.31) and (3.32), which agree well with the computed values. Equation (3.31) relies separately upon the values for c_1 and c_2 appearing in (3.29). While the first of these can be determined from fitting Nu, the data do not give a reliable estimate for c_2, so the latter was chosen to fit μ_1 and μ_2 simultaneously (using $c_2 = 0.037$). Substituted into (3.29) we thus have

$$Nu \sim 0.128693\, Ra^{0.33175}(\log Ra)^{0.0325} + 0.037.$$

Trying to anticipate the exact exponents is a difficult enterprise in numerology given the absence of an accompanying derivation, and not overlooking that the final data points are perceptibly noisy; hence these values must be regarded as provisional, but the data do not permit significant departure from the values stated if all the tests for consistency are to hold. Perturbing the algebraic power by ± 0.00005 or the logarithmic power by ± 0.0005 gives noticeably worse agreement in replotting figure 7(a). Key to the accuracy of this determination as well is that, and again in contrast with Chan's

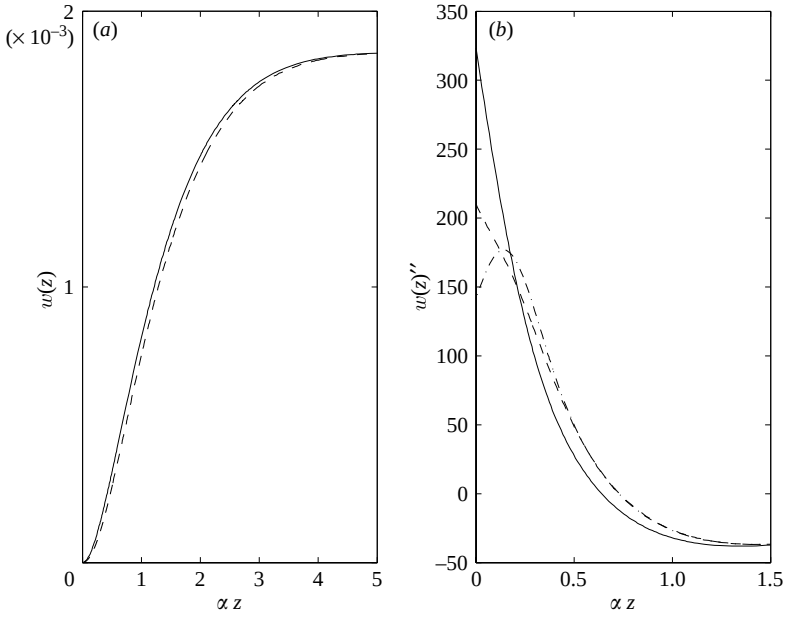

FIGURE 8. (*a*) Superposition of w (solid) from a 1-α solution and $w_{2,1}$ (dashed) from a 2-α solution at a common reference value of α. (*b*) The same superposition, but the second derivative in each case, with $w''_{3,1}$ (dash–dot) from the 3-α solution of largest available Ra shown for comparison.

proposed elaboration to a multi-α solution, log–log corrections here do not appear to enter at the same order as indicated in Appendix B for the 1-α solution.

A complementary approach to the determination of scalings is the superposition of curves representing w, θ, and their derivatives at a range of values of Ra. When the exponents sought are simple rational numbers, this is a useful and elementary exercise. Variations in the overlaid curves are produced not only by explicit adjustments of μ and ν in the process of fitting but also by variation in higher-order corrections over the finite range of Ra sampled. In seeking an exponent that evidently is exceedingly close to 1/3 these two effects are not easily distinguished, if at all. So while plots of this nature may help to confirm the values identified above, they are not useful to find the values *a priori*.

Instead it is more instructive to look at $w_{2,1}$, here selected at $Ra = 6.763 \times 10^{13}$ with $\alpha_{2,1} = 540.943$, and compare it to w from a 1-α solution with α_1 having the same value, which occurs for $Ra = 1.618 \times 10^{12}$. Plotted as a function of $\xi = \alpha z$ using the common value of α, one might expect the intermediate layer solutions to coincide as they satisfy the same equation and certainly the same boundary conditions for $\xi \to \infty$. While in figure 8(*a*) w and $w_{2,1}$ are reasonably similar, figure 8(*b*), showing the second derivative of each, exhibits a first-order change in the character of the match coming from the sublayer. Where w'' shows a slope monotonically increasing towards the origin, reflecting the underlying $\sqrt{\log(1/\xi)}$ singularity in (B 4), $w''_{2,1}$ shows a clear change in the character of that match at approximately the point where the two curves cross. This effect is more transparent with the third curve, which shows $w''_{3,1}$. Note, however, that the 3-α solution is for $\alpha_{3,1} = 44.109$. Reaching the desired value of 540.943 would require an increase in Ra by about 10^3 beyond the highest

point computed. In lieu of this, we have arbitrarily rescaled $w''_{3,1}$ in the plot so that its amplitude matches $w''_{2,1}$.

The structure of Chan's 1-α solution – specifically the appearance of log–log terms – is singularly sensitive to the intermediate layer conditions imposed in the limit of $\xi \to 0$. With the modification of the boundary conditions those terms immediately disappear and, while a (weak) logarithmic dependence persists in the 2-α bound for Nu, the rapid decay of correction terms, as detailed in the discussion above for μ_1 and μ_2, allows a robust characterization of this solution branch in advance of the needed analytical development. Free-slip boundary conditions will prove less numerically obliging.

Finally, computations at 4-α carried to $Ra = 10^{11}$ show Nu, $\alpha_{4,4}$ and $\alpha_{4,3}$ all apparently consistent with a limiting dependence of $Ra^{1/3}$. We anticipate that the emergence of this scaling will become apparent for $\alpha_{4,1}$ and $\alpha_{4,2}$ as well, once Ra is sufficiently far above the bifurcation at $Ra = 2.09 \times 10^8$. At $Ra = 10^{12}$ for example, $\alpha_{4,1}$ is only 3.2 after rising from a minimum of 2.96 at $Ra = 5 \times 10^9$. (By comparison we were able to carry the 3-α solution from its initial bifurcation at $Ra = 6.74 \times 10^6$ to $Ra = 1.14 \times 10^{13}$.) A plot of $\log|\mu_1 - \mu_2|$ gives persuasive evidence that $\mu = 1/3$ but, unlike the case of the balance parameter for the 3-α no-slip solution, there appears to be an intervening algebraic transient ahead of a constant term in the asymptotic form for Nu, suggesting at least some possible distinctions between 3- and 4-α solutions. So the behaviour of the lesser wavenumbers may not be as simple as we have proposed and the failure of scale separation perhaps confined to fewer wavenumbers. Computation extended to $Ra \approx 10^{16}$ should resolve this point decisively.

We have not computed 5-α solutions and beyond but it seems that, from 3-α onward, all branches will asymptote to $Ra^{1/3}$, with only the prefactor affected, and that some absence of scale separation is characteristic of the saturated bound. Our estimates of the prefactor for Nu are 0.138006795 and 0.13835 for three- and four-wavenumber solutions respectively. The inconsequential change suggests that computations on higher branches serve little practical purpose.

In conclusion, it is a curious feature that the dual nature of this variational problem is reflected as well in the character of the fields that saturate the bound. It has long been thought that the MHB approach yielded the correct asymptotic bound but inevitably only after undergoing an infinite bifurcation sequence of nesting boundary layers. The progression found here is 1, 2, ∞. Subsequent bifurcations simply modify the leading constant (approaching the limit from below of course).

Coming from the other direction, a number of successes in application of the CDH method has encouraged the view that simple, one-parameter, test fields suffice to capture the saturated limit and yet, as we have demonstrated in Part 1, that view cannot be maintained in the case of convection at infinite Prandtl number; a more complex structure is required. To summarize, conservative bounds are not assured of immediate saturation with elementary test fields, while a multi-α expansion may saturate in a small number of steps.

6. Free-slip numerical results

6.1. 1-α *results*

Now we consider the 1-α solution for free-slip boundary conditions, which contrasts markedly with that for no-slip. This problem was first studied by Chan (1970), who predicted that the upper bound consisted of a single-wavenumber solution behaving as $Nu \sim Ra^{1/3}$, and with no ensuing bifurcation from that state. A careful numerical

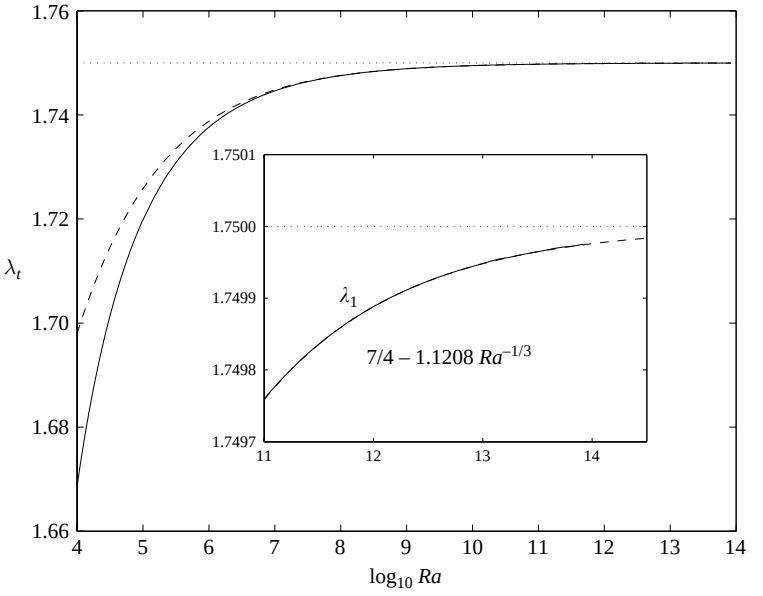

FIGURE 9. The balance parameter λ_1, with limiting value of 7/4. The dashed line shows an asymptotic fit, the dotted line the limit.

treatment of the 1-α solution is presented by Vitanov (1998) who, in his equation (29), gives the following scalings:

$$Nu \sim 0.3254 Ra^{1/3}, \quad \alpha_1 \sim 0.2011 Ra^{1/6} \quad \text{as} \quad Ra \to \infty. \tag{6.1}$$

For an exponent of 1/3, consistent with the expansion given in (3.20), the limiting value of λ_1 is, as in § 5.2, 7/4. Using the same single-parameter fit as in (5.6), here we obtain $\tilde{c}_1 = -1.1223$. But we have an analytic prediction for c_1 (derived in § 7.1) and these data permit reliable estimation of c_2 (≈ 0.9420), so we can in this instance compare the freely fitted value to that implied by (3.21), which works out to $\tilde{c}_1 = -1.1205$. The difference appears within the probable range of fitting error. The result using the empirical value of $\tilde{c}_1$, shown in figure 9 (with added inset scale to match the earlier figure 5), gives excellent agreement for $Ra > 10^8$. From the self-consistency of this fit we conclude that Vitanov's exponent for Nu is borne out. (Slight bumps in the computed λ_1 for Ra larger than about 10^{13} reflect the encroaching loss of resolution.)

But in figure 10 we see that Vitanov's assumption that α_1 scales as $Ra^{1/6}$ is invalid. As we shall shortly prove, $\alpha_1 \to 5.5377856128012329$ as $Ra \to \infty$. This is in notable contrast to all other upper bounds problems of which we are aware, where α is consistently a monotone increasing function of the control parameter in the problem. The reasons for this, as well as the success of Vitanov's prediction for Nu, are explored in § 7.1.

As with no-slip, in lieu of computing the constants appearing in the correction terms to Nu, for which see (C 7), here too we simply make use of the expected form, regarding higher-order constants as parameters to be fitted in an appropriate manner reflecting the asymptotic nature of the expansion. The result, namely

$$\frac{Nu}{0.32498941162098 Ra^{1/3}} = 1 - 2.7373 Ra^{-1/3} - (2.1352 \log Ra - 0.8815) Ra^{-2/3}, \tag{6.2}$$

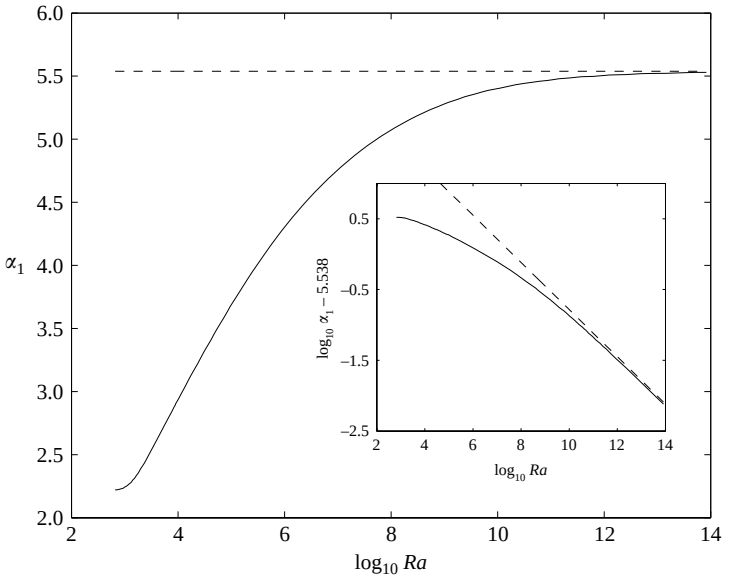

FIGURE 10. α_1 showing convergence to an $O(1)$ number with inset showing that the residual decays algebraically with $Ra^{-1/3}$ after about $Ra = 10^9$.

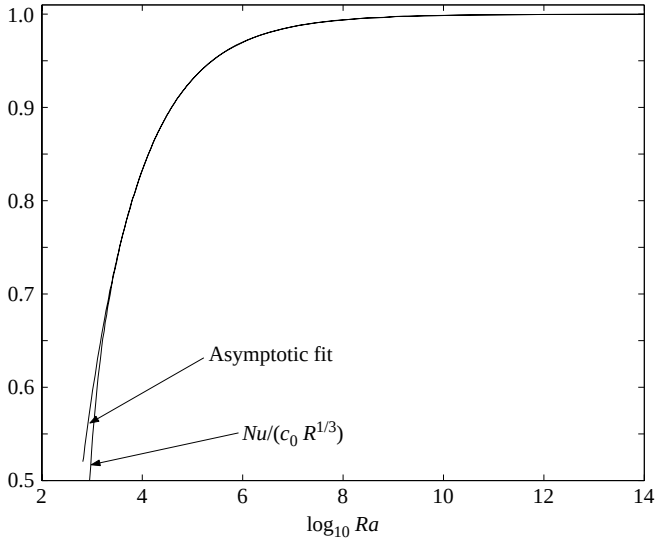

FIGURE 11. Comparison of the 1-α reduced Nusselt number to an asymptotic fit.

is plotted in figure 11, along with the actual ratio. As before, the leading-order contribution is implicitly confirmed by pivoting the asymptotic expansion of the ratio about a leading term of unity.

6.2. *Multi-α results*

Straus (1976*a*) did the first exploration of the possible bifurcation to multi-α solutions for free-slip boundaries, concluding that no bifurcation of the 1-α occurs for

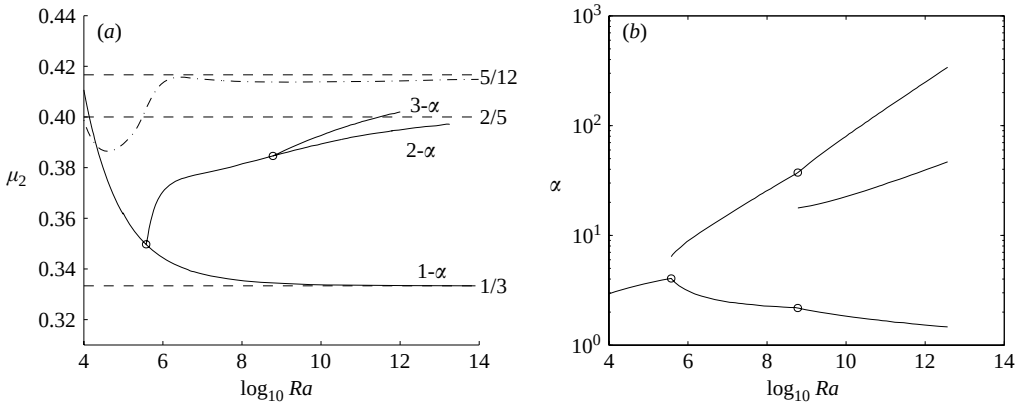

FIGURE 12. (*a*) The free-slip μ_2. Branches are labelled by the corresponding mode number, k-α. Dashed lines are included for comparison at 1/3 (the limiting exponent for 1-α), at 2/5 (the limiting exponent for 2-α), and at 5/12 (a bound on the exponent for the N-α result based on the result from Part 1, with the running conservative estimate appearing as the adjacent dash-dotted line). The circles represent the point of bifurcation from mode k to $k+1$. No points have been obtained on the four-mode branch after the third circle. (*b*) Bifurcation of the corresponding horizontal wavenumbers $\alpha_{k,j}$.

$Ra < 2.3 \times 10^5$. This is corroborated by our determination that the transition takes place at 3.7713469×10^5.

We have already observed that the 1-α Nusselt function scales as $Ra^{1/3}$. Calculations of the asymptotics for 2-α reveal a $Ra^{2/5}$ scaling, the analytic basis of which we present shortly. The 3-α solution is found to scale as $Ra^{31/75}$, consistent with a limiting exponent of 5/12, coinciding with the conservative free-slip bound presented in Part 1, and as speculated originally in Plasting (2004). The bifurcation to a 4-α solution occurs at around $Ra = 7 \times 10^{11}$ but no points on the 4-α branch have yet been obtained owing to numerical difficulties. (This does not seem to point to any underlying pathology in the equations themselves, however.) To give the reader an overview, we show μ_2 in figure 12(*a*) along the one-, two-, and three-mode solution branches.

In figure 12(*b*) we show the accompanying α-bifurcation. The distinguished feature of the free-slip α-bifurcation is saturation of the lowest wavenumber. This has been noted earlier for the 1-α solution and is seen for 2- and 3-α solutions as well. We conjecture that this obtains for all subsequent bifurcations.

Most of discussion for the 2-α solution is presented in Appendix D but we note here a feature common to the 2- and 3-α solutions. As previously found for no-slip, μ_1 and μ_2 individually approach a common limit more slowly than does their difference. In the case of the 2-α solution, equations (D 26)–(D 27) give reason to expect (3.25) to apply, hence a slow transient that scales as $Ra^{-1/5}$. Such a term provides a plausible fit as seen in figure 13, where the limit of 2/5 is assumed, and two transients of $Ra^{-1/5}$ and $Ra^{-2/5}$ fitted to the data for $Ra > 2.6 \times 10^{10}$. The data at smaller Ra serve as an independent check of the expansion; a log plot of that difference shows a successor scale of $Ra^{-3/5}$. (A plot of Nu and the associated empirical fit appears in figure 14.) On this observation, it is not surprising that an intermediate term before the constant is also encountered in the solution for 3-α. Once more, plots of the fields w and $\widehat{\theta}$ are of limited use for the reasons noted previously. For this, the last of our numerical study, it appears that the proper form for the expansion of Nu is a subtle

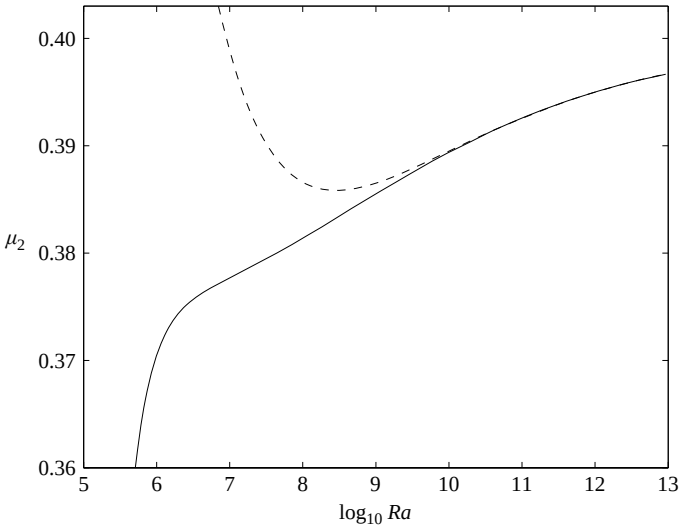

FIGURE 13. Empirical determination of μ_2 and a fit according to the formula following (3.25).

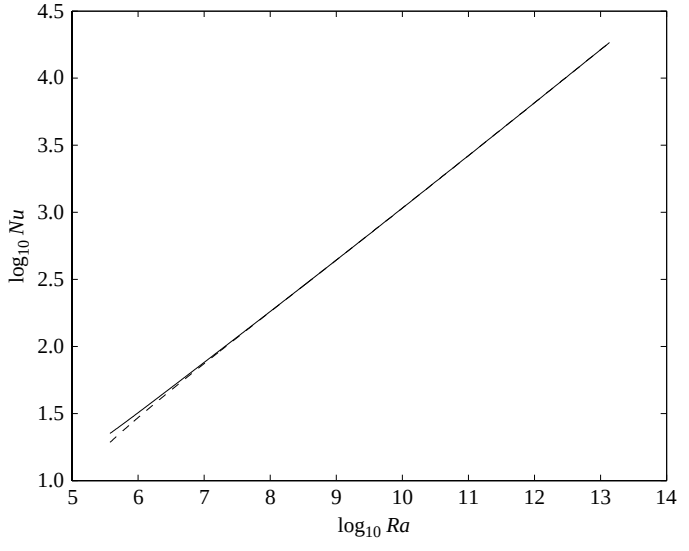

FIGURE 14. Nusselt number as a function of Ra for the 2-α free-slip solution. A second, dashed, curve is superimposed, following the empirical fit $Nu = 0.10100Ra^{2/5} + 0.70965Ra^{1/5} - 7.166$.

generalization of the form given in (3.25), namely

$$Nu \sim 0.068197\, Ra^{31/75} + 0.329473\, Ra^{4/15} - 0.504659. \tag{6.3}$$

On an initial approach to the data, the previously useful diagnostic variables $\mu_{1,2}$ appear of little help. The reason is that, while $\mu_{1,2}$ certainly asymptote to 31/75, for the form in (6.3), if $\mu_{1,2}$ are each expressed as we have so far done, as a series, there are twelve independent transients of order greater than Ra^{-1}. For exponents as in (6.3) having a non-simple ratio, one must revert to the rational form, here (and

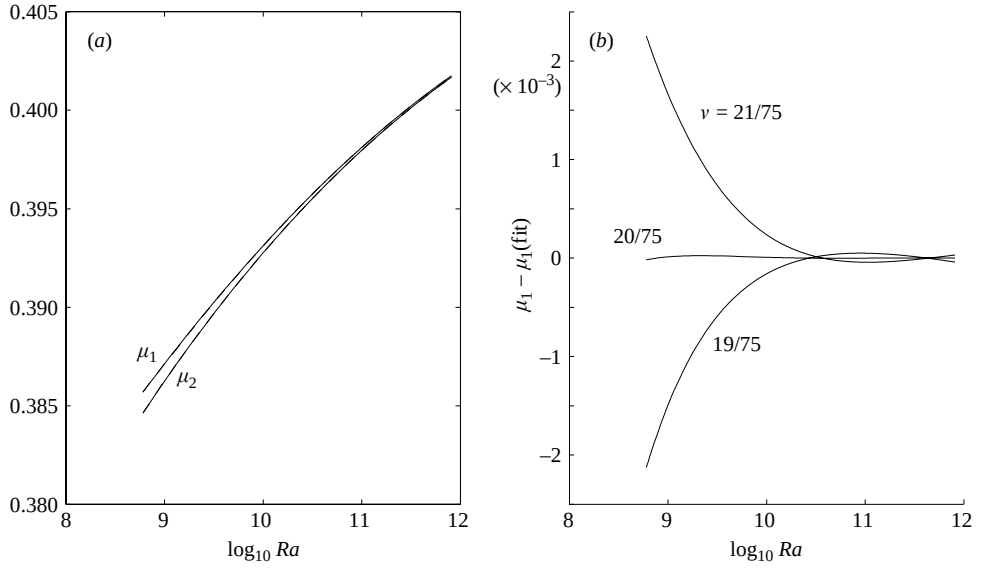

FIGURE 15. (*a*) Computed and fitted exponent estimates $\mu_{1,2}$ for the *Nu* relation proposed in (6.3). (*b*) Sensitivity of the fit to change in the second exponent in (6.3), for $\mu = 31/75$.

invoking the coefficients in (6.3) symbolically for greater clarity)

$$\mu_1 = \frac{31/75\, c_1\, Ra^{31/75} + 4/15\, c_2\, Ra^{4/15}}{c_1\, Ra^{31/75} + c_2 Ra^{4/15} + (c_3 - 1)}.$$

The computed values of μ_1 are used to estimate c_2/c_1 and $(c_3 - 1)/c_1$ based on a least-squares fit to the rational form above. Figure 15(*a*) compares the computed and fitted values of $\mu_{1,2}$; the difference is imperceptible. The c_k given in (6.3) are determined from a direct fit for *Nu* itself. The resulting ratio of c_2/c_1 agrees with the value fixed by fitting μ_1 with a relative error of about 10^{-4}. The second ratio agrees to 10^{-2}. Here μ_2 proves unreliable for fitting purposes, so instead we use the results from μ_1, but adjust $(c_3 - 1)/c_1$ to c_3/c_1 based on the value of c_1 obtained from *Nu*.

As may be clear, the 3-α results are the most tentatively established of this study. Indeed, given the two independent exponents and three coefficients of (6.3), unconfined as yet by any analysis, it is only to be expected that any smooth curve such as *Nu*(*Ra*) can be fit with high fidelity, but with little ability meaningfully to discriminate among candidate exponent pairs. For our purpose, however, it is not the minimization of least-square error *per se* (which error tends anyway to be a shallow minimum insofar as exponents are concerned) but rather the distribution of the error that advantages one fit over another. When *Nu* is fitted with functions unrelated to the terms in its asymptotic expansion, the resulting error curve is of a nature generic to any least-squares fit. The proper asymptotic fit has in comparison an error that is distinctly one-sided. Unfortunately, this is not a unique prescription given data of moderate precision, computed over a limited range and thus (6.3) remains provisional in nature, not definitive. Using μ_1 in lieu of *Nu* provides relatively greater selectivity for the exponents. In figure 15(*b*) we fix the first exponent, $\mu = 31/75$, and vary the second by $\pm 1/75$ about 4/15 (in each case optimizing the remaining coefficients). It will be seen that the middle value is manifestly the distinguished one. It remains, however, that a range of rational $\mu = p/q$ exists in the vicinity of 31/75, among which values the

only heuristic discriminator is a presumption that $p+q$ should be as small as possible (as opposed, e.g. to $\mu = 1025/2478$, which fits μ_1 marginally better). While the choice taken reflects that heuristic, it is not free of subsidiary complication. In particular the behaviour of the largest wavenumber remains less certain. While it is possible that $\alpha_{3,3} \sim cRa^{6/25}$, such a result has, in contrast to the case of 2-α, no transparent relation to the stated form for Nu, although it does suggest $\alpha_{N,N} \sim cRa^{(1-5^{1-N})/4}$, at once rationalizing all three branches explored here and coinciding in the limit of $N \to \infty$ with the conservative result reported in Part 1. Lastly, (6.3) does not exhaust the possible forms one might consider although, among those with only two terms larger than a constant, it appears a distinguished choice. While a form with three terms might well arise, limits on both the accuracy of the data and the available range in Ra make it unlikely that one can usefully constrain the possibilities without a reasoned argument to confine the class of analytic forms explored, particularly insofar as the appearance of logarithms is concerned.

With this (tentative) identification of μ, we can finally anticipate the rest of the members in the multi-α sequence, namely $Nu \sim cRa^{\mu^{(k)}}$ where

$$\mu^{(k)} = \frac{5}{12}\left(1 - \frac{1}{5^k}\right), \qquad k = 1, 2, \ldots . \tag{6.4}$$

As earlier observed, the optimal solution thus saturates with an exponent of 5/12, the same value found for the conservative model presented in Part 1. Note that the sequence beginning with (3.25) and (6.3) prefigures a general form with progressively less attenuated transient contributions. This is paralleled in the form of the series found by extended Richardson extrapolation to describe the exponent for the conservative model, with terms in that case of $Ra^{k/12}$ for $k = 5, 4, \ldots$. Anticipating such features is crucial to a convincing fit of data of necessity confined to a limited range in Ra.

While the geometric sequence in (6.4) puts infinite-Prandtl-number convection with free-slip boundary conditions in more familiar territory than the novel domain inhabited by no-slip, it is nonetheless decidedly not the territory first identified by Busse. The key element from which much follows is the discovery that α saturates in the 1-α solution. Compounding this anomaly is that the traditional view of how multi-α solutions make successive contributions of $\overline{w_k\theta_k}$ sum to unity is wholly confounded by the free-slip solutions. Both of these features are explored at length in § 7 and the appendices, where we treat the 1- and 2-α solutions. The obscure relation of wavenumber to Nu noted for the 3-α solution hints that even the complications of the 2-α solution, which are considerable, do not completely exhaust the variational possibilities. In this respect too free-slip conditions depart from the Busse scenario, where bifurcations assume a fixed character right from the beginning. Without any data from the 4-α branch, it is a bald assertion, if a reasonable hope based on the experience of no-slip, that the 3-α solution is at last the template for all remaining members in the series. But, as the analysis of the 3-α solution evidently shares little immediate overlap with the antecedent cases, important though its delineation is, we have chosen not to pursue it here.

7. Asymptotic solutions for free-slip

In their paper on convection for arbitrary Prandtl number, Vitanov & Busse (1997) comment that 'the [multi-α] method seems to fail in the case of stress-free boundaries'. The novel character of the balances we explore in this section has some resonance with that remark.

In the discussion to follow, we adopt the normalization given by Chan, namely

$$w \to \langle w\widehat{\theta}\rangle^{-1/2} Ra^{-1/2} w \qquad \text{and} \qquad \widehat{\theta} \to \langle w\widehat{\theta}\rangle^{-1/2} Ra^{1/2}\theta.$$

With this choice† (2.10) becomes

$$F = Nu - 1 = \frac{1 - \dfrac{1}{Ra}\|\nabla\theta\|^2}{\langle(1 - \overline{w\theta})^2\rangle}, \tag{7.1}$$

here maximized subject to $\langle w\theta\rangle = 1$ and (2.2) which, following the variable change above, becomes

$$\nabla^4 w + \nabla_H^2 \theta = 0. \tag{7.2}$$

As before, ∇_H^2 is the horizontal Laplacian, $\langle\cdot\rangle$ denotes a volume average, and $\overline{(\cdot)}$ a horizontal average. Boundary conditions are free-slip, as stated in (2.4).

The associated Euler–Lagrange equations can be simplified (equations 28(a, b) in Chan 1971) to solving the two equations

$$\frac{1}{RaF}\nabla^6\theta + \nabla^4\left[\left(1 - \overline{w\theta} - \frac{\lambda}{F}\right)w\right] + \left(1 - \overline{w\theta} - \frac{\lambda}{F}\right)\nabla^4 w = 0, \tag{7.3}$$

$$\nabla^4 w + \nabla_H^2\theta = 0, \tag{7.4}$$

where

$$\lambda = \frac{1}{2Ra}\|\nabla\theta\|^2 - 1. \tag{7.5}$$

To recover the balance parameter as given at (3.7), the present definition for λ has to be rescaled as $\lambda \to -2\lambda$.

Owing to the special form of the nonlinearity in equation (7.3), multi-α solutions (Busse 1969*b*, 1970) can be sought of the form

$$[\,w(\boldsymbol{x}), \theta(\boldsymbol{x})\,] = \sum_{n=1}^{N} [\,w_n(z), \theta_n(z)\,]\phi_n(x, y), \tag{7.6}$$

where $\nabla_H^2\phi_n = -\alpha_n^2\phi_n$ and $\overline{\phi_n\phi_m} = \delta_{mn}$ (the Kronecker delta function). Again without loss of generality, isotropy in the (x, y)-plane permits the choice

$$\phi_n = \sqrt{2}\cos\alpha_n x. \tag{7.7}$$

(We adopt the prefactor of $\sqrt{2}$ for convenience in what follows.)

The equations are still too difficult to solve exactly but we present here an asymptotic solution for $N = 1$, valid as $Ra \to \infty$. We address $N = 2$ in Appendix D.

7.1. *The* 1-α *solution*

We look for a solution to maximizing F using the single-wavenumber ansatz

$$[\,w(\boldsymbol{x}), \theta(\boldsymbol{x})\,] = \sqrt{2}\,[\,w_1(z), \theta_1(z)\,]\cos\alpha_1 x. \tag{7.8}$$

Numerical evidence suggests that α_1 remains $O(1)$ as $Ra \to \infty$. This motivates the pursuit of an asymptotic solution arranged into two regions: a boundary layer of size

† Because of notational needs for the boundary layers discussed here, the caret on θ, used previously to denote a zero-mean field, is reserved as a marker for boundary layer structure. This conforms to Chan's original notation.

$O(\delta)$ where $\partial/\partial z = O(1/\delta) \gg \alpha_1$, and the interior where $\partial/\partial z = O(\alpha_1) = O(1)$. This assumption differs considerably from the 'usual' multi-α ansatz (Busse 1969*b*, 1970; Chan 1971; Kerswell 1996; Kerswell & Soward 1996; Kerswell 2002), where α_1 scales as an increasing function of Ra so that there are naturally three layers: an inner layer where $\partial/\partial z = O(1/\delta) \gg \alpha_1$, an intermediate layer where $\partial/\partial z = O(\alpha_1) \gg 1$, and an interior where $\alpha_1 \gg \partial/\partial z = O(1)$.

The most evident characteristic of the 1-α numerical solution is that $\overline{w\theta}$ is graphically indistinguishable from unity except near the boundaries, where it must vanish. This behaviour acts to minimize the denominator of (7.1) and thus to maximize F.

In seeking a solution we assume symmetry about the layer midplane $z = 1/2$ and focus our attention on the domain $z \in [0, 1/2]$. Defining a boundary layer variable $\zeta = z/\delta$ and an interior variable $\xi = \alpha_1 z$, we define boundary layer functions

$$\widehat{w}(z) = w/(c_1\delta), \quad \widehat{\theta}(z) = c_1\delta\,\theta, \tag{7.9}$$

where c_1 is a free scalar, and interior functions

$$\tilde{w}(z) = \alpha_1 w, \quad \tilde{\theta}(z) = \theta/\alpha_1. \tag{7.10}$$

In both cases the scalings are chosen to ensure $\widehat{w}\widehat{\theta} = \tilde{w}\tilde{\theta} = O(1)$ (and subscripts for w and θ have been suppressed). At leading order, the equations (7.3) and (7.4) become

$$\tilde{w}\,\tilde{\theta} = 1, \qquad \left(\frac{\mathrm{d}^2}{\mathrm{d}\xi^2} - 1\right)^2 \tilde{w} = \tilde{\theta}, \tag{7.11}$$

in the interior and

$$\widehat{\theta}^{(VI)} + \left[\left(1 - \overline{\widehat{w}\widehat{\theta}}\right)\widehat{w}\right]^{(IV)} = 0, \qquad \widehat{w}^{(IV)} = 0, \tag{7.12}$$

in the boundary layer, where the thickness δ is chosen as $(c_1^2 RaF)^{-1/4}$ to give a coefficient of unity for $\widehat{\theta}^{(VI)}$ (the superscripts indicate the number of ζ derivatives). We now proceed by solving the interior problem

$$\tilde{w}\left(\frac{\mathrm{d}^2}{\mathrm{d}\xi^2} - 1\right)^2 \tilde{w} = 1, \tag{7.13}$$

subject to the two symmetry conditions at the midplane, $\tilde{w}'(\alpha_1/2) = \tilde{w}'''(\alpha_1/2) = 0$ (the prime denotes a derivative with respect to ξ) and two boundary conditions at the wall. The latter are determined by the requirement of matching to the inner solution $\widehat{w}$. From (7.12), $\widehat{w}$ is a cubic polynomial in ζ. The boundary conditions (2.4) disallow both a constant and quadratic term and hence $\widehat{w}$ is restricted to linear and cubic terms. But if the linear term is present, then a cubic term cannot simultaneously be matched with the outer solution $\tilde{w}$ at leading order, hence we need only consider the simplest possible solution, namely $\widehat{w} = \zeta$ (where the constant of proportionality is set to unity by a suitable choice of the parameter c_1). That is, we need $\tilde{w} \sim c_1\xi$ as $\xi \to 0$ and hence the interior equation (7.13) is to be solved subject to $\tilde{w}(0) = 0$. This alone assures a suitable match insofar as c_1 is concerned. Here we simply assert that the appropriate second condition is $\tilde{w}''(0) = 0$, reserving a justification of that statement to Appendices B and C.

The resulting problem is a delicate one owing to the singularity of $\tilde{w}^{(IV)}$ at $\xi = 0$: hence we provide a complete characterization of the solution in (B 2). The conclusion is that a solution $\tilde{w}(\xi, \alpha_1)$ exists which importantly defines $c_1(\alpha_1) = \tilde{w}'(0, \alpha_1)$. At this point, $\tilde{w}$ and $\tilde{\theta} = 1/\tilde{w}$ are known up to the value of α_1, which is determined at the

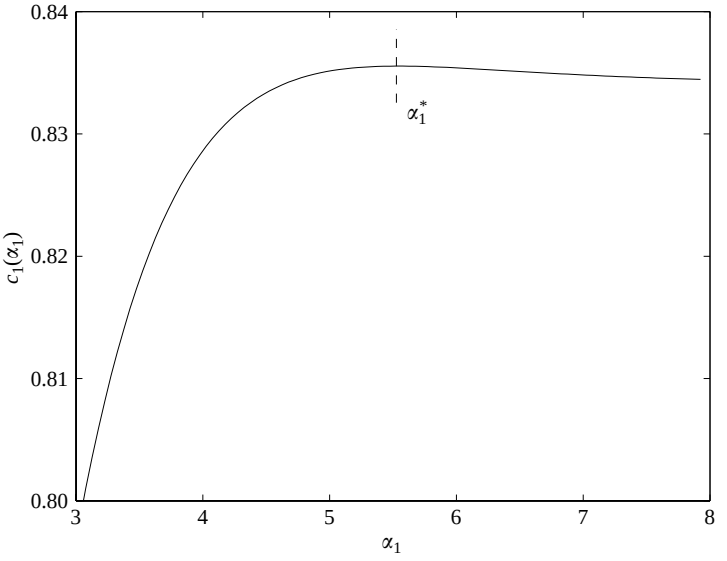

FIGURE 16. Dependence of the slope c_1 at the origin on α_1, showing that a maximum is reached at a finite wavenumber, α_1^*.

very end of the analysis. What remains before this is to calculate $\widehat{\theta}$. Knowing $\widehat{w} = \zeta$, the equation for θ can be rewritten as

$$\widehat{\theta}^{(VI)} + \left[(1 - \zeta\widehat{\theta})\zeta\right]^{(IV)} = 0, \tag{7.14}$$

to be solved subject to $\widehat{\theta}(0) = 0$. The four solutions of (7.14) that satisfy this boundary condition and also behave algebraically as $\zeta \to \infty$ are given in (A 5). Knowing that $\widehat{w} = \zeta$, the solution for which $\widehat{\theta} \sim 1/\zeta$ asymptotically is selected, namely

$$\widehat{\theta} = \sqrt{\frac{\pi\zeta}{8}}\,\Gamma(3/4)\left[I_{1/4}(\zeta^2/2) - L_{1/4}(\zeta^2/2)\right], \tag{7.15}$$

where I_ν is the modified Bessel function and L_ν is the modified Struve function. Now the value of F can be calculated to leading order

$$F = \frac{1 - \dfrac{1}{Ra}\|\nabla\theta\|^2}{\langle(1 - \overline{w\theta})^2\rangle} \approx \frac{1 - I/(Ra\,c_1^2\delta^3)}{\delta J} = \frac{c_1^{2/3}(\alpha_1)}{(4\,I)^{4/3}}Ra^{1/3}, \tag{7.16}$$

where

$$I = 2\int_0^\infty \widehat{\theta}'^2\,\mathrm{d}\zeta \approx 0.53091206824548,$$
$$J = 2\int_0^\infty (1 - \zeta\widehat{\theta})^2\,\mathrm{d}\zeta = 3I \approx 1.59273620473644,$$

and the final expression for F in (7.16) is obtained following substitution for δ in the intermediate expression and a little algebra. Finally, the last expression for F is maximized over α_1, which corresponds to maximizing c_1, the slope at the origin. Again, this is the point of departure from all previous examples: the slope is not a monotone function of α_1; as seen in figure 16 it overshoots $c_1(\infty)$ by a few percent, approaching

its asymptotic limit from above. The maximum occurs for $\alpha_1^* = 5.5377856128012329$, which confirms the initial ansatz that α_1 saturates at a value of $O(1)$, and predicts that $c_1(\alpha_1^*) = 0.8355433652593106$. Substituting the values indicated, the predicted asymptotic bound is then

$$F_{max} \sim 0.32498941162098\, Ra^{1/3} \qquad \text{as } Ra \to \infty. \tag{7.17}$$

As noted in the Appendix, (C 7) provides an explicit correction term of order $Ra^{-1/3}\log Ra$ (with a subdominant contribution of order $Ra^{-1/3}$). Figure 11 in § 6.1 is seen to confirm all of these details.

Finally, the Vitanov (1998) 1-α prediction that $Nu \sim 0.3254 Ra^{1/3}$ lies remarkably close to the leading-order result for F given above and yet he assumes $\alpha_1 \to \infty$ as $Ra \to \infty$, in keeping with other upper bound problems. One sees on reflection that the close correspondence is attributable to the marginal overshoot illustrated in figure 16, with the result that $c_1(\alpha_1^*)$ differs only slightly from $c_1(\infty) = 0.834210$. The inconsistency in Vitanov's analysis is that he has selectively to include higher-order terms, otherwise α_1 is undetermined. (It is clear from his figure 4 that the numerical results up to $Ra = 10^7$ are more consistent with α_1 remaining $O(1)$ than that $\alpha_1 \sim Ra^{1/6}$ as $Ra \to \infty$.)

We believe that the results of this section, in conjunction with the free-slip portions of Appendices A–C, constitute the first complete asymptotic analysis of *any* 1-α upper bound solution in the sense of a fully consistent match. The purpose of this development is to support the general hypothesis in § 8, where we shall argue that the entire fate of the multi-α sequence is determined by the possibility of a match of the 1-α boundary layer to the interior. For this reason, that the match is obtained for free-slip needs to be established beyond any possible doubt.

7.2. *Generalization from the* 1-α *solution*

The novel nonlinear balance above, with α_1 tending to a constant, presages an equally intricate balance for succeeding multi-α solutions. We do not yet have a satisfactory understanding of the general case but do present a largely complete theory in Appendix D for the case of 2-α. The key result is depicted in figure 17. In striking contrast to all known examples of multi-α solutions, the vertical flux in the innermost layer, $\overline{w_2\theta_2}$ (notation as in (7.8)), rises rapidly from zero but then fails to saturate in the adjacent overlap region. Rather, it diverges as $Ra^{1/5}$. The outer layer responds with the same scaling but the opposite sign such that the sum of the two remains $O(1)$.

In concluding this section, we aim briefly to shed further light on the odd circumstance that the wavenumber remains $O(1)$. For that purpose, it is instructive to consider the generalized problem

$$\left.\begin{aligned} (\mathrm{D}^2-1)^2\tilde{w} = \frac{1}{\tilde{w}}, \qquad & \tilde{w}'(\alpha_1/2) = \tilde{w}'''(\alpha_1/2) = 0, \\ \tilde{w}(0) = 0, \qquad & \beta\tilde{w}'(0) + (1-\beta)\tilde{w}''(0) = 0, \end{aligned}\right\} \tag{7.18}$$

regarding $\tilde{w}'(0)$ as a parametric function of β. Free-slip is not singular in having a finite value of α_1 at which the slope at the wall is maximized. Rather, this persists in the mixed boundary condition over a finite range, as one can immediately anticipate from (B 3). Done as a shooting problem, the numerical solution requires extended precision at values of about $\alpha_1 \geqslant 4$, so tracking the result is time-consuming (based on the Taylor series extended precision solver in Maple). Figure 18 shows both α_1^* and the accompanying slope as a function of increasing β over a range where the answers

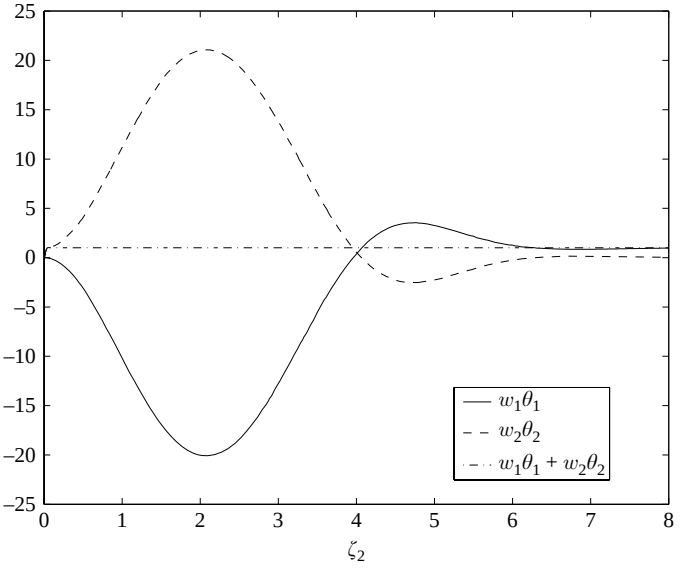

FIGURE 17. Overshoot of $\overline{w\theta}$ (scaling as $Ra^{1/5}$), characteristic of the asymptotic 2-α free-slip solution. For this plot $Ra = 6.09 \times 10^{11}$.

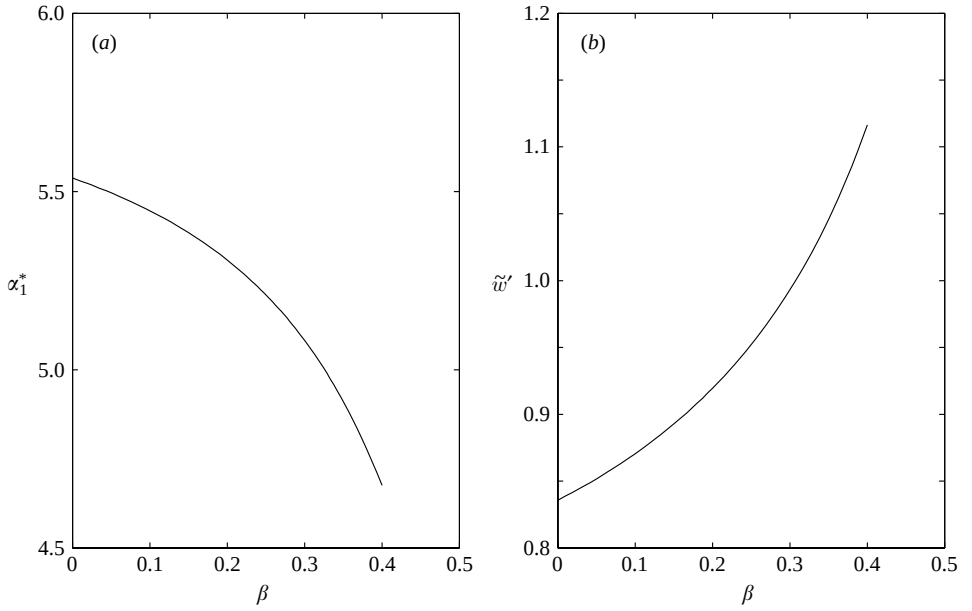

FIGURE 18. Parameters for solution of the generalized problem defined at (7.18)

.

are thought to be accurate to at least ten significant digits. Apart from that we can anticipate continuity of the 1-α solution branch for a finite range of $\beta > 0$, a deeper motivation for presenting this generalization is that we shall find in Appendix D.1 that (7.18) appears again as equation pair (D 12) and (D 15) for the leading-order interior solution of the 2-α problem (though missing a statement of conditions on $\tilde{w}_1(\zeta_1)$

as $\zeta_1 \to 0$). Recurrence of (7.18) follows on the observation that the accompanying wavenumber, $\alpha_{2,1}$, also tends to a constant, 1.9662, as apparently does $\alpha_{3,1}$, suggesting that (7.18) remains the appropriate interior equation in all cases, solved subject to particular boundary conditions determined by matching at the origin. The relation of continuity in the 1-α solution to successive bifurcations in the N-α family is a point to which we shall return in the conclusion.

While arguments in Appendix D.1 rely on the thesis that $\alpha_{2,1}$ tends to some constant, completing that discussion so as to derive the particular value selected lies well beyond the scope of this paper. However, the general nature of the missing elements can be anticipated by reference to Appendix D, where the needed ingredients for the required match stemming from the inner limit of the outer layer are given.

8. Mixed boundary conditions

For a first synthesis of the two boundary conditions, we look to the comparison of optimal background fields illustrated in figure 19. Because we have not yet determined all the relevant scaling exponents that occur in a leading-order expansion of the free-slip 3-α solution, the boundary layer presentations here are simply scaled by Ra^{μ} with $\mu = 1/3$ for no-slip (the saturated value) and $\mu = 31/75$ for free-slip (the third member in the geometric progression to 1/4). It is reasonable that the structures shown have largely attained their asymptotic character. Each τ exhibits undershoot of a few percent. The striking difference is seen in the outer region (figure 19*c*). Here the no-slip undershoot leaves a negligible residue; the recovery to $\tau = 1/2$ takes place almost entirely in a boundary layer. By contrast, for free-slip only about one-third of that recovery takes place in the boundary layer, the remaining two-thirds gives rise to a roughly linear interior profile of τ with slope of about 1/10. From this distinction we see why the background field in Part 1 – allowing for a residual interior slope – yields the correct scaling for free-slip but fails for no-slip. The disparity in interiors ultimately derives from the fact that matching is possible with (B 2) (as shown at length in Appendix C) but not with (B 4), where subdominant terms are required to effect the match (hence the exponential, rather than algebraic, recovery in the no-slip τ). From this understanding of the relevant makeup of τ, one can hope to craft a still more refined version of the recent arguments by Doering *et al.* (2005) in order to provide a rigorous justification of the exponents advanced here on the basis of numerical and asymptotic reasoning.

The unifying synthesis hence is this: the essence of the upper bound solution for infinite Prandtl number is that (B 2) is a regular limit of the general solution of (7.18), while (B 4) is not. We argue that the subsidiary multi-α structure is completely controlled by this classification of the 1-α solution in all upper bound problems. We further propose that a geometric progression (as e.g. in the well-documented case of plane Couette flow) occurs if, and only if, the 1-α solution for the midlayer is continuable to adjacent boundary conditions via

$$\beta w'(0) + (1-\beta) w''(0) = 0 \tag{8.1}$$

as a regular perturbation. This is assured whenever the leading-order midlayer equation is linear, barring the unlikely case of a regular or irregular singular point at the wall. An immediate consequence is that the 2-α and successor branches for the no-slip solution cannot follow the exponent sequence given in equation (93) of Chan (1971). This is consistent with figure 8, which clearly illustrates the departure from the boundary conditions singularly associated with (B 4). But that the solution

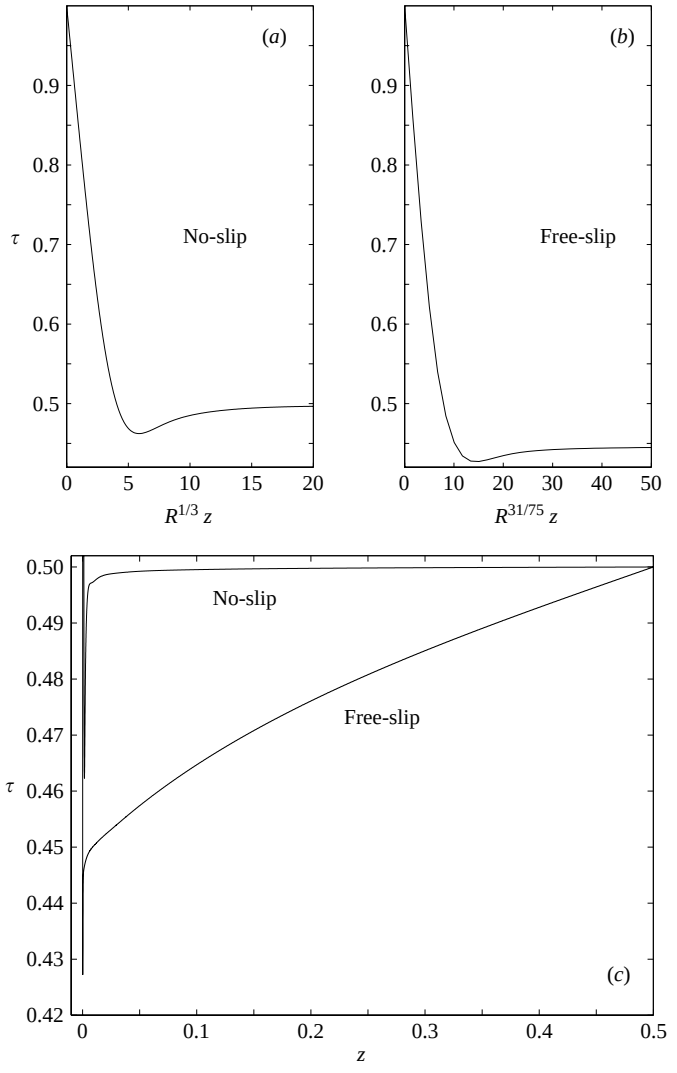

FIGURE 19. Comparison of the optimal background field, τ, for no-slip and free-slip boundary conditions. The no-slip result is a 4-α solution at $Ra = 4.59 \times 10^{10}$. The free-slip is a 3-α solution at $Ra = 8.13 \times 10^{11}$.

instead saturates at the particular limiting exponent of 1/3, and does so coincident with the 3-α bifurcation, has of course to derive from subsequent considerations.

Similarly, that in reaching $Nu < c\,Ra^{5/12}$, the free-slip branches have a smallest wavenumber that saturates at a finite value and a divergent $\overline{w_k\theta_k}$ product (for 2-α and above), rests on an intricate structure that we have elucidated only in the case of 1- and 2-α (and even then with certain lacunæ for the latter). While the continued saturation is a natural enough corollary of the postulate on regularity, the divergence is surely not.

Notwithstanding that significant features of the multi-α solutions transcend a complete characterization of the 1-α solution space for the generalized boundary condition (8.1), we can begin to collect the seemingly disparate results from table 1 into a more coherent pattern following the further observation that (8.1) refers to the midlayer solution. The combination of mixed-order derivatives means that the form

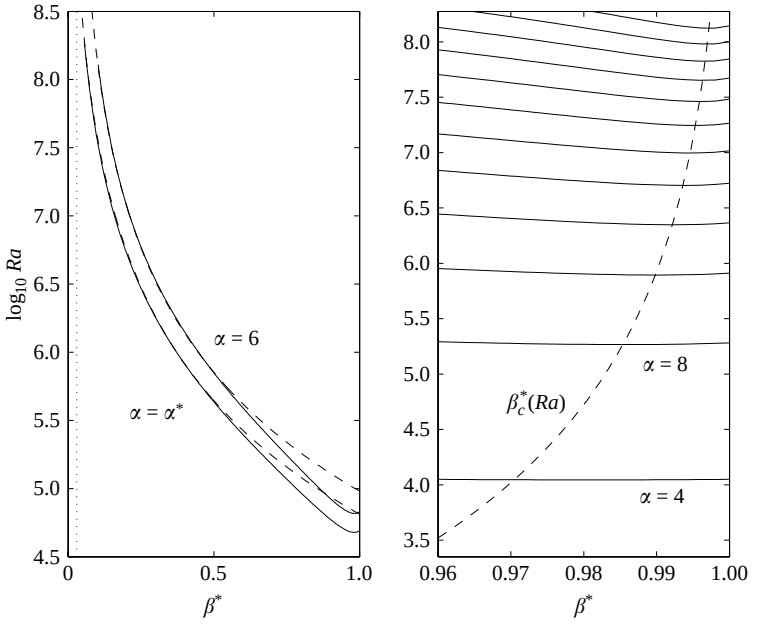

FIGURE 20. The transition from free-slip to no-slip behaviour.

in general changes if referred to either interior or wall-layer coordinates, introducing a dependence on Ra. For this purpose we introduce the variable β^* to discuss possible domains of interest with reference to the mixed boundary condition, as applied to w in (3.2)–(3.5) (and presuming, by the extension of 'natural boundary conditions', the same is applied to q).

Numerical experiments with the mixed condition (cf. (E 4)) lead us to the simple two-part characterization depicted in figure 20. The first distinguishing feature of contours of constant α is confined to a boundary layer in the vicinity of $\beta^* = 1$. This is the locus of points satisfying the condition $\partial\alpha(\beta^*, Ra)/\partial\beta^* = 0$, graphically indicated by the dashed curve, $\beta_c^*(Ra)$, plotted in figure 20(b), and which is well fitted by

$$\beta_c^* \sim 1 - 0.3033 Ra^{-1/4}. \tag{8.2}$$

(Given the 1-α no-slip result that $\alpha \sim Ra^{1/4}$, the form attained by β_c^* can hardly be put down to coincidence.)

We observe that this curve serves at least qualitatively to define a border between regions we shall term generalized free-slip and no-slip. More precisely, a 1-α computation carried out along the curve $\beta^* = 1 - cRa^{-3/10}$ gives ample evidence of a limit in which the controlling factor of Nu is $Ra^{3/10}$ (for any c), whereas $\beta^* = 1 - cRa^{-1/10}$ yields the limit $Nu < c\,Ra^{1/3}$. We propose that the exponent 1/4 is the critical value dividing the (β^*, Ra)-plane into the two regions. While the limits become numerically more delicate to confirm, computations along $\beta_c^* \equiv 1 - cRa^{-1/4\pm\epsilon}$ for $\epsilon \to 0$ are thus predicted to give the free-slip or no-slip scaling for ϵ positive or negative respectively. A deductive basis for (8.2) is desirable, though far from apparent. In view of the considerable complications of the no-slip solution, particularly the considerations in Appendix C.2, an approach to breakdown at β_c^* coming from the free-slip side may be more feasible. A suggestion of the form such a breakdown might take is the parametric failure of a match paralleling that between the outer limit of the inner solution, given in (C 4), with the inner limit of the outer solution in (C 5).

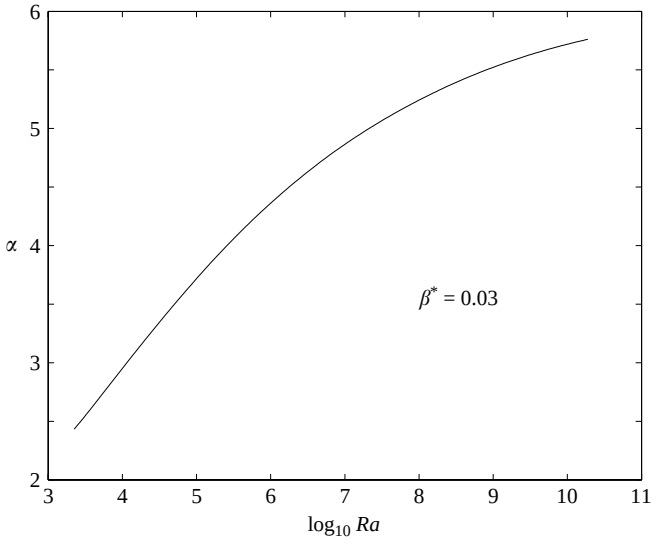

FIGURE 21. Saturation of the wavenumber for generalized free-slip.

To speak of generalized free-slip, however, we must also address the behaviour of α itself. This is the second part of the characterization remarked on above. We have already seen evidence in figure 18 that the solutions of the midlayer equation attaining maximum slope $w'(0)$ for finite α continue over a finite range in β (again, referred to midlayer coordinates). In figure 20(a), we plot two contours of constant α from the full 1-α solution: the first at the value $\alpha = \alpha^* = 5.5377856128012329$ (i.e. the saturation value for free-slip), the second at $\alpha = 6$. Evidently the first contour acts as a separatrix, with all contours for $\alpha < \alpha^*$ that commence at $\beta^* = 1$ on the right intersecting the vertical line $\beta^* = 0$, and the α^* contour itself tangent to that axis as $Ra \to \infty$. The data on that contour are consistent with a power law, $\beta^*(\alpha^*, Ra) \sim c_1 Ra^{-0.36}$, the extension of which is plotted as a dashed line. Arguing that the curve for $\beta^*(\alpha = 6, Ra)$ must obey an asymptotic relation with the same power of Ra, a consistent fit requires that we introduce a second constant, thus $\beta^*(\alpha, Ra) = c_0(\alpha) + c_1(\alpha) Ra^{-0.36}$. In this instance we find $c_0 \approx 0.03$. We can test this proposal by doing a computation at fixed $\beta^* = 0.03$ to see if indeed $\alpha \to 6$ as $Ra \to \infty$, along the dotted line in figure 20(a).

Figure 21, carried about two decades further in Ra than the data used from figure 20 to extract c_0, is in reasonable accord with that prediction. The choice of $\alpha = 6$ is principally in order that a plausibly demonstrated limit in Ra is obtained quickly enough to require little computation, but otherwise arbitrary and thus entirely representative. All contours, that is, with $\alpha \geqslant \alpha^*$ emerge from $\beta^* = 1$, drop to a minimum at β_c^*, and then turn upward, eventually becoming vertical. The asymptotic expression of this is contained in the coefficient function we have denoted by $c_0(\alpha)$, and whose inverse $\alpha = c_0^{-1}(\beta^*)$ succinctly expresses the second defining feature of generalized free-slip: that α tends to a constant as $Ra \to \infty$. Thus $c_0^{-1}(0) = 5.53...$ and $\lim_{\beta^* \to 1} c_0^{-1} \to \infty$, with c_0^{-1} a monotone increasing function.

All of the numerical results described thus far refer to 1-α solutions. Recall, however, that the initial hypothesis is a stronger one. We suggest the same division into generalized free-slip and no-slip applies to the multi-α solutions, also as demarcated by β_c^*, and with the significant codicil that multi-α solutions defined over a finite region of β^* as $Ra \to \infty$ will always approach their N-α limit as a geometric series.

In this view the no-slip condition ought to coincide with the result established in Part 1 of $Nu < c\,Ra^{7/20}$, and would do so as a conventional geometric progression, were it not that exact no-slip is singular in the manner illustrated at such length in Appendix B.†

Although couched in too specific a language of boundary-layer theory to illuminate the most general basis for the singular classification of upper bound problems, this picture nonetheless offers an appealing unified view of all the results reported. It suggests the origin of the peculiar gap between the conservative no-slip bound from Part 1 and the result found here of $Nu < 0.139\,Ra^{1/3}$ (although it does not immediately suggest how better to pose the conservative model). Also, it possibly sheds light on Constantin & Doering (1999) (and its successors), which established a no-slip bound of $Nu < c\,Ra^{1/3}(\log Ra)^{2/3}$ by making use of an additional, pointwise, logarithmic bound for the second derivative of the vertical velocity. That estimate uses classical methods in functional analysis for singular operators of so-called Calderon–Zygmund type. The nature of the arguments to establish the bound depart considerably from the CDH method in that the relevant quadratic form is no longer positive semidefinite, so it is not self-evident that – in spite of enforcing more constraints – the estimate so obtained must of necessity yield a tighter bound. It might be better viewed as a bound relative to 7/20, on which it does improve, recognizing that the exact no-slip bound with exponent of 1/3 rests in an essential way on the singular nature of the $\beta^* \to 1$ limit, which the rigorous estimates used in Constantin & Doering (1999), Yan (2004), and Doering *et al.* (2005) in no way reflect.

At the same time, the fundamental observation here of $\beta^* = 1$ representing a singular limit must not be thought unambiguously to represent some essential physical aspect of infinite-Prandtl-number convection. As repeatedly emphasized in Ierley & Worthing (2001), determining when a given set of constraints is 'congruent', i.e. leads to a smooth variational solution, does not relate in any simple way to the smooth or non-smooth behaviour of even substantially similar sets; each set is thus *sui generis*. There is hence no basis on which to argue that the two particular integral constraints used here enjoy a privileged role in the physics of convection. Far from it. Given some other, congruent, collection of constraints applied to infinite-Prandtl-number convection, a geometric series is more than likely to be obtained for no-slip, implying a different form for the equivalent $\beta_c^*(Ra)$ as well.

Naturally if additional constraints are used for no-slip then, however achieved, the resulting bounds certainly cannot exceed the present superconvergent 3-α solution. That is, a more tightly constrained problem must satisfy $Nu \leqslant 0.139 Ra^{1/3}$ on all its SC-neutral branches. We might in consequence expect such added constraints will be found to alter only the prefactor, although a reduction below 1/3 cannot rigorously be excluded. Nonetheless, additional constraints for free-slip would seem the more likely candidate for exponent reduction. Pertinent to that possibility, Jimenez & Zufiria (1987) give an estimate of $Nu \sim 0.21\,Ra^{1/3}$ for an exact solution of the equations with free-slip boundary conditions, after maximizing heat flux over the wavenumber of the solution (which estimate is numerically confirmed in Ierley & Worthing (2001)). This constitutes a firm lower bound on range of improvement for free-slip.

† Because of its relative simplicity, a survey of the influence of (8.1) on the conservative bound is probably an instructive point of comparison. As $\alpha \sim Ra^{1/4}$ for both boundary conditions, one does not expect a necessary coincidence of β_c^* for the conservative model with the one defined above although, for consistency, the conservative border cannot lie further to the left.

9. Conclusions

Conditioned, perhaps, by the (growing) number of elegant upper bounds for various flows, a view that turbulence itself must also be 'nice' in some asymptotic sense occasionally asserts itself. In justifying the relevance of variational bounds, various writers have thus often appealed to the idea that the optimizing fields themselves may have a suggestive and immediate physical relation to the realized flows, though variational calculus is notorious for inducing pathologies.

But the 1-α basis of classification proposed here aside, there is very little else about ensuing details of even the variational problem for infinite-Prandtl-number convection that could merit the term 'nice'; moreover the divergence of $w_k\theta_k$ for free-slip (or near-slip) boundary conditions is far more suggestive of a wholly variationally induced peculiarity than some physical mode of instability.

Howard (1972) proposes a pragmatic, frankly utilitarian, view of bounds on flow quantities:

> One sometimes gets the impression, especially from reading general books about physics, that many people regard a variational formulation as an essential component of a true and deep understanding of the fundamental character of almost anything. This idealistic but rather narrow-minded attitude, a bit akin to the once-popular view that planetary orbits must obviously be circles, probably limits scientific progress somewhat, but when variational relationships are present or can be introduced it is prudent to be aware of the fact and look for ways in which they can be put to use.

Such a measured view better describes the aim of this work and also the nature of its findings. One must speak carefully of what physical significance, if any, can ultimately be said to attach to this study. A circumspect statement is simply that the no-slip boundary condition is more sensitive to the $\sigma \to \infty$ limit than is free-slip. In what respects this tentative distinction is mirrored by realized turbulent flows in the same limit, and for very large Ra, remains very much an open question, than which few could be of greater interest.

Such guarded optimism notwithstanding, within the field of upper bound theory proper it is remarkable that a problem long the subject of intense study should yet continue to turn up major surprises. Surely the central one, and the signal advance of this work, is the identification of singularity as a departure from the canonical N-α geometric series and a tentative understanding of the underlying cause on which that distinction turns. But the results established here for free-slip must also figure as a principal contribution since, pivotal though the geometric series is, it rests on the more solidly grounded expectation commencing with Busse (1969*b*) (and most generally elaborated in Kerswell (2002)) that maximization of flow quantities proceeds from an interweaving of contributions from successive wavenumbers such that $\overline{w\theta}$ (or equivalent) rises to a constant immediately outside the innermost layer. But universally the manner in which that has to date been demonstrated has the variables in question remaining order one. The free-slip divergence exhibited here, no less than the singularity of no-slip, derives from what we can now see as the defining property of infinite-Prandtl-number convection regarded as an upper bound problem based on the power integrals: the nonlinearity of (7.18), the leading-order interior expansion of the Euler–Lagrange equation for w.

It is a pleasure for G. R. I. to note the many happy months spent on sabbatical as a visitor to the Mathematics Department of the University of Bristol, whose staff and students were uniformly and unfailingly gracious in their hospitality. He is also happy to acknowledge the generous funding received from EPSRC grant GR/S02204/01 in

support of that visit. R. R. K. gratefully acknowledges the EPSRC for its support of his participation in this work under grant GR/A92613/01.

Development of some of the key material in the appendices on asymptotic expansions for higher-order matching benefited greatly from discussion with Professor Otto Ruehr of the Michigan Technological University. In particular he generously contributed the analysis of the ${}_pF_q$ expansion (C 26) for the case of no-slip, where the exact constants in (C 28) are exceptionally difficult to derive. Having his example greatly facilitated finding the equivalent, easier, result for free-slip in (C 4).

We wish to thank Charlie Doering and Lou Howard for stimulating conversations during the summer GFD program at Woods Hole in 2002, which encouraged us to undertake the present exploration. We also wish to thank the anonymous reviewers of this paper, whose remarks encouraged both some key rearrangements in the interest of clarity and the helpful addition of figure 19.

Appendix A. Summary of the 1-α boundary layer expansion

A.1. *Slip*

The leading-order equation for the free-slip wall-layer is given by

$$\widehat{\theta}^{(VI)} + [(1-\zeta\widehat{\theta})\zeta]^{(IV)} = 0. \tag{A 1}$$

There are four solutions consistent both with the boundary condition at the origin and algebraic behaviour at infinity. These are

$$\widehat{\theta}^{(1)} = \zeta, \tag{A 2}$$

$$\widehat{\theta}^{(2)} = 1 + \frac{\Gamma(3/4)}{\sqrt{2}}\left[\sqrt{\zeta}\, I_{1/4}(\zeta^2/2) - \frac{1}{\zeta^{3/2}}\left(3I_{3/4}(\zeta^2/2) + \zeta^2 I_{7/4}(\zeta^2/2)\right)\right], \tag{A 3}$$

$$\widehat{\theta}^{(3)} = \Gamma(3/4)\sqrt{\frac{\pi\zeta}{8}}\left(I_{1/4}(\zeta^2/2) - L_{1/4}(\zeta^2/2)\right), \tag{A 4}$$

$$\widehat{\theta}^{(4)} = \frac{\pi^{3/2}}{4\Gamma(3/4)}\left[\sqrt{\zeta}\, I_{1/4}(\zeta^2/2) - \frac{3}{\zeta^{3/2}} L_{3/4}(\zeta^2/2) - \sqrt{\zeta}\, L_{7/4}(\zeta^2/2)\right] - \frac{\zeta^2}{5}. \tag{A 5}$$

The respective asymptotic behaviours of these, found from the equivalent integral representations, are given by

$$\widehat{\theta}^{(1)} \sim \zeta, \qquad \widehat{\theta}^{(2)} \sim 1, \qquad \widehat{\theta}^{(3)} \sim \frac{1}{\zeta}, \qquad \widehat{\theta}^{(4)} \sim \frac{1}{\zeta^2}.$$

The appropriate solution of (7.15) (and equation (23) in Vitanov 1998) is $\widehat{\theta}^{(3)}$. In its representation in (A 4), I_ν is the modified Bessel function, and L_ν is the modified Struve function. To facilitate computation of the integrals I and J arising for the 1-α solution, we note that the full asymptotic expansion of $\widehat{\theta}^{(3)}$ is

$$\widehat{\theta}^{(3)} \sim \sum_{n=0}^{\infty} \frac{16^n \Gamma(n+1/2)\,\Gamma(n+1/4)\,\Gamma(3/4)}{\sqrt{2}\pi^{3/2}\zeta^{4n+1}} = \frac{1}{\zeta} + \frac{2}{\zeta^5} + \frac{60}{\zeta^9} + \frac{5400}{\zeta^{13}} + \ldots. \tag{A 6}$$

A.2. *No-slip*

The leading-order equation for the no-slip wall layer is given by

$$\widehat{\theta}^{(VI)} + [(1-\zeta^2\widehat{\theta})\zeta^2]^{(IV)} = 0. \tag{A 7}$$

In this case there are five solutions compatible with the boundary conditions at the wall:

$$\widehat{\theta}_0 = \sqrt{\zeta} I_{1/6}(\zeta^3/3), \tag{A 8}$$

$$\widehat{\theta}_1 = \zeta^5 {}_1F_2([1], [11/6, 5/3]; \zeta^6/36), \tag{A 9}$$

$$\widehat{\theta}_2 = 9\Gamma(2/3)\zeta^3 + 83^{1/3}2^{5/6}\pi^{3/2}\zeta^{-5/2}\left[L_{5/6}(\zeta^3/3) + \zeta^3 L_{11/6}(\zeta^3/3)\right], \tag{A 10}$$

$$\widehat{\theta}_3 = \sqrt{\zeta} L_{1/6}(\zeta^3/3), \tag{A 11}$$

$$\widehat{\theta}_4 = \zeta^2 {}_1F_2([1], [7/6, 4/3]; \zeta^6/36), \tag{A 12}$$

but each diverges exponentially. From this set we form the four differences $\widehat{\theta}^{(k)} = \widehat{\theta}_0 - \phi_k \widehat{\theta}_k$ for $k = 1 \ldots 4$ with a suitable choice of ϕ_k. The resulting difference functions have, in order, an asymptotic limit of ζ^{1-k}.

Note that $\widehat{\theta}^{(3)} = \widehat{\theta}_0 - \widehat{\theta}_3$ is the choice that occurs in the 1-α problem analysed by Chan (it emerges that $\phi_3 = 1$). The exact solution thus assumes the form

$$\widehat{\theta}^{(3)} = \frac{\sqrt{\pi\zeta}}{6^{5/6}}\Gamma\left(\frac{2}{3}\right)\left[I_{1/6}(\zeta^3/3) - L_{1/6}(\zeta^3/3)\right]$$
$$\sim \sum_{n=0}^{\infty} \frac{\Gamma(n+1/2)\,\Gamma(n+1/3)\,\sqrt{3}\,\Gamma(2/3)\,36^n}{2\,\pi^{3/2}\,\zeta^{6n+2}} = \frac{1}{\zeta^2} + \frac{6}{\zeta^8} + \frac{432}{\zeta^{14}} + \ldots \tag{A 13}$$

and the relevant integral in the computation of F is given to higher accuracy as

$$I = \langle(\widehat{\theta}^{(3)'})^2\rangle + \langle(1 - \widehat{w}_1\widehat{\theta}^{(3)})^2\rangle = 1.1106455446632808.$$

(The notation of I follows Chan's usage.)

A.3. *On the numerical determination of free-slip boundary layer scalings*

Diagnosis of numerical results for this problem always pivots about the innermost layer. In most cases w in this region takes the form $c_1\zeta^k$, where $k = 1$ for free-slip boundaries and $k = 2$ for no-slip, but the arbitrariness in c_1 does not permit one to ascribe a unique relation as a function of Ra between z, the exterior coordinate, and ζ the boundary layer variable. Rather one looks to θ, whose governing equation, for the free-slip w, assumes the form (A 7).

As observed, this equation has four admissible solutions, $\theta^{(k)}(\zeta)$. The computed solution for the relevant exact θ invariably reaches a maximum near the wall. So too does each of the four admissible solutions. What is desired is an algorithm both for uniquely determining the boundary layer scale as a function of Ra and also for fixing the amplitude dependence. In general we do not wish, contrary to the particular case of the 1-α no-slip solution, simply to integrate the governing equation four times in order to reduce the order of the equation – thus discarding several possible solutions. To do so, we would need to know more about the details of the match to the succeeding layer and we are here instead devising a numerical procedure to approach the diagnosis without prejudice as to the form of the match. Having elucidation of that as the aim of the diagnosis, we proceed as follows.

For a succession of values of Ra, we take the computed θ, locate the point z_m associated with the boundary layer maximum and finally compute $\theta(z_j)$ for $0 \leqslant z_j \leqslant \rho z_m$, where ρ is a suitable value (typically 1.5 or so in order to have a sufficient range past the maximum to distinguish among the various algebraic rates of decay, but also not so far as to intrude into the next layer). We now have a double

fitting procedure, namely to find

$$\min_{\phi_k,\nu} \sum_{j=1}^{J} \left(\theta(z_j) - \sum_{k=1}^{4} \phi_k(Ra)\theta^{(k)}(\nu(Ra)z_j) \right)^2 . \tag{A 14}$$

The result of this minimization provides a unique relation, $\zeta = \nu(Ra)z$, as well as the amplitude dependence for each of the four fundamental solutions. These solutions form a complete set for (A 7) but this observation has to be supplemented by noting that θ is, of course, not a solution of (A 7) because θ itself is an infinite sum of boundary layer terms, only the first of which satisfies the homogeneous form above, though homogeneous solutions recur at higher order also, as needed to satisfy boundary conditions at the origin. On the assumption that inhomogeneous solutions are either higher order than the relevant homogeneous contributions or, if of the same order as one or more of the former, then at least numerically small over the region sampled, this diagnostic procedure is then a fully objective method of determining the constitution of the matched asymptotic expansion, in contrast to various informal methods more typically applied. The stated assumption is verified at (C 18) in the case of application to the 1-α free-slip solution, and observed empirically to hold in the instance of 2-α.

As the computed solution is given in spectral form, we can as easily evaluate it at one point as another. Nonetheless, in practice it is easiest to evaluate it at an equally spaced set of 100–200 values z_j (relative to the location of the maximum, and thus a function of Ra), and then to use cubic spline interpolation on previously stored vectors containing finely tabulated values of the four fundamental solutions in order to compute the variational quantity above over a range of values of ϕ_k and ν in the course of minimization.

Appendix B. Intermediate layer: the leading-order 1-α solution

B.1. *Formal expansions about the origin*

B.1.1. *Slip*

The solution for the fourth-order problem

$$(\mathrm{D}^2 - 1)^2\tilde{w} - 1/\tilde{w} = 0 \tag{B 1}$$

subject to $\tilde{w} = \tilde{w}'' = 0$ at the origin leaves us with the two boundary conditions which impose that the solution is symmetric about the midplane, namely

$$\tilde{w}'(\alpha/2) = \tilde{w}'''(\alpha/2) = 0.$$

This is constructively viewed as a shooting problem, which shows that we require a solution in the vicinity of the origin having two free (shooting) parameters. In the free-slip case, such a solution can be found in a form generalized from that given in Vitanov (1998), specifically

$$\begin{aligned}\tilde{w} = {} & c_1\xi + c_3\xi^3 + c_5^{(1)}(c_1, c_3)\xi^5 + c_7^{(1)}(c_1, c_3)\xi^7 + \ldots \\ & + \left(\frac{\xi^3}{6c_1} + c_5^{(2)}(c_1, c_3)\xi^5 + c_7^{(2)}(c_1, c_3)\xi^7 + \ldots \right) \log\xi \\ & + \left(c_7^{(3)}(c_1, c_3)\xi^7 + \ldots \right) (\log\xi)^2 + O(\xi^9(\log\xi)^3).\end{aligned} \tag{B 2}$$

In the instance that we instead impose $\tilde{w}(0) = 0$ and general values of $\tilde{w}'(0) = c_1$, $\tilde{w}''(0) = c_2$, and $\tilde{w}'''(0) = c_3$, the solution can be written as the sum of (B 2) plus a

contribution (given here explicitly to avoid invoking a yet more general nomenclature for the coefficients) of the form

$$\delta\tilde{w} = c_2\left\{\xi^2 + \left(1 - \frac{1}{4\,{c_1}^2}\right)\frac{\xi^4}{6} + \frac{c_2\,\xi^5}{120\,{c_1}^3} + \left(\frac{1}{2} - \frac{7}{36\,c_1^2} + \frac{c_3}{3\,c_1^3} - \frac{c_2^2}{6\,c_1^4} - \frac{11}{240\,c_1^4}\right)\frac{\xi^6}{60} + \left(\frac{c_2}{9\,c_1^3} - \frac{c_2\,c_3}{2\,c_1^4} + \frac{121\,c_2}{2520\,c_1^5} + \frac{c_2^3}{6\,c_1^5}\right)\frac{\xi^7}{140} + \ldots + \left[\frac{\xi^6}{1280\,c_1^4} - \frac{c_2\,\xi^7}{1680\,c_1^5} + \ldots\right]\log\xi\right\}. \tag{B 3}$$

This generalization allows us easily to accommodate the mixed boundary condition described in the main body of the text, namely $\beta\tilde{w}'(0) + (1-\beta)\tilde{w}''(0) = 0$. In that case we regard $c_2 = c_2(c_1;\beta)$ as a dependent variable and the resulting solution still has the two free variables, $c_{1,3}$, which are chosen to satisfy conditions at the midline. From the form of $\delta\tilde{w}$, the case of $\beta \to 0$ poses no difficulty, for then $c_2 \to 0$ and $\tilde{w}$ smoothly limits to the result given in (B 2). For $\beta \to 1$, however, $c_1 \to 0$ and both the explicit coefficients in (B 3) as well as those in (B 2) diverge. Hence no-slip is a singular limit, with a solution to whose characterization we now turn.

B.1.2. *No-slip*

The no-slip solution is more involved, with a series solution in the form

$$\tilde{w}(\xi) = \sqrt{\log 1/\xi}\sum_{j=1}^{\infty}\xi^{2j}\sum_{k=1}^{\infty}(\log 1/\xi)^{1-k}\sum_{m=1}^{k}c_{j,k,m}(\log\log 1/\xi)^{m-1}. \tag{B 4}$$

For later reference it is useful to observe that the inner limit of this takes the form

$$\sum_{j=1}^{\infty}(\zeta_1 g_1)^{2j}\sum_{k=0}^{\infty}\tilde{c}_{j,k}(\log 1/\zeta_1)^k, \tag{B 5}$$

where the $\tilde{c}_{j,k}$ depend upon $\log 1/g_1$ and the $c_{j,k,m}$. The only solution compatible with no-slip conditions is that for $c_{1,1,1} = 1$ and $c_{1,2,1} = c(\alpha)$, with all other coefficients determined from these values. In other words, only one free matching parameter is available for the limit of $\xi \to \infty$.† Explicit expressions for the first few terms are

$$\tilde{w}(\xi) = \sqrt{\log 1/\xi}\left\{\xi^2\left[1 + \frac{1}{\log 1/\xi}\left[c - \frac{1}{8}\log\log 1/\xi\right] - \frac{1}{128(\log 1/\xi)^2} \times \left[(64c^2 + 32c + 60) - (16c+4)\log\log 1/\xi + (\log\log 1/\xi)^2\right] + \ldots\right] + \xi^4\left[\frac{1}{6} + \frac{1}{48\log 1/\xi}\left[(8c+2) - \log\log 1/\xi\right] + \ldots\right] + \xi^6\left[\frac{1}{120} + \ldots\right]\right\}.$$

As with (B 2), it is merely an exercise in algebra to continue this expansion as far as desired. While the appearance of (B 4) is at first glance forbidding, it is instructive to note that the singular solution of the elementary transcendental equation

$$z = \log(z/\varepsilon)$$

† Actually, $c_{1,1,1} = \pm 1$, but the second solution is simply the negative of the first so there is no loss of generality in confining our attention to $c_{1,1,1} = 1$.

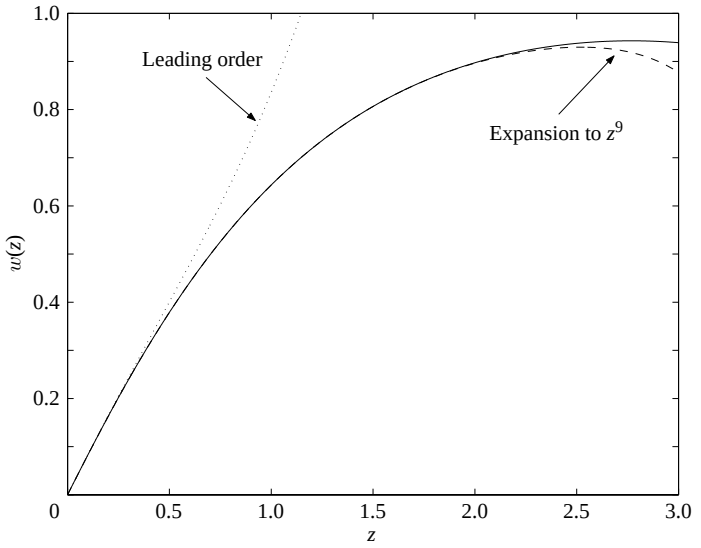

FIGURE 22. Comparison of one- and nine-term truncations of (B 2) to the exact solution.

(the regular solution is the standard Lambert function) is of the form

$$z = \log 1/\varepsilon + \sum_{k=1}^{\infty} (\log 1/\varepsilon)^{1-k} \sum_{m=1}^{k} c_{k,m} (\log\log 1/\varepsilon)^m,$$

$$= \log 1/\varepsilon \left[1 + \frac{\log\log 1/\varepsilon}{\log 1/\varepsilon - 1} + \frac{(\log\log 1/\varepsilon)^2}{2(\log 1/\varepsilon - 1)^3} + \frac{(\log\log 1/\varepsilon)^3 (1 + 2\log 1/\varepsilon)}{6(\log 1/\varepsilon - 1)^5} + \ldots \right],$$

that is to say, of the same basic form as the inner two sums in (B 4) (albeit with elementary $c_{k,m}$, which yield the second line directly).

B.2. *Numerical solution*

B.2.1. *Slip*

We used (B 2) with coefficients determined up to and including ξ^7 to determine the vector $(\tilde{w}, \tilde{w}', \tilde{w}'', \tilde{w}''')$ at a point near the origin from which to begin shooting to $\xi = \alpha_1/2$.† The value of α_1 is varied until the maximum of c_1 is reached (as illustrated in figure 16). From this procedure we find

$$\left.\begin{aligned} \alpha_1 &= 5.5377856128012329, \\ c_1 &= 0.8355433652593106, \\ c_3 &= -0.1640002693966280. \end{aligned}\right\} \tag{B 6}$$

The expansion is corroborated in figure 22, where the series is computed to order ξ^9 and compared to direct numerical solution of the $\tilde{w}$ equation. (The leading-order behaviour is indicated by a dotted line.)

B.2.2. *No-slip*

The issue of matching aside (for which see Appendix C. 2), the contrast of the formal solution (B 4) with that for free-slip boundary conditions (B 2) is more apparent than

† Note that the solution is less sensitive to the value of α_1 hence it is less accurately fixed than is the desired slope, c_1. We therefore resorted to 128-bit arithmetic to ensure greater overall accuracy.

real; at first glance it is difficult to see how to make use of this expansion since one needs to satisfy two boundary conditions at the midline ($\xi = \alpha_1/2$), not one. But because here $\alpha_1 \to \infty$, rather than saturating at a finite value, it is plausible to apply the single condition $\tilde{w}(\xi) \to 1$ for $\xi \to \infty$ in order to determine a unique c (in the expectation that derivatives of $\tilde{w}$ will automatically vanish).†

Practical numerical use of (B 4) is another matter. It transparently cannot converge for $|\xi| \geqslant 1$, but it is more likely that the series does not converge at all. By comparison there is little doubt that (B 1) with free-slip boundary solutions has a convergent solution in the classical sense. Based on examination of the $\tilde{w}$ expansion to

$$\left[\frac{\log\log 1/\xi}{\log 1/\xi}\right]^{30},$$

it emerges that the divergence is essentially captured in the bare subseries

$$^{(2)}\tilde{w}(\xi) = \xi^2 \sqrt{\log 1/\xi} \sum_{k=1}^{\infty} c_{1,k,1} (\log 1/\xi)^{1-k}. \tag{B 7}$$

The innermost summand can, by rearrangement, be accurately summed as an adjunct to this form. Define

$$\tilde{c}_{1,k,1}(\xi) = \sum_{j=k}^{\infty} c_{1,j,j-k+1}\, \chi(\xi)^{j-k}, \tag{B 8}$$

where

$$\chi(\xi) \equiv \frac{\log\log 1/\xi}{\log 1/\xi},$$

and replace c in (B 7) above by $\tilde{c}$ to recover all the terms in ξ^2 in (B 4). This series of functions defined in (B 8) is accurately evaluated with a Padé sum (Baker 1975) of moderate order (e.g. typically 20*S* for [10,10] and $|\chi| < 1$.) Interestingly, each $\tilde{c}_{1,k,1}$ so evaluated ($k = 1 \ldots 6$) indicates a first-order pole at, or quite near, $\chi(\xi) = 4$ when $c_{1,2,1} = 0$. But χ is bounded by e^{-1} for real ξ, so the singularities are not realized. We did not explore the dependence of this pole location on a range of $c_{1,2,1}$. The difficulty in summing (B 7) is basically unchanged following substitution of revised values obtained from (B 8) since the latter are comparatively weak functions of χ for the range of interest. Terms in the 'bare' sum (B 7) turn out, for large index, to be asymptotically similar to a series of the form

$$\sum_{n=0}^{\infty} c_1 \Gamma(n+\alpha_1)\Gamma(n+\beta_1) \left(\frac{2}{\log 1/\xi}\right)^{2n} + c_2 \Gamma(n+\alpha_2+\mathrm{i}\beta_2)\Gamma(n+\alpha_2-\mathrm{i}\beta_2) \left(\frac{2}{\log 1/\xi}\right)^{2n+1}, \tag{B 9}$$

which is usefully recognized as

$$c_1 \Gamma(\alpha_1)\Gamma(\beta_1)\ {}_3F_0\left([1, \alpha_1, \beta_1]; \frac{4}{\log^2 \xi}\right) + \frac{2c_2 |\Gamma(\alpha_2 + \mathrm{i}\beta_2)|^2}{\log 1/\xi}\ {}_3F_0\left([1, \alpha_2 + \mathrm{i}\beta_2, \alpha_2 - \mathrm{i}\beta_2]; \frac{4}{\log^2 \xi}\right), \tag{B 10}$$

† Applying two midline symmetry conditions for a finite domain, as for the free-slip case, is doubtless possible where the second free parameter emerges from a subdominant series of terms not captured with the present asymptotic expansion. Such terms, however, can only further complicate the already formidable difficulties of summation.

where

$$\begin{array}{lll} c_1 = -0.0886909381, & \alpha_1 = -0.3225964958, & \beta_1 = 1.066702846, \\ c_2 = \ \ 0.1705855590, & \alpha_2 = \ \ 0.8759758375, & \beta_2 = 0.4664575889. \end{array}$$

If terms in (B 4) are grouped in powers of $\log\log 1/\xi$, the next set, linear in that quantity, also tends to a similar pair of series with the constants

$$\begin{array}{lll} c_3 = \ \ 0.0111804302, & \alpha_3 = \ \ 0.3750000000, & \beta_3 = 0.720350910, \\ c_4 = -0.0108524652, & \alpha_4 = -0.6852998399, & \beta_4 = 0.4352998399. \end{array}$$

but now the even terms having the form $\alpha_3 \pm \mathrm{i}\beta_3$ and the odd terms the real form, and thereafter alternating in succession.

The form (B 9) is a generalized Stieltjes function and can be associated with a finite value directly by means of its integral representation. Alternatively we can appeal to the equivalent expression in terms of the Barnes generalized hypergeometric function ${}_3F_0$.†

The hypergeometric function ${}_3F_0([1,\alpha,\beta];z)$ formally satisfies a third-order ordinary differential equation whose general solution can be expressed in the convergent form

$$\frac{\nu_1}{z}{}_1F_2\left([1],[2-\alpha,2-\beta];\frac{1}{z}\right) + \nu_2\, z^{-(\alpha+\beta)/2} I_{\beta-\alpha}\left(\frac{2}{\sqrt{z}}\right) + \nu_3\, z^{-(\alpha+\beta)/2} I_{\alpha-\beta}\left(\frac{2}{\sqrt{z}}\right). \tag{B 11}$$

With this approach, summing the divergent series amounts to a determination of the values of $\nu_{1,2,3}$ which match the particular solution singled out by the ${}_3F_0$. This is most readily done on the negative real axis first and then having due regard for branch cuts in interpreting the solution elsewhere in the complex plane. The imaginary portions of $\nu_{2,3}$ change sign for $\pi < \arg(z) \leqslant 2\pi$. The result is

$$\nu_1 = \frac{-1}{(1-\alpha)(1-\beta)}, \quad \nu_2 = \frac{\pi^2}{\Gamma(\alpha)\Gamma(\beta)\sin\pi(\alpha-\beta)}\left(\frac{1}{\tan\pi\beta} - \mathrm{i}\right),$$
$$\nu_3 = \frac{-\pi^2}{\Gamma(\alpha)\Gamma(\beta)\sin\pi(\alpha-\beta)}\left(\frac{1}{\tan\pi\alpha} - \mathrm{i}\right)$$

(where the arguments are ordered such that $\beta > \alpha$). This is a special case of the general identity

$$\begin{aligned} {}_{p+1}F_0([1,\{\alpha_k\}];z) \sim & \prod_{k=1}^{p}\left(\frac{1}{1-\alpha_k}\right){}_1F_p\left([1],[2-\{\alpha_k\}];-\frac{1}{z}\right) \\ & + \frac{\pi^p}{\prod_{k=1}^{p}\Gamma(\alpha_k)}\sum_{k=1}^{p}\left(\frac{1}{\tan\pi\alpha_k} - \mathrm{i}\right) z^{-\alpha_k}{}_0F_{p-1}\left([1+\alpha_k-\{\alpha_j^*\}];-\frac{1}{z}\right) \\ & \times \prod_{j=1}^{p^*}\frac{1}{\Gamma(1+\alpha_k-\alpha_j)\sin\pi(1+\alpha_k-\alpha_j)}, \end{aligned}$$

where $*$ denotes the restriction $j \neq k$.

In general each of the functions in (B 10) is real only for negative real argument. With the positive definite argument appearing here, they are naturally complex, with

† There is an extensive literature on this subject. In particular see Ichinobe (2001), which derives a unique Borel sum for the general case of ${}_qF_{p-1}$ with $q > p$.

an imaginary component whose asymptotic expansion, derived from $K_{\alpha-\beta}$, is

$$\mathrm{Im}\,\{{}_3F_0([1,\alpha,\beta];x)\} \sim -\frac{\pi^{3/2}}{\Gamma(\alpha)\Gamma(\beta)}\,\mathrm{e}^{-2/\sqrt{x}}x^{1/4-(\alpha+\beta)/2}\left[1+\frac{4(\alpha-\beta)^2-1}{16}\sqrt{x}+O(x)\right]$$

as $x \to 0^+$. Substituting in the original argument of ${}_3F_0$ from (B 10), the leading-order behaviour of the first term is

$$-\mathrm{i}c_1\pi^{3/2}\,\xi\,(\log 1/\xi)^{\alpha_1+\beta_1-1/2}\left(1+O\left((\log 1/\xi)^{-1}\right)\right).$$

While the analytic continuation of the solution naturally induces an imaginary component on the positive real axis, if we revert to the integral representation for the solution, it is clear that a generalized Cauchy principal value exists. For ${}_3F_0$, this amounts to simply discarding exponentially small terms from (B 11), leaving the correct (purely real) asymptotic representation of that principal value. As an elementary illustration, note that the asymptotic expansion previously given in (A 6) can be rewritten as

$$\zeta^{-1}\,{}_3F_0\left([1,1/4,1/2];\frac{16}{\zeta^4}\right).$$

Applying the results above, $\nu_1 = -8/3$, so the first term in the convergent representation is thus

$$-\frac{\zeta^3}{6}\,{}_1F_2\left([1],[3/2,3/2+1/4];\frac{\zeta^4}{16}\right).$$

But this is simply a standard hypergeometric representation of

$$-\Gamma(3/4)\sqrt{\frac{\pi\zeta}{8}}\,L_{1/4}(\zeta^2/2).$$

The remaining pair of terms reduces to

$$\Gamma(3/4)\sqrt{\frac{\pi\zeta}{8}}\left[I_{1/4}(\zeta^2/2)+(1-\mathrm{i})\,\frac{\sqrt{2}}{\pi}\,K_{1/4}(\zeta^2/2)\right]$$

and hence (A 6) is confirmed to be the correct asymptotic expansion of (A 4) as the modified Bessel function K is exponentially small. The same considerations are easily seen to apply, *mutatis mutandis*, to the asymptotic expansion for the no-slip boundary layer solution (A 13), so it is then not surprising that the midlayer should have its asymptotic expansion about $\xi = 0$ expressed essentially in terms of ${}_3F_0$.

The determination of $c_{1,2}$ and the other coefficients above, while here evaluated as a numerical exercise, can be derived from an asymptotic solution of the recurrence relation associated with (B 4) by the discrete analogue of Laplace's method, with the above as the leading-order term and an asymptotic series of algebraic corrections in $1/n$ thereafter. At issue is simply whether the technical complications for general $c_{k,l,m}$ merit the effort to carry the analysis to completion.† Even given such a result

† The recurrence relation for the series by equating independent terms in the differential equation, each of the form $\xi^{2i}\ (\log 1/\xi)^j(\log\log 1/\xi)^k$, to zero. The general expression so determined cannot be reduced to fewer than twenty–two double sums, each quadratic in the $c_{l,m,n}$. This form is evaluated for sequentially increasing values of i and j: for a given (i,j) pair, the complete group of c coefficients associated to $k = 1 \ldots j$ is determined as the solution of a tridiagonal system. The associated matrix (whose entries are found from previously determined values of c) remains well-conditioned to large order.

to facilitate the immediate problem of summing (B 7), it would have to be modified further for the corrections induced by (B 8), the initial tendency of which we have sketched above. One can alternatively view the corrections as leading to revised coefficients $[c_{1,2}(\chi\,;c), \alpha_{1,2}(\chi\,;c), \beta_{1,2}(\chi\,;c)]$ by means of the Padé sums developed in (B 8) (the values above are $c_{1,2}(0,0)$, etc.) leaving one to evaluate the single pair of modified ${}_3F_0$ functions as a Borel sum.

For completeness we remark that one might use optimal asymptotic truncation but this places severe limits on accuracy, particularly for derivatives of $\tilde{w}$, and appears to preclude a determination of c based on shooting. Rather, following Chan's approach, we use the Green's function for the no-slip problem, which can be written

$$G(x,z) = 1/4(1+|z-x|)\mathrm{e}^{-|z-x|} - 1/4(2xz+x+z+1)\mathrm{e}^{-x-z},$$

and which we note is symmetric under the interchange of x and z. Chan restates the nonlinear differential equation as an iterative integral one, namely

$$\tilde{w}_{n+1}(z) = \int_0^\infty \frac{G(x,z)}{\tilde{w}_n(x)}\,\mathrm{d}x. \tag{B 12}$$

The integral can be broken down into

$$\int_0^\delta + \int_\delta^\gamma + \int_\gamma^\infty \mathrm{d}x,$$

where the first quadrature must be designed accurately to evaluate terms of the form

$$\int_0^\delta x^j(\log 1/x)^{-k/2}(\log\log 1/x)^m\,\mathrm{d}x,$$

with $j \geqslant 0$, $k \geqslant 1$ and $0 \leqslant m \leqslant (k-1)/2$. The last integral is done analytically, with errors that can be bounded based on the large-ξ behaviour of $\tilde{w}$, namely

$$\tilde{w} \sim 1 + c_1\mathrm{e}^{-1/2\sqrt{2^{3/2}+2}\,\xi}\cos(1/2\sqrt{2^{3/2}-2}\,\xi + c_2).$$

Any standard quadrature scheme is adequate in the midrange, $\delta < \xi < \gamma$, where $1/\tilde{w}(x)$ is perfectly well behaved, as is $G(x,z)$ save for being only C^2 at $x=z$. (In our computation we used $\delta = 0.1$ and $\gamma = 35$.)

Figure 23 shows residuals after subtraction of both the one-term approximation, $\xi^2\sqrt{\log 1/\xi}$, and also the optimal asymptotic truncation of (B 4). Over the range of ξ shown, the latter corresponds to keeping all terms up to, and including,

$$\left(\frac{\log\log 1/\xi}{\log\xi}\right)^8,$$

with an expected relative error of not more than about 3×10^{-5}. The value of c is varied to produce the least residual, with a resulting estimate of $c = 0.1248$, notably less precise than for the free-slip case. The limit on accuracy of the truncation precludes the possibility of significant further refinement, and happens to coincide with the estimated limit on accuracy of the computed solution of the integral equation. While computation falls short of being a proof, figure 23 does indicate consistency between the numerically determined solution of (B 1), recast as an integral equation, and the determination of c based on the optimal asymptotic truncation of (B 4).

Finally it remains to discuss the matching of (B 2) and (B 4) with the innermost layer.

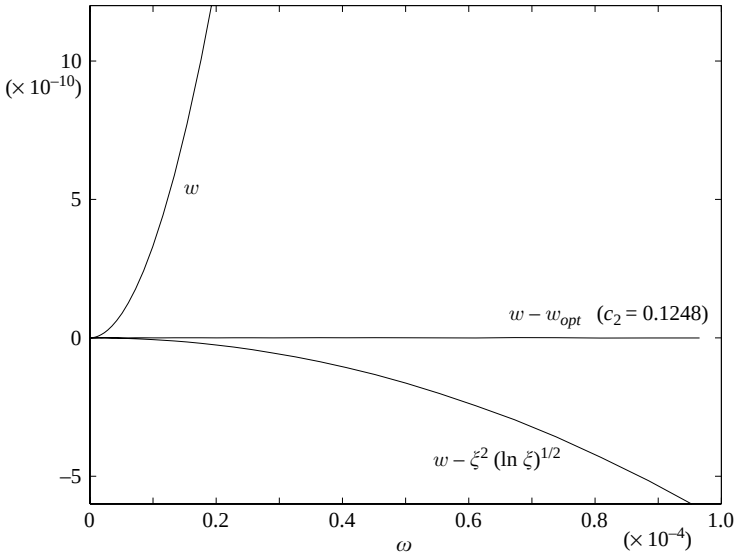

FIGURE 23. Determination of the single parameter in the no-slip expansion (B 4).

Appendix C. Matching of 1-α intermediate and wall layers

C.1. *Free-slip*

We have so far simply assumed the two boundary conditions in (B 1) at $\xi = 0$, with the remarkable consequence of α_1 tending to a constant. This assumption, while evidently correct on the numerical evidence, is not a trivial point. In the main body of the paper, we have established a match such that

$$\lim_{\zeta\to\infty} c_1\delta\widehat{w} = \lim_{\xi\to 0}\frac{1}{\alpha_1}\tilde{w} = \frac{c_1\,\xi}{\alpha_1},$$

but this constitutes only half a solution. Looking for a match of (B 2) that accounts for c_3 as well can be considered to close the problem in the sense that we will then have established a global relation, i.e. one linking both free conditions at $\zeta = 0$ to the value of the solution on the midline determined by imposing $\tilde{w}'(\xi = \alpha_1/2) = \tilde{w}'''(\xi = \alpha_1/2) = 0$, and hence justified the complete statement of the leading-order midlayer problem. In view of the considerable novelty of the free-slip solution, we suggest this is a point worth establishing beyond doubt.

Noting that the relevant term in (B 2) is cubic in ξ indicates the need of a boundary-layer expansion to three terms. We represent the general series as

$$w = \frac{c_1\,g_1}{\alpha_1}\sum_{k=0}^{\infty} g_1^k\widehat{w}_{1,k}, \qquad \theta = \frac{\alpha_1}{c_1\,g_1}\sum_{k=0}^{\infty} g_1^k\widehat{\theta}_{1,k}. \tag{C 1}$$

In the main body of the text, where only the leading-order problem is considered, the notation is slightly different. The relation is $g_1 = \alpha_1\delta$. Because there are frequent points of comparison with Chan for the equivalent expansion of no-slip, we have preferred to adopt his g_1 as the common notation throughout this appendix.

The $\widehat{w}$ equations are

$$\widehat{w}_{1,0}^{(IV)} = 0, \quad \widehat{w}_{1,1}^{(IV)} = 0, \quad \widehat{w}_{1,2}^{(IV)} = \widehat{\theta}_{1,0}/c_1^2 + 2\widehat{w}_{1,0}''.$$

Again, $\widehat{w}_{1,0} = \zeta$. For the moment we pass over the homogeneous solutions for $\widehat{w}_{1,1}$ and look for the solution of the third equation. The form $\widehat{w}_{1,2}$ can be found explicitly†:

$$\widehat{w}_{1,2} = \left[\gamma_1\zeta + \gamma_3\zeta^3 + \frac{\zeta\,\Gamma^2(3/4)}{\sqrt{8\pi}\,c_1^2}\,{}_2F_3\left(\left[-\frac{1}{2}, -\frac{1}{4}\right], \left[\frac{1}{2}, \frac{3}{4}, \frac{5}{4}\right]; \frac{\zeta^4}{16}\right) - \frac{\zeta^7}{5040\,c_1^2}\,{}_3F_4\left(\left[1, 1, \frac{5}{4}\right], \left[2, \frac{9}{4}, \frac{5}{2}, \frac{11}{4}\right]; \frac{\zeta^4}{16}\right)\right]. \quad (C\,2)$$

The coefficients $\gamma_{1,3}$ allow for the homogeneous solutions at second order. The remainder is a particular solution. The generalized hypergeometric representation is computationally useful only for small to moderate argument since each of the ${}_pF_q$ functions above grows like $\exp(\zeta^2/2)$, see 5.11.2(8) in Luke (1969). A complete asymptotic statement is problematic for general ${}_pF_q$, even in the case of ${}_2F_2$, as noted in Ierley & Ruehr (1986). Asymptotic results are instead facilitated by the equivalent integral representation of this particular solution, for the derivation of which, both in this and the case of no-slip, we are indebted to Otto Ruehr who, in addition provided the asymptotic expansion of the resulting no-slip integral, which is notably difficult to establish. Setting aside the factors of c_1^2, the relevant integral is

$$\frac{1}{12}\int_0^1 \frac{\mathrm{d}s}{\sqrt[4]{1-s^2}} \int_0^\zeta y(\zeta - y)^3 \mathrm{e}^{-sy^2/2}\mathrm{d}y + \frac{\Gamma^2(3/4)\zeta}{\sqrt{8\pi}}. \quad (C\,3)$$

From (C 3) it can be shown that the limiting behaviour of the particular solution is

$$\frac{\zeta^3\log\zeta}{6} + \frac{\zeta^3}{12}\left[\gamma + \frac{\log 2}{2} - \frac{\pi}{4} - \frac{11}{3}\right] + \frac{\Gamma^2(3/4)\zeta^2}{2^{3/2}} + \frac{1}{12\zeta} + \frac{1}{28\zeta^5}\ldots, \quad \zeta\to\infty. \quad (C\,4)$$

(The hypergeometric form in (C 2) and (C 4), carried to three more terms, suffice to cover essentially the entire range of ζ, with a practical cross-over at about $\zeta = 3$.)

To match this we observe first a special property of the form that the expansion in (B 2) takes. For a general change of scale, $\xi = g_1\zeta$, it proves convenient to introduce a relation

$$g_1 = \mathrm{e}^{6(\nu-1)c_1c_3}$$

defining ν as an alternative variable. With this notation, it can be easily verified that the resulting series is (to all orders) as in (B 2) but with ξ replaced by $g_1\zeta$ in the algebraic terms, ζ in the log terms, and c_3 replaced by νc_3. The parameter c_3, in other words, functions as a scale parameter for the solution (e.g. with the 'natural' scale, $g_1 = \exp(-6c_1c_3)$, all terms in (B 2) containing c_3 vanish). With this notation the inner limit of the outer solution is conveniently written as

$$g_1c_1\zeta + g_1^3\left(\nu c_3\zeta^3 + \frac{\zeta^3}{6c_1}\log\zeta\right) + O(g_1^5). \quad (C\,5)$$

Comparison shows that we must take

$$c_1\gamma_3 = \nu c_3 - \frac{1}{12c_1}\left[\gamma + \frac{\log 2}{2} - \frac{\pi}{4} - \frac{11}{3}\right], \qquad \gamma_1 = 0. \quad (C\,6)$$

Strictly, the appearance of ν in this match indicates that (C 1) has to be generalized as a double expansion in g_1 and $\log g_1$ but as this affects terms beyond the order considered

† A caution to readers: as of this writing, Maple v.9 does not correctly integrate powers, z^j, times the generalized hypergeometric function of argument z^k when, as is nearly always the case here, $j \geqslant k-1$. These simply have to be done by hand.

here, we omit that formal development in the interest of brevity. It suffices here to note that the quantity $\langle(1-\overline{w\theta})^2\rangle$ appearing in the denominator of (7.16) is corrected to

$$\delta J\left(1-\frac{2^{4/3}\,\alpha_1^2}{9\,c_1^{10/3}\,I^{1/3}}\,Ra^{-2/3}\left(\frac{2}{3}\,\log Ra+\gamma+\frac{\log 2}{2}-\frac{\pi}{4}-\frac{11}{3}\right)\int_0^\infty \mathrm{d}\zeta(1-\zeta\theta_{1,0})\theta_{1,0}\zeta^3\right)$$
$$\approx\delta J\,\left(1+(3.9599150\,\log Ra-20.9575070)Ra^{-2/3}\right). \tag{C 7}$$

The same considerations show that K and L in (25) of Vitanov (1998), in that work assumed constant, are both $O(\log Ra)$. Inversion of (C 7) in (7.16) changes the sign of the correction and is to be compared to the purely empirical values given in (6.2). The difference between the two is attributable to similar corrections arising from two other integrals, linear in $\theta_{1,2}$. These are somewhat troublesome to evaluate, having products of various derivatives of ${}_pF_q$ present as inhomogeneous terms in the governing equation for $\theta_{1,2}$.

Certainly, without the second parameter c_3 in the solution for the middle layer, a discussion of matching at second order is seriously incomplete. But even with this term, it is seen that the matching procedure fails at $O(g_1^3\zeta^2)$ owing to the term in ζ^2, which cannot be countered with a homogeneous solution of the equation for $\widehat{w}_{1,2}$ without violating the boundary condition that $\widehat{w}''_{1,2}(0)=0$. This incompatibility is a recurring problem at all orders, i.e. one can never match a term from the inner layer of the form $g_1^j\zeta^k$ for $j\neq k$. The inner layer does generally mix orders since individual asymptotic expansions are independent of g_1 (though not of its log, through ν) and this fact naturally introduces a sequence of powers of ζ, but all with a common prefactor in g_1. Neglect of mixed-order terms in the match is equivalent to saying that the wall layer is completely passive, that is, adapts to an imposed exterior solution, and of course this is not true; there is some modification of the interior, that is, a scale sensitivity lacking in (B 2) and which sensitivity would be reflected in, for example, the needed quadratic correction.

What is required to effect a match is a suitable expansion, the structure of which is not hard to anticipate, namely

$$\mathring{\omega}_1=\sum_{n=0}^{\infty} g_1^n\mathring{\omega}_{1,n}, \tag{C 8}$$

$$\mathring{\theta}_1=\sum_{n=0}^{\infty} g_1^n\mathring{\theta}_{1,n}, \tag{C 9}$$

where $\mathring{\theta}_{1,0}=1/\mathring{\omega}_{1,0}$. (Again following Chan, we now switch from $\tilde{w}$ used in the main text to $\mathring{\omega}$ in order to make free-slip and no-slip as notationally similar as possible.) We also take

$$-\frac{\lambda}{F}=\widehat{\lambda}\,g_1+O(g_1^2),\qquad \widehat{\lambda}=\frac{7\,I}{2\,\alpha_1},$$

with the numerical value of I as given in (7.17). As earlier, we rescale z with α_1. The equations for the next corrections, $\mathring{\omega}_{1,1}$ and $\mathring{\theta}_{1,1}$, are a coupled set given by

$$(\mathrm{D}^2-1)^2\mathring{\omega}_{1,1}=\mathring{\theta}_{1,1}, \tag{C 10}$$

$$(\mathrm{D}^2-1)^2(\mathring{\omega}_{1,0}^2\mathring{\theta}_{1,1})+\mathring{\omega}_{1,0}\mathring{\theta}_{1,1}(\mathrm{D}^2-1)^2\mathring{\omega}_{1,0}+(\mathrm{D}^2-1)^2(\mathring{\omega}_{1,1})$$
$$+\frac{\mathring{\omega}_{1,1}}{\mathring{\omega}_{1,0}}(\mathrm{D}^2-1)^2\mathring{\omega}_{1,0}=2\widehat{\lambda}\,(\mathrm{D}^2-1)^2\mathring{\omega}_{1,0}. \tag{C 11}$$

It is helpful to eliminate $\mathring{\theta}_{1,1}$ using the first equation and get a single, eighth-order, equation for $\mathring{\omega}_{1,1}$.

The eight homogeneous solutions have to be deduced individually as the origin is an irregular singular point. The key one is that required to match the term of order ζ^2 in (C 4). The relevant series expansion begins as

$$\mathring{\omega}_{1,1}^{(2)} = \xi^2 + \left(\frac{\log \xi}{270\, c_1^2} - \frac{1}{8640\, c_1^4} - \frac{7}{2700\, c_1^2} + \frac{c_3}{45\, c_1} - \frac{1}{216} \right) \xi^6 + \ldots, \tag{C 12}$$

with the same constants $c_{1,3}$ as in (B 2). This and three further solutions, which behave as 1, $\xi^2 \log \xi$, and $\xi^3 \log \xi$, respectively are invoked here and at higher order as needed to match the outer limit of successive contributions to the inner solution.

The remaining four solutions have forms that can be guessed fairly readily. These are

$$\mathring{\omega}_{1,1}^{(1)} = \xi - \frac{\log \xi}{720\, c_1^4}\, \xi^5 + \left(\frac{\log^2 \xi}{15120\, c_1^6} + \ldots \right) \xi^7 + \ldots, \tag{C 13}$$

$$\mathring{\omega}_{1,1}^{(3)} = \xi^3 + \left(\frac{\log \xi}{210\, c_1^2} - \frac{1}{100800\, c_1^4} - \frac{149}{44100\, c_1^2} + \frac{c_3}{35\, c_1} - \frac{11}{4200} \right) \xi^7 + \ldots, \tag{C 14}$$

$$\mathring{\omega}_{1,1}^{(4)} = \xi^4 + \left(-\frac{\log \xi}{45\, c_1^2} + \frac{7}{450\, c_1^2} - \frac{2\, c_3}{15\, c_1} + \frac{7}{90} \right) \xi^6 + \ldots, \tag{C 15}$$

$$\mathring{\omega}_{1,1}^{(5)} = \xi^5 + \left(-\frac{\log \xi}{21\, c_1^2} + \frac{149}{4410\, c_1^2} - \frac{2\, c_3}{7\, c_1} + \frac{13}{210} \right) \xi^7 + \ldots. \tag{C 16}$$

We now seek a homogeneous correction in the form

$$\frac{\Gamma^2(3/4)}{2^{3/2} c_1} \mathring{\omega}_{1,1}^{(h)} \quad \text{where} \quad \mathring{\omega}_{1,1}^{(h)} = \left[\lambda_1^{(h)} \mathring{\omega}_{1,1}^{(1)} + \mathring{\omega}_{1,1}^{(2)} + \lambda_3^{(h)} \mathring{\omega}_{1,1}^{(3)} + \lambda_4^{(h)} \mathring{\omega}_{1,1}^{(4)} + \lambda_5^{(h)} \mathring{\omega}_{1,1}^{(5)} \right], \tag{C 17}$$

and the coefficients $\lambda_k^{(h)}$ are chosen so that $\mathring{\omega}'_{1,1}(\alpha/2) = \mathring{\omega}'''_{1,1}(\alpha/2) = \mathring{\omega}^{(V)}_{1,1}(\alpha/2) = \mathring{\omega}^{(VII)}_{1,1}(\alpha/2) = 0$. The last two conditions arise from reduction of the pair of fourth-order equations for $\mathring{\omega}_{1,1}$ and $\mathring{\theta}_{1,1}$ into a single equation. This disposition of the homogeneous solutions contrasts with no-slip, where we need to determine the far-field behaviour of each as exponential growth or decay, omitting all the former. But the latter must then be paired with the available local expansions about the origin. In view of the complexity of the governing equations, that connection problem can only be solved numerically while here it could be completed essentially analytically given sufficient care in Padé summation of the series involved.

The leading terms for the particular solution for $\mathring{\omega}_{1,1}$ take the form

$$\mathring{\omega}_{1,1}^{(*)} = \frac{1}{360 c_1^3}\, \xi^5 \log \xi + O(\xi^7 (\log \xi)^2). \tag{C 18}$$

Boundary conditions at the midline are satisfied as in (C 17), giving an augmented particular solution of $\widehat{\lambda}\, \mathring{\omega}_{1,1}^{(p)}$ where

$$\mathring{\omega}_{1,1}^{(p)} = \left[\lambda_1^{(p)} \mathring{\omega}_{1,1}^{(1)} + \mathring{\omega}_{1,1}^{(*)} + \lambda_3^{(p)} \mathring{\omega}_{1,1}^{(3)} + \lambda_4^{(p)} \mathring{\omega}_{1,1}^{(4)} + \lambda_5^{(p)} \mathring{\omega}_{1,1}^{(5)} \right], \tag{C 19}$$

with the $\lambda_k^{(p)}$ determined in the same manner as the $\lambda_k^{(h)}$.

	(h)	(p)
λ_1	−0.958768	−0.278473
λ_3	−0.528599	+0.068177
λ_4	+0.186566	−0.046239
λ_5	−0.050859	+0.020484

TABLE 2. Computed coefficients λ_k in (C 17) and (C 19)

The necessary inclusion of $\mathring{\omega}_{1,1}^{(1)}$ in (C 17) and (C 19) means that the slope of the wall layer at the origin, γ_1 – previously taken as zero – is instead given by

$$\gamma_1 = \frac{\lambda_1^{(h)}\Gamma^2(3/4)}{2^{3/2}g_1c_1} + \frac{\lambda_1^{(p)}\widehat{\lambda}}{g_1}. \tag{C 20}$$

Formally this correction should be incorporated as a term of order $O(g_1^2)$, that is a homogeneous contribution to $\widehat{w}_{1,1}$, which accounts for the appearance of g_1 in the denominators above, but this is a minor detail if we do not pursue matching beyond $O(g_1^3)$. The remaining terms introduced through (C 14)–(C 16) are higher order in g_1 when carried to the inner layer and need not be considered further. We have a tentative reason now to regard the match as satisfactorily resolved at $O(g_1^3)$ and require only for numerical confirmation.

Comparison requires care in defining the constants. We use a well-resolved computation at $Ra = 3.769 \times 10^{11}$ with $\alpha_1 = 5.49356168$. For this α_1 we require the associated $c_{1,3}$ (in place of the limiting values indicated in Appendix B), found as a byproduct of computing $\mathring{\omega}_{1,0}$ to be

$$c_1 = 0.835541474428, \quad c_3 = -0.164064858206.$$

The values of $c_{1,3}$ uniquely determine the linear solutions of (C 10)–(C 11), so we turn now to a determination of the λ_k.

We have carried out the expansions of (C 12)–(C 16) and (C 18) up to order ξ^{11}. Because derivatives up to order seven from these expansions are required as initial conditions, a desire for high accuracy suggests commencing integration with as small a value of ξ as possible. Working against this with finite-precision arithmetic, however, is that the seventh derivative of $\mathring{\omega}_{1,1}^{(1)}$ scales as ξ^{-2} for $\xi \to 0$. Comparison of double-precision integrations commencing at $\xi = 10^{-5}$ and 10^{-6} shows relative differences of about 10^{-7} in the resulting derivative values at $\xi = \alpha_1/2$, so these values were refined using extended precision starting from $\xi = 10^{-8}$. Table 2 shows the values of the $\lambda_k^{(h,p)}$ so computed. We now fix

$$g_1 = \left(\frac{4\,I}{c_1^2 R}\right)^{1/3} = 0.001102361082$$

using the leading-order result for F (cf. the line following (7.12)).

In § 7 we give the rescaling from the CDH basis to Chan as

$$w \to \langle w\widehat{\theta}\rangle^{-1/2} Ra^{-1/2} w \qquad \text{and} \qquad \widehat{\theta} \to \langle w\widehat{\theta}\rangle^{-1/2} Ra^{1/2}\theta,$$

in accord with his normalization that $\langle w\theta\rangle = 1$. For an examination of the first correction beyond leading order, it is thus necessary to rescale with care, recognizing that the asymptotic solution as constructed thus far leads to $\langle w\theta\rangle = 1 + a_1 g_1 + O(g_1^2)$

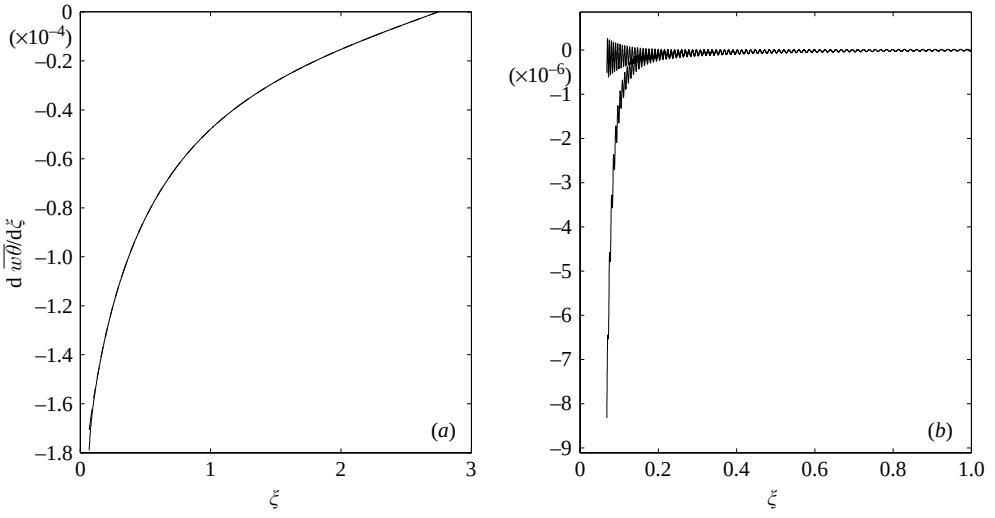

FIGURE 24. (*a*) A comparison of the computed and predicted $\mathrm{d}\overline{w\theta}/\mathrm{d}\xi$ for free-slip boundary conditions. (*b*) The error in the prediction.

where

$$a_1 = 2/\alpha_1 \int_0^{\alpha_1/2} \frac{\Gamma^2(3/4)}{2^{3/2}\, c_1}\, L\left(\mathring{\omega}_{1,1}^{(h)}\right) + \widehat{\lambda}\, L\left(\mathring{\omega}_{1,1}^{(p)}\right) \mathrm{d}\xi$$
$$- 2/\alpha_1 \int_0^{\infty} \left[1 - \sqrt{\frac{\pi}{8}}\Gamma(3/4)\, \zeta^{3/2}\left(I_{1/4}(\zeta^2/2) - L_{1/4}(\zeta^2/2)\right)\right] \mathrm{d}\zeta, \quad \text{(C 21)}$$

and

$$L \equiv \left[\mathring{\omega}_{1,0}\left(\mathrm{D}^2 - 1\right)^2 + \mathring{\omega}_{1,0}^{-1}\right].$$

The first term accounts for the interior $\overline{w\theta}$ correction found in this section, the second for the deficit due to the rise of the leading-order boundary layer from zero at the wall to its asymptotic value of unity.

For a first comparison we can, however, sidestep delicate corrections to the normalization, which need primarily arises if we look at the difference $\alpha_1 w - \mathring{\omega}_{1,0}$, and instead focus on

$$g_1 L'\left(\frac{\Gamma^2(3/4)}{2^{3/2}\, c_1}\, \mathring{\omega}_{1,1}^{(h)} + \widehat{\lambda}\mathring{\omega}_{1,1}^{(p)}\right),$$

where the prime denotes $\mathrm{d}/\mathrm{d}\xi$. One can prove the convenient and altogether remarkable identity

$$L'(\mathring{\omega}_{1,1}^{(h)}) = \left[\frac{4\, c_1^2 - 1 - 24\, c_1^2\, \lambda_4^{(h)}}{24\, c_1^2 \lambda_4^{(p)}}\right] L'(\mathring{\omega}_{1,1}^{(p)}) \quad \text{(C 22)}$$

and, details of matching coefficients aside, we have then the elementary prediction that

$$\frac{\mathrm{d}\overline{w\theta}}{\mathrm{d}\,\xi} = \text{const}\, L'(\mathring{\omega}_{1,1}^{(h)}) \quad \text{(C 23)}$$

for a suitable choice of a single constant. For this comparison we first normalize the CDH solution, as in § 7, to $\langle w\theta \rangle = 1$. In figure 24, we use an empirically determined value for the constant, -1.315806×10^{-4}. Figure 24(*b*), showing the difference, clearly illustrates the vestigial influence of the wall layer. Its contribution is easily computed

to be $-8g_1^4/\xi^5$ and a second line has been plotted showing that contribution – which does not require an interior match – subtracted out. What remains is a rapid oscillation, largest at the ends of the intervals. This reflects the numerical resolution limit of the solution. Note that a relation like (C 22) does not hold in general. It fails, for example, in the case of the (augmented) homogeneous solution based on $\xi^3 \log \xi$. Hence that the correct solution is composed of the specific constituents $\mathring{\omega}_{1,1}^{(h,p)}$ stated is decisively established.

To confirm their predicted amplitudes, we turn finally to the expansion

$$\alpha_1 w \sim \mathring{\omega}_{1,0} + g_1 \left[\frac{\Gamma^2(3/4)}{2^{3/2} c_1} \mathring{\omega}_{1,1}^{(h)} + \widehat{\lambda} \mathring{\omega}_{1,1}^{(p)} \right].$$

As Chan's variational formulation is predicated on $\langle w\theta \rangle$ held fixed at unity, while the posited solution has $\langle w\theta \rangle \sim 1 + a_1 g_1$, we can restore the required normalization by the transformation

$$\mathring{\omega}_{1,1} \to \mathring{\omega}_{1,1} + \gamma_1 \mathring{\omega}_{1,0} \qquad \mathring{\theta}_{1,1} \to \mathring{\theta}_{1,1} + \frac{\gamma_1}{\mathring{\omega}_{1,0}}.$$

With this transformation (C 10) is unchanged, while in (C 11), $\widehat{\lambda} \to \widehat{\lambda} - 2\gamma_1$. By solving for γ_1 from

$$\gamma_1 = -a_1(\gamma_1)/2$$

where $\widehat{\lambda}$ in (C 21) is replaced by $\widehat{\lambda} - 2\gamma_1$, then $\langle w\theta \rangle = 1$ holds at $O(g_1)$. This computation gives $\gamma_1 = 0.81837990$, which predicts a constant in (C 23) of -1.31242×10^{-4}, consistent with the empirical determination reported above. The renormalized forms for w and θ now assume the form

$$\alpha_1 w \sim \mathring{\omega}_{1,0} + g_1 \left[\frac{\Gamma^2(3/4)}{2^{3/2} c_1} \mathring{\omega}_{1,1}^{(h)} + \widehat{\lambda} \mathring{\omega}_{1,1}^{(p)} \right] + g_1 \gamma_1 \left[\mathring{\omega}_{1,0} - 2 \mathring{\omega}_{1,1}^{(p)} \right], \tag{C 24}$$

$$\theta/\alpha_1 \sim \mathring{\omega}_{1,0}^{-1} + g_1 \left[\frac{\Gamma^2(3/4)}{2^{3/2} c_1} \mathring{\theta}_{1,1}^{(h)} + \widehat{\lambda} \mathring{\theta}_{1,1}^{(p)} \right] + g_1 \gamma_1 \left[\mathring{\omega}_{1,0}^{-1} - 2 \mathring{\theta}_{1,1}^{(p)} \right], \tag{C 25}$$

where $\mathring{\theta}^{(h,p)}$ are found from the corresponding $\mathring{\omega}^{(h,p)}$ by use of (C 10). Figure 25 compares the interior error in the leading-order approximations for w and θ with the error of (C 24)–(C 25). The perceptive reader will note that, while the second-order errors in w and θ are evidently well resolved in figure 25, the equivalent error in $\mathrm{d}\overline{w\theta}/\mathrm{d}\xi$ as presented in figure 24 appears to be beyond the resolution limit of the computation. The reason for the discrepancy is subtle. The linear eighth-order operator deriving from (C 10)–(C 11) applies to $\mathring{\omega}_{1,k}$ for all $k \geqslant 1$; hence we can anticipate a contribution from the homogeneous solution $\mathring{\omega}_{1,1}^{(h)}$ at every order. The empirical determination for the constant appearing in (C 23) unavoidably includes all of these and hence the residual plotted in figure 24 is not strictly second order. Lastly, it will be evident how to use the above expressions in conjunction with the boundary layer expansions to compose uniform asymptotic approximations valid over the entire interval in z.

We have now completed the free-slip asymptotic match, confirming the development of (C 10)–(C 19) in every particular and thus vindicating the boundary conditions asserted in § 7.1 for the interior $\tilde{w}$ equation, so we turn finally to the match for no-slip.

C.2. *No-slip*

As one might anticipate from the crucial role above of c_3, the absence of an equivalent second free parameter in (B 4) means that the matching must have a somewhat different character than the free-slip case, as indeed appears.

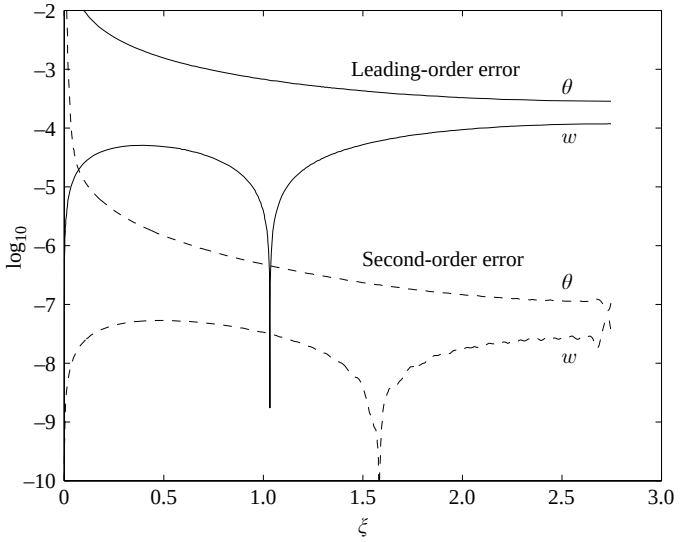

FIGURE 25. The logarithm (base 10) of the leading- and second-order errors in the interior predictions for θ and w.

One can first simply integrate the asymptotic relations in the wall hierarchy order by order to see if a consistent match might possibly be made to (B 4). Following that programme (and cancelling superfluous terms) we obtain

$$\begin{aligned}
&\widehat{\omega}_{1,0} \sim \zeta_1^2,\\
&\widehat{\omega}_{1,1} \sim \zeta_1^2\left[\frac{1}{2}\log 1/\zeta_1 + \gamma_1\right],\\
&\widehat{\omega}_{1,2} \sim \zeta_1^2\left[-\frac{1}{8}\log^2 1/\zeta_1 + \gamma_1 \log 1/\zeta_1 + \gamma_2\right],\\
&\widehat{\theta}_{1,0} \sim \zeta_1^{-2},\\
&\widehat{\theta}_{1,1} \sim \zeta_1^{-2}\left[-\frac{1}{2}\log 1/\zeta_1 + 2\gamma_1 + \frac{1}{4}\right],\\
&\widehat{\theta}_{1,2} \sim \zeta_1^{-2}\left[\frac{3}{8}\log^2 1/\zeta_1 - \left(\frac{3}{8} + \frac{9\gamma_1}{2}\right)\log 1/\zeta_1 + \text{const}\right],
\end{aligned}$$

where the constants γ_1 and γ_2 in each case are determined by matching to the middle layer.

But as the detailed solution for $\widehat{w}_{1,2}$ with free-slip boundary conditions illustrates, this is not a complete characterization of all possible terms (though all the ones above are certainly present). As with the free-slip case, the detailed solutions for Chan (equations 44a,b) using the related expansion (47a,b) quickly become infeasible to follow but one can again produce an exact particular solution for $\widehat{\omega}_{1,1}$, namely

$$\begin{aligned}
\widehat{\omega}_{1,1} = &\frac{\zeta_1{}^5\sqrt[3]{2}\sqrt{3}}{480\pi}\,{}_4F_5\left(\left[\frac{1}{3},\frac{1}{2},\frac{2}{3},\frac{5}{6}\right],\left[\frac{7}{6},\frac{4}{3},\frac{3}{2},\frac{5}{3},\frac{11}{6}\right];\frac{\zeta_1^6}{36}\right)\Gamma^3(2/3)\\
&-\frac{\zeta_1{}^8}{20160}\,{}_5F_6\left(\left[\frac{5}{6},1,1,\frac{7}{6},\frac{4}{3}\right],\left[\frac{3}{2},\frac{5}{3},\frac{11}{6},2,\frac{13}{6},\frac{7}{3}\right];\frac{\zeta_1{}^6}{36}\right). \qquad \text{(C 26)}
\end{aligned}$$

Once again for the asymptotic behaviour it is preferable to use the integral representation, namely

$$\frac{1}{18}\int_0^1 \frac{\mathrm{d}s}{\sqrt[3]{1-s^2}}\int_0^\zeta y(\zeta-y)^3\mathrm{e}^{-sy^3/3}\,\mathrm{d}y. \tag{C 27}$$

The asymptotic expansion of this is

$$\frac{\pi^{3/2}6^{2/3}\sqrt{3}\zeta^3}{162\,\Gamma(5/6)}+\frac{\zeta^2}{2}\log 1/\zeta+\left(\frac{1}{4}-\frac{\gamma}{6}+\frac{\log(3)}{24}+\frac{\pi\sqrt{3}}{72}\right)\zeta^2 - \frac{\Gamma^2(2/3)\sqrt[3]{2}\sqrt[3]{3}}{6}\zeta+\frac{\Gamma^4(2/3)\sqrt[6]{3}}{12\pi}+\frac{1}{140\zeta^4}+O(\zeta^{-10}). \tag{C 28}$$

The term of order ζ^3 will be ubiquitous in particular solutions at every order, simply arising from a first constant of integration. This can always be removed by invoking a homogeneous solution.

Comparison of these results with the exact solution in (B 4) shows that Chan's prescription for the wall to intermediate layer match is not quite complete in two respects:

(i) If the amplitude scaling for the wall is taken as

$$A_1=\frac{g_1^2}{\alpha_1}\sqrt{\log 1/g_1},$$

then the second term in $\widehat{\omega}_{1,2}$ is unaccounted for following the previously established result that $\gamma_1=c$ from the match for $\widehat{\omega}_{1,1}$.†

(ii) Once again we have terms which go unmatched in the asymptotic expansion of the particular solution of the wall layer (C 28), which have no opposite number from the inner limit but which also cannot be eliminated by appeal to homogeneous solutions.

The resolution of the first point requires that we return to (B 4). Identification of the amplitude parameter A_1 in Chan's equation (42) is predicated on the g_1 dependence of the coefficient $\tilde{c}_{1,0}$ in the inner limit of the middle layer solution. This is formally a divergent series, which begins

$$A_1\sim\frac{1}{\alpha_1}g_1^2\left(\log\frac{1}{g_1}\right)^{1/2}\left[1+\frac{c-(1/8)\log\log 1/g_1}{\log 1/g_1}+\ldots\right]. \tag{C 29}$$

The character of this should not be wholly surprising; the value of c is the signature of the global match to the interior solution (albeit one that is challenging to determine), and the asymptotic expansion of the innermost boundary layer must in some fashion reflect that. Indeed the want of any such relation in the original exposition is one of its most curious features. Fortunately, the role of this parameter is purely to establish a reference scale; nothing in the results above for $(\widehat{\omega},\widehat{\theta})$ is directly affected, it is only when the explicit match is effected that the full series must be used. With this replacement, the apparent anomaly in the matching of $\widehat{\omega}_{1,2}$ is resolved.

Resolution of the second point, a match to the linear and constant terms in (C 28), is now a familiar exercise with the free-slip case acting as a guide. The equations are simply the homogeneous form of (C 10)–(C 11). The origin is again an irregular singular point. Prompted by the greater complication of no-slip, we here seek only the leading term for each of the eight homogeneous solutions. For this it suffices to

† Notice the distinction with free-slip: there the identification of γ_3 with the term vc_3 led to an unexpected $\log Ra$ contribution owing to c_3 being a scale parameter. Here the single parameter c plays no special role in the expansion and the term it induces in the boundary layer is unchanged in order.

let $\mathring{\omega}_{1,0} = \xi^2\sqrt{\log 1/\xi}$. Each solution has a first term of the form $\xi^\mu(\log 1/\xi)^\nu$ for $\mu = [0, 1, 2, 3]$. The corresponding ν are $[\pm 1/6, \pm 1/2, \pm 1/2, \pm 1/6]$. The inner limits of the first four, that is for $\mu = 0, 1$, are candidates for the required match.

But, as previously anticipated, the required constituents must be composed so as to eliminate the four growing exponentials in the far field. As for matching, all that matters is the value of μ, not ν, and this process will identify a subspace of solutions we can label as $\mathring{\omega}_{1,1}^{(k)^*}$ for $k = 1..4$ with inner limit ζ^{k-1}. Each will project on all four decaying exponentials. This match is unlike free-slip in that there are no induced wall corrections. While conceptually easy, producing the equivalent of (C 17) is more difficult in practice. We have first to compute the coefficients that accompany the two solutions with the required inner limits, $\mathring{\omega}_{1,1}^{(1,2)^*}$. In the case of $\mathring{\omega}_{1,1}^{(1)^*}$, for example, this is of the form

$$\lambda_1 = \frac{\Gamma^4(2/3)\sqrt[6]{3}}{12\pi}\left[1 + \left(\frac{\log\log 1/g_1}{24} + \frac{43}{108} - \frac{c}{3}\right)(\log 1/g_1)^{-1} + O\left(\left(\frac{\log\log 1/g_1}{\log 1/g_1}\right)^2\right)\right]^{-1}\left[\lambda_{1/6}^{(1)}(\log 1/g_1)^{1/6} + \lambda_{-1/6}^{(1)}(\log 1/g_1)^{-1/6}\right]. \tag{C 30}$$

The computation is a two-step process. First we determine the constants $\lambda_{\pm 1/6}^{(1)}$, which derive from the numerical connection problem outlined above. Next, the series above must be carried out well beyond the few terms shown since, for values of Ra reasonably within reach, g_1 is of the order of 10^{-2} and the ratio of logs is about 1/3. Even apart from the marginal accuracy in the present estimate of c in the second half of appendix B, the use of (C 30) immediately reopens the issue of summability. It may be that a comparatively few terms in (C 30), in conjunction with Padé summation, could provide the needed accuracy (and similarly for the coefficient of $\mathring{\omega}_{1,1}^{(2)^*}$). In view of the diverse sources of numerical uncertainty, we have not explored this possibility although it should be added that, if one could show explicit agreement of this expansion at the level of agreement of the curves in figure 24, this would at once confirm the postulated solution (B 4), the associated value of c, and, precisely as for free-slip, the global consistency of the midlayer problem as posed.

Insofar as Chan's leading-order prediction of the 1-α heat flux,

$$Nu < c\, Ra^{3/10}(\log Ra)^{1/5},$$

is concerned, the main modification of that argument is driven by the renormalization of the expansion parameter noted above. This induces only additive corrections to the prefactor; it does not change the leading order. Figure 2 in the main text, relying on the form suggested here for such corrections, gives reasonable evidence that these are as indicated. Additional terms of a similar character, comparable in origin to those explicitly exhibited in (C 7) for free-slip, certainly emerge from the match above as well, though their constructive derivation appears incomparably more difficult.

Appendix D. Expansions for the 2-α free-slip solution

D.1. *The indicial equations*

We look for a solution maximizing F using the two-wavenumber ansatz

$$[\, w(\boldsymbol{x}), \theta(\boldsymbol{x})\,] = \sqrt{2}\sum_{n=1}^{2}[\, w_n(z), \theta_n(z)\,]\cos\alpha_n x. \tag{D 1}$$

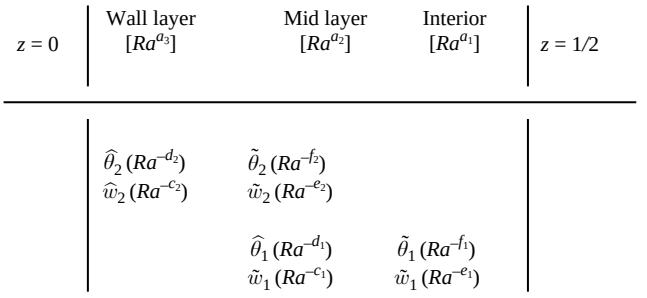

FIGURE 26. Schematic relation of the boundary layers.

Based upon the 1-α analysis and numerical computations for the 2-α branch, we look for a three-layer 2-α solution where $\alpha_1 = O(Ra^{a_1})$ and $\alpha_2 = O(Ra^{a_2})$ $(a_2 > a_1)$ as $Ra \to \infty$. The second wavenumber solution $[w_2(z), \theta_2(z)]$ appears to be arranged over two layers: an innermost (third) layer of thickness $O(Ra^{-a_3})$, within which we define

$$\widehat{w}_2 = Ra^{-c_2} w_2, \qquad \widehat{\theta}_2 = Ra^{-d_2}\theta_2, \qquad \zeta_3 = Ra^{a_3} z, \tag{D 2}$$

and an intermediate (second) layer of thickness $O(Ra^{-a_2})$ $(a_2 < a_3)$ where $\partial/\partial z = O(\alpha_2)$, within which we define

$$\tilde{w}_2 = Ra^{-e_2} w_2, \qquad \tilde{\theta}_2 = Ra^{-f_2}\theta_2, \qquad \zeta_2 = Ra^{a_2} z. \tag{D 3}$$

The scalings are chosen so that the fields marked with a caret or tilde are $O(1)$.

The first wavenumber solution $[w_1(z), \theta_1(z)]$ is arranged over the intermediate layer and an outer (first) layer of thickness $O(Ra^{-a_1})$, but the latter is the interior hence $a_1 = 0$, as in the 1-α solution, once again reflecting the $O(1)$ saturation of the lowest wavenumber. In the intermediate layer, we define

$$\widehat{w}_1 = Ra^{-c_1} w_1, \qquad \widehat{\theta}_1 = Ra^{-d_1}\theta_1, \tag{D 4}$$

and in the interior

$$\tilde{w}_1 = Ra^{-e_1} w_1, \qquad \tilde{\theta}_1 = Ra^{-f_1}\theta_1, \qquad \zeta_1 = Ra^{a_1} z. \tag{D 5}$$

For consistency we also define $O(1)$ wavenumbers $\tilde{\alpha}_1 = Ra^{-a_1}\alpha_1$ and $\widehat{\alpha}_2 = Ra^{-a_2}\alpha_2$. Given that $a_1 = 0$, there are then ten indices to find in order to fix the asymptotic scaling of the solution and, in turn, the scaling for the Nusselt number. This is our objective rather than a complete solution for each variable in each layer. The diagram in figure 26 shows the relation of the fields. Six of the ten equations needed can either be anticipated *a priori* or else discovered by cursory examination of numerical results. The remaining four equations are determined by matching of inner and outer expansions. While matching w_n is elementary, the matches for θ_n are not. The match of $\widehat{\theta}_2$ to $\tilde{\theta}_2$ is particularly sensitive. A numerical method suited to its diagnosis is outlined in Appendix A, culminating in equation (A 14), from which the determination of the needed constituents follows. To the extent that each match for θ_n is resolved strictly by appeal to numerical evidence, the logic in this section is incomplete but the arguments required to fill in the gaps would be out of proportion to the largely formal gain in rigour.

The numerical evidence is highly suggestive that $\overline{w\theta} \approx 1$ everywhere except in the innermost layer, where $\overline{w\theta}$ rises smoothly from 0 to 1. This implies $F = O(Ra^{a_3})$, so we define $\widehat{F} = FRa^{-a_3}$. It will turn out as well for consistency that $(1 - \overline{w\theta}) = O(\lambda/F) = O(Ra^{-a_3})$, with considerable consequences for the solution in the intermediate layer.

In the innermost layer, the equations for $\widehat{w}_2$ and $\widehat{\theta}_2$ are

$$Ra^{4a_3-2a_2+2c_2}\,\widehat{w}_2^{IV} = \widehat{\alpha}_2^2\widehat{\theta}_2\,, \tag{D 6}$$

$$Ra^{a_3-1-2c_2}\,\frac{1}{\widehat{F}}\widehat{\theta}_2^{VI} + [(1-\widehat{w}_2\widehat{\theta}_2)\widehat{w}_2]^{IV} + (1-\widehat{w}_2\widehat{\theta}_2)\widehat{w}_2^{IV} = 0. \tag{D 7}$$

As in the 1-α solution, we take the leading balance in the $\widehat{w}_2$ equation to be $\widehat{w}_2^{IV} = 0$ (which gives only an inequality for the indices) and the last term in equation (D 7) drops out as before. Similarly, as we then expect $\widehat{w}_2 = c\zeta_3$, in order to recover (7.14), we take

$$c_2 = \tfrac{1}{2}(a_3 - 1). \tag{D 8}$$

The distinction in the 2-α problem will be seen in the need for two of the four solutions of (A 5) in order to effect a proper match.

The equations in the intermediate layer for $\tilde{w}_2$ and $\widehat{w}_1$ to leading order are

$$Ra^{2a_2+e_2-f_2}\left[\frac{\mathrm{d}^2}{\mathrm{d}\zeta_2^2} - \widehat{\alpha}_2^2\right]^2 \tilde{w}_2 = \widehat{\alpha}_2^2\tilde{\theta}_2, \tag{D 9}$$

and

$$\widehat{w}_1^{IV} = 0. \tag{D 10}$$

An interesting balance in the first equation requires that

$$2a_2 = f_2 - e_2 \tag{D 11}$$

and we so assume. The alternative possibility, that $\tilde{w}_2$ satisfies a homogeneous equation, can quickly be ruled out. (As above, assumption of the form of the equation for $\widehat{w}_1$ provides only an inequality for the indices. Both inequalities are found to be satisfied after the fact.)

The interior equation for $\tilde{w}_1$ is

$$Ra^{2a_1+e_1-f_1}\left[\frac{\mathrm{d}^2}{\mathrm{d}\zeta_1^2} - \tilde{\alpha}_1^2\right]^2 \tilde{w}_1 = \tilde{\alpha}_1^2\tilde{\theta}_1. \tag{D 12}$$

Again we look for a distinguished balance of terms and thus require

$$2a_1 = f_1 - e_1. \tag{D 13}$$

For the wall and interior regions, that $\overline{w\theta} \approx 1$ immediately implies

$$d_2 = -c_2 \quad \text{and} \quad e_1 = -f_1. \tag{D 14}$$

In the interior we must also have

$$\tilde{w}_1\tilde{\theta}_1 = 1. \tag{D 15}$$

In the intermediate layer, where

$$\overline{w\theta} = Ra^{d_1+c_1}\tilde{w}_2\tilde{\theta}_2 + Ra^{e_2+f_2}\widehat{w}_1\widehat{\theta}_1, \tag{D 16}$$

and we observe that $\tilde{w}_2\tilde{\theta}_2$ and $\widehat{w}_1\widehat{\theta}_1 \gg O(1)$, it follows first that

$$e_2 + f_2 = c_1 + d_1, \tag{D 17}$$

and in addition that

$$\tilde{w}_2\tilde{\theta}_2 = -\widehat{w}_1\widehat{\theta}_1. \tag{D 18}$$

Where (D 15) serves to define $\tilde{\theta}_1$, (D 18) reveals an unavoidable ambiguity that our simple approach to determining the indicial exponents alone cannot resolve. The equations for $\tilde{\theta}_2$ and $\widehat{\theta}_1$ are not closed, as they each require there be a finite residual from the quantity $1-\overline{w\theta}-\lambda/F$, but enforcing (D 18) precludes representing this in terms of the variables given. This difficulty is addressed in the next section.

The remaining four indicial equations arise through matching. The elementary inner equations for $w_{1,2}$ render two of these matches immediate. For w_2, since $\widehat{w}_2$ emerges out of the intermediate layer like ζ_3 this must match onto $Ra^{a_3-a_2}\zeta_2$ and hence a match to $\tilde{w}_2$ requires

$$e_2 = a_3 - a_2 + c_2. \tag{D 19}$$

Similarly for w_1, where $\widehat{w}_1$ emerges out of the intermediate layer like ζ_2, we have

$$e_1 = a_2 - a_1 + c_1. \tag{D 20}$$

On first view, the numerical solutions suggest that $\widehat{\theta}_2 \to$ constant as $\zeta_3 \to \infty$, rather than the 1-α asymptotic behaviour of $1/\zeta_3$. While the governing equation does admit such a solution, namely $\widehat{\theta}^{(2)}$ given in (A 3), this interpretation of the outer limit of the wall layer is not correct. Examining a sequence of numerical solutions with the aid of the fitting procedure defined by (A 14) shows that $\widehat{\theta}_2$ consists of two of the four solutions of (A 1); the 'normal' solution with an asymptotic limit of $1/\zeta_3$, but also an exact elementary solution, $\widehat{\theta}_2 = \zeta_3$, of smaller order within the wall layer. But, on passing to an outer limit expressed in terms of ζ_2 for the match, the second of these is amplified by $Ra^{2(a_3-a_2)}$ relative to the first, and the role of dominant and subdominant interchanged. Strictly this should lead back to revision of our initial ansatz in equations (D 2)–(D 5), but we defer a formal development in that direction to the next section, where the intermediate layer in particular is carefully addressed. Arguing here more informally, if the subdominant contribution in the wall layer is assumed to scale as $Ra^{d_2-\delta}$, then if $\widehat{\theta}_2$ is to match onto $\tilde{\theta}_2$, we require

$$f_2 = d_2 - \delta + a_3 - a_2. \tag{D 21}$$

In lieu of producing an eleventh equation to close the set, we shall assume that $\delta = a_3 - a_2$, an assertion anyway verified by (and also originally discovered from) the fitting procedure defined by (A 14).

The direct consequence of $\widehat{\theta}_2$ tending to ζ_3 is that $w_2\theta_2$ continues to increase beyond 1 as $\zeta_3 \to \infty$ and consequently $\widehat{w}_1\widehat{\theta}_1$ has to grow from 0 to compensate for it. This is the most obvious feature in the numerical calculations, with a typical result shown in figure 17, and it bears emphasizing that this overshoot, which we shall shortly infer to scale as $Ra^{1/5}$, is without precedent in the literature on upper bounds. Indeed owing to the divergence in the individual products, this feature is also the reason for which numerical solutions fail: the needed cancellation transcends the capacity of double precision to resolve, setting a decidedly finite limit on the possible range of Ra. By contrast, solutions with no-slip boundary conditions exhibit no inherent constraint; attaining larger Ra simply requires more resolution.

Finally, we look to the match for θ_1. Since $\widehat{w}_1\widehat{\theta}_1$ has to decrease down to $O(1)$ but $\widehat{w}_1 \sim \zeta_2$ as $\zeta_2 \to \infty$, $\widehat{\theta}_1$ must decrease faster than $1/\zeta_2$. Here we face the difficulty earlier noted, that the equation for $\widehat{\theta}_1$ is not closed in terms of the variables available, so we cannot derive its limiting behaviour by dominant balance (for example). As

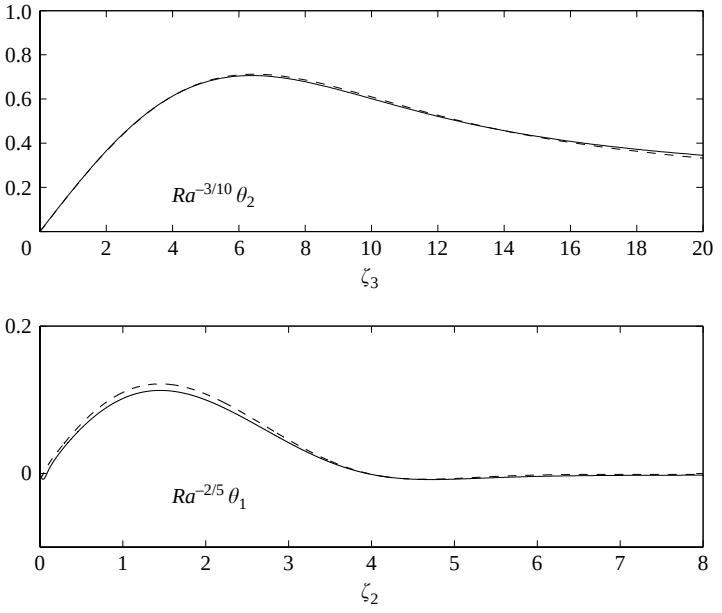

FIGURE 27. Confirmation of the boundary layer scalings deduced in § D.1. Results for $Ra = 2.315 \times 10^{10}$ and 6.093×10^{11} are plotted according to the scalings $\widehat{\theta}_2 = Ra^{-3/10}\theta_2$ and $\widehat{\theta}_1 = Ra^{-2/5}\theta_1$, with boundary layer coordinates $\zeta_3 = Ra^{2/5}z$ and $\zeta_2 = Ra^{1/5}z$ respectively.

with our inference just above about δ, we are forced to rely on numerical evidence, which supports a simple algebraic decay of $\widehat{\theta}_1 \sim 1/\zeta_2^2$. Assuming this, it follows that

$$f_1 = d_1 - 2(a_2 - a_1). \tag{D 22}$$

This is the tenth and final indicial equation.

Collecting all ten equations, the scaling indices that result are

$$a_2 = -c_1 = \tfrac{1}{5}, \quad a_3 = d_1 = \tfrac{2}{5}, \quad f_2 = d_2 = -c_2 = \tfrac{3}{10}, \tag{D 23}$$

$$e_1 = f_1 = 0, \quad e_2 = -\tfrac{1}{10}, \tag{D 24}$$

implying that for the 2-α solution

$$Nu \sim Ra^{2/5} \qquad \text{as } Ra \to \infty. \tag{D 25}$$

Numerical corroboration for these scalings is very good as shown in figure 27 for $\widehat{\theta}_1$ and $\widehat{\theta}_2$, as well as figure 14, showing Nu.

D.2. *Intermediate layer*

The aim in this section is not – as in Appendix C – a detailed dissection of matching, but only to exhibit an ordered expansion that could in principle permit such a match to the wall (and interior). The point here is that the extreme degree of cancellation in $1 - \overline{w\theta}$ for 2-α free-slip leads to a remarkably intricate set of coupled simultaneous equations.

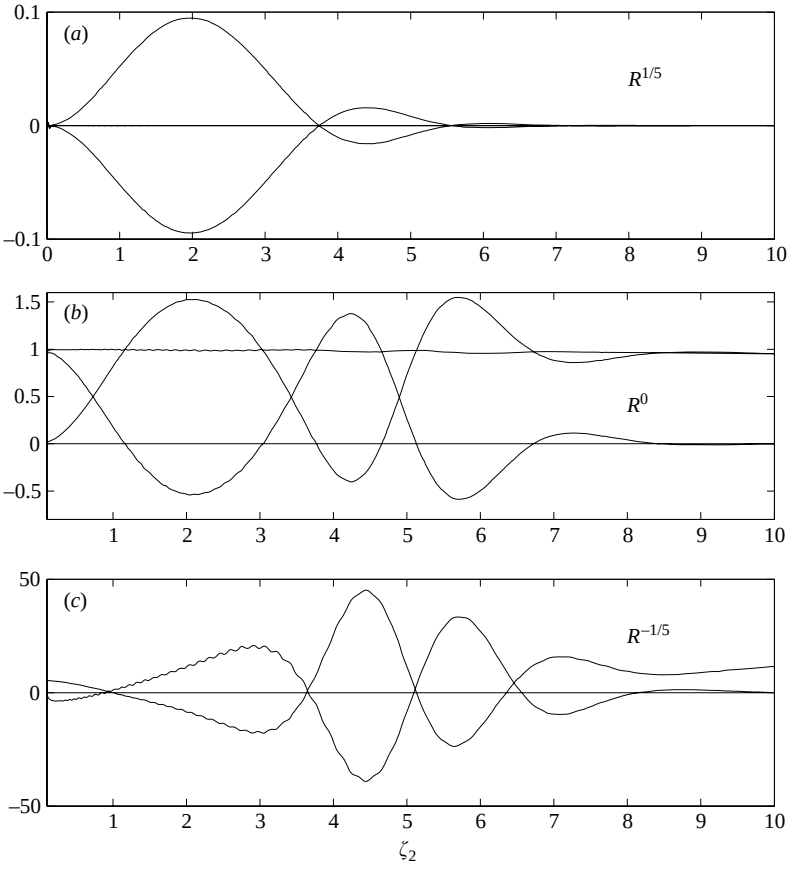

FIGURE 28. Successive order balances in the delicate cancellation of $\widehat{w}_1\widehat{\theta}_1$ against $\tilde{w}_{2,}\tilde{\theta}_2$.

Following on from the results for the indicial exponents derived above, we are led to expansions of the form

$$\tilde{w}_2 = Ra^{-1/10}\sum_{k=0}^{\infty}\tilde{w}_{2,k}(\zeta_2)\,\epsilon^k, \qquad \tilde{\theta}_2 = Ra^{3/10}\sum_{k=0}^{\infty}\tilde{\theta}_{2,k}(\zeta_2)\,\epsilon^k, \tag{D 26}$$

$$\widehat{w}_1 = Ra^{-1/5}\sum_{k=0}^{\infty}\widehat{w}_{1,k}(\zeta_2)\,\epsilon^k, \qquad \widehat{\theta}_1 = Ra^{2/5}\sum_{k=0}^{\infty}\widehat{\theta}_{1,k}(\zeta_2)\,\epsilon^k, \tag{D 27}$$

where $\epsilon = Ra^{-1/5}$. As there can be no confusion within this section, we confine the notation to a single subscript for α.

In this instance we require that $1 - \tilde{w}_2\tilde{\theta}_2 - \widehat{w}_1\widehat{\theta}_1$ be $O(Ra^{-2/5})$, which gives us three algebraic relations that must be satisfied. These are given by

$$\widehat{w}_{1,0}\widehat{\theta}_{1,0} + \tilde{w}_{2,0}\tilde{\theta}_{2,0} = 0, \tag{D 28}$$

$$\widehat{w}_{1,0}\widehat{\theta}_{1,1} + \widehat{w}_{1,1}\widehat{\theta}_{1,0} + \tilde{w}_{2,0}\tilde{\theta}_{2,1} + \tilde{w}_{2,1}\tilde{\theta}_{2,0} = 1, \tag{D 29}$$

$$\widehat{w}_{1,0}\widehat{\theta}_{1,2} + \widehat{w}_{1,1}\widehat{\theta}_{1,1} + \widehat{w}_{1,2}\widehat{\theta}_{1,0} + \tilde{w}_{2,0}\tilde{\theta}_{2,2} + \tilde{w}_{2,1}\tilde{\theta}_{2,1} + \tilde{w}_{2,2}\tilde{\theta}_{2,0} = 0. \tag{D 30}$$

Figure 28 shows the extent to which these relations can be verified by the available numerical results. In particular, absolute accuracy and the concomitant restriction

of the dynamic available range of Ra limit the number of components in (D 26)–(D 27) that can be determined by extrapolation. Unavoidably there is a successive degradation of accuracy for increasing index. Hence, while the first relation is satisfied to better than graphical precision, in the second there is perceptible variation about the expected constant value of unity and figure 28(c) provides only a qualitative sense of the cancellation at $O(Ra^{-1/5})$. The extrapolation for $\widehat{w}_{1,k}$ and the other variables is not in any way conditioned on the observed cancellation (except indirectly through suggesting the overall scaling of the expansion) and hence this furnishes an independent test of the proposed algebraic relations. While the errors in figure 28(c) raise the prospect that perhaps the cancellation is not complete at that order, that the residue is, rather, an artifact of extrapolation is demonstrated by simply computing $1-\overline{w\theta}$ using the full fields, from which result it is unambiguously found that the residual scales as $Ra^{-2/5}$.

The w equations are

$$\mathrm{D}^4\widehat{w}_{1,0} = 0, \tag{D 31}$$

$$\mathrm{D}^4\widehat{w}_{1,1} = \alpha_1^2\widehat{\theta}_{1,0}, \tag{D 32}$$

$$\mathrm{D}^4\widehat{w}_{1,2} = \alpha_1^2(\widehat{\theta}_{1,1} + 2\mathrm{D}^2\widehat{w}_{1,0}), \tag{D 33}$$

and

$$\nabla_2^4\tilde{w}_{2,j} = \alpha_2^2\tilde{\theta}_{2,j}, \qquad j = 0, 1, 2, \tag{D 34}$$

where $\nabla_2^{2k} = (\mathrm{D}^2 - \alpha_2^2)^k$. But the only elementary solution to emerge from this is $\widehat{w}_{1,0} = \widehat{c}_{1,0}\,\zeta_2$.

The θ equations are

$$\widehat{F}^{-1}\mathrm{D}^6\widehat{\theta}_{1,0} + \mathrm{D}^4(\rho_0\widehat{w}_{1,0}) = 0, \tag{D 35}$$

$$\widehat{F}^{-1}\mathrm{D}^6\widehat{\theta}_{1,1} + \mathrm{D}^4(\rho_0\widehat{w}_{1,1} + \rho_1\widehat{w}_{1,0}) + \rho_0\widehat{\theta}_{1,0} = 0, \tag{D 36}$$

$$\widehat{F}^{-1}\mathrm{D}^6\widehat{\theta}_{1,2} + \mathrm{D}^4(\rho_0\widehat{w}_{1,2} + \rho_1\widehat{w}_{1,1} + \rho_2\widehat{w}_{1,0}) + \rho_0\widehat{\theta}_{1,1} + \rho_1\widehat{\theta}_{1,0} = 2\alpha_1^2(\mathrm{D}^2(\rho_0\widehat{w}_{1,0}) + (\rho_0 - 1)\mathrm{D}^2\widehat{w}_{1,0}), \tag{D 37}$$

$$\nabla_2^4(\rho_0\tilde{w}_{2,0}) + \rho_0\tilde{\theta}_{2,0} = 0, \tag{D 38}$$

$$\widehat{F}^{-1}\nabla_2^6\tilde{\theta}_{2,0} + \nabla_2^4(\rho_0\tilde{w}_{2,1} + \rho_1\tilde{w}_{2,0}) + \rho_0\tilde{\theta}_{2,1} + \rho_1\tilde{\theta}_{2,0} = 0, \tag{D 39}$$

$$\widehat{F}^{-1}\nabla_2^6\tilde{\theta}_{2,1} + \nabla_2^4(\rho_0\tilde{w}_{2,2} + \rho_1\tilde{w}_{2,1} + \rho_2\tilde{w}_{2,0}) + \rho_0\tilde{\theta}_{2,2} + \rho_1\tilde{\theta}_{2,1} + \rho_2\tilde{\theta}_{2,0} = 0, \tag{D 40}$$

where, to facilitate analysis, we have introduced a critical auxiliary variable, ρ, defined by

$$1 - \widehat{w}_1\widehat{\theta}_1 - \tilde{w}_2\tilde{\theta}_2 - \lambda/F = Ra^{-2/5}\sum_{k=0}^{\infty}\rho_k(\zeta_2)\epsilon^k. \tag{D 41}$$

(Note that the last parameter in the problem, λ, must also be expanded, that is

$$\lambda_0 = \frac{\langle|\nabla\widehat{\theta}_{2,0}|^2\rangle}{2Ra} - 1,$$

with subsequent terms following in an obvious fashion. But these constants are subsumed in the present discussion by constants of integration associated with the ρ_k and need only be incorporated at the point of carrying out a detailed match of the layers, which is, as earlier indicated, beyond the purpose of the discussion here.)

The fifteen equations (D 28)–(D 40) for w, θ and ρ constitute a minimal coupled nonlinear set, that is, the interactions of the intermediate layer seem no further

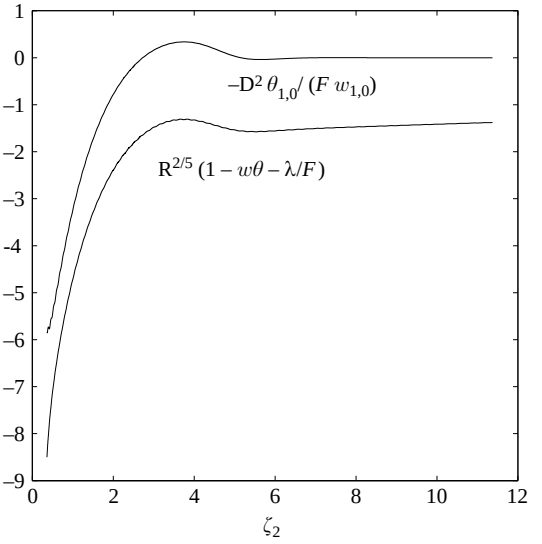

FIGURE 29. Numerical confirmation of one result for the proposed midlayer expansion.

reducible. Determination of the numerous coefficients in homogeneous solutions of the governing equations has to be done in concert with matching to expansions of appropriate degree in both the wall and the interior layers. This is a project well beyond the scope of this paper. Instead, we conclude this section with several elementary analytic and numerical observations.

As for (D 31), so too in (D 35) an elementary result suggests itself, namely

$$\rho_0(\zeta_2) = -\frac{\mathrm{D}^2\widehat{\theta}_{1,0}}{\widehat{F}\,\widehat{w}_{1,0}},$$

and from this one can eliminate ρ_0 as an unknown. Figure 29 compares this prediction to the actual ρ_0. The similarity is evident enough, but with a roughly constant offset remaining between the two. The offset suggests that we allow for homogeneous solutions, that is,

$$\rho_0(\zeta_2) = -\frac{\mathrm{D}^2\widehat{\theta}_{1,0}}{\widehat{F}\,\widehat{w}_{1,0}} + c_1 + c_2/\zeta_2, \tag{D 42}$$

on the presumption that matching will determine c_1 and c_2 (on numerical evidence there is no need to invoke the remaining two homogeneous solutions).

The computed solution provides a variety of results, some easily reconciled with the above scheme and some not. One of the easier numerical observations is the fit

$$\tilde{w}_{2,0} \approx c_1\alpha_2\zeta_2\,\mathrm{e}^{-\alpha_2\zeta_2} - c_2\,\mathrm{e}^{-\alpha_2\zeta_2},$$

where $c_{1,2}$ are order one. These are simply the homogeneous solutions of (D 34).

A second, purely empirical, fit is

$$\tilde{\theta}_{2,0} = \mathrm{e}^{\mu k_2\zeta_2}, \qquad \zeta_2 \to \infty,$$

where $\mu \approx -1.45 + 2.12\mathrm{i}$. But given (D 34), this means that there must be some of this oscillatory exponential also in $\tilde{w}_{2,0}$ in addition to the homogeneous solutions noted. While it is awkward trying to subtract the homogeneous terms, by computing $(\mathrm{D}^2-\alpha_2)^2 w_2$, these are annihilated and the (oscillatory) remainder does coincide with

θ_2. (Strictly speaking this numerical comparison of raw fields is a superposition of all orders in (D 34) but clearly the first term dominates the comparison.)

It appears that (D 32) holds accurately through the intermediate layer. By integrating $\widehat{\theta}_{1,0}$ four times, one can discriminate the homogeneous and particular solutions in $\widehat{w}_{1,1}$. In any event the interior equation

$$(\mathrm{D}^2 - 1)^2 \tilde{w}_{1,0} = 1/\tilde{w}_{1,0}$$

does not satisfy free-slip boundary conditions (as indicated by the numerical results) and the series solution is hence not the 1-α solution in (B 2). This has a bearing on the point central to the thesis of this paper, that this alteration in the boundary condition is a smooth perturbation of the solution in (B 2). Establishing the explicit details is the key step required to show that $\alpha_1 \to 1.9662$ for the 2-α solution. More specifically, the altered boundary condition arises either directly owing to a particular solution of (D 32), whose outer limit is ζ_2^2, or from a homogeneous solution required at the origin to make the particular solution satisfy free-slip boundary conditions.

For small ζ_2, a power series expansion of (D 28)–(D 40) could be carried out to confirm aspects of the match to the inner layer. Similar analysis can probably establish the relevant asymptotic relations $\zeta_2 \to \infty$, in particular a determination of the characteristic polynomial, one of whose root pairs is (μ, μ^*) observed above.

What is lacking is a rational deductive derivation for the origin of (D 28-D 40) rather than, as here, a numerically guided search for a set of relations whose consistency is shown after the fact.

D.3. *Second wall layer*

Expanding solutions in the innermost ($Ra^{-2/5}$) layer, we have

$$\widehat{w}_{2,0}^{IV} = \widehat{w}_{2,1}^{IV} = 0,$$

for which the relevant solutions are each $c\,\zeta_3$ for a suitable constant c.

The equation for $\widehat{\theta}_{2,0}$ follows from simplification using the indicated solution for $\widehat{w}_{2,0}$:

$$\mathscr{L}\widehat{\theta}_{2,0} \equiv \frac{1}{\widehat{F}} \frac{\mathrm{d}^6 \widehat{\theta}_{2,0}}{\mathrm{d}\zeta_3^6} - \frac{\mathrm{d}^4}{\mathrm{d}\zeta_3^4}((1 - \zeta_3 \widehat{\theta}_{2,0})\zeta_3) = 0.$$

The solution singled out is $\widehat{\theta}_{2,0} = c\,\widehat{\theta}^{(3)}$ (cf. Appendix A for details).

At next order, $\widehat{\theta}_{2,1}$ satisfies the inhomogeneous equation

$$\mathscr{L}\widehat{\theta}_{2,1} = 2\frac{\mathrm{d}^4}{\mathrm{d}\zeta_3^4}(\zeta_3^2 \widehat{\theta}_{2,0}). \tag{D 43}$$

While the particular solution for this has an involved integral representation, we only need to note that the right-hand side vanishes for $\widehat{\theta}_{2,0} \sim 1/\zeta_3$ and it is, rather, the homogeneous solutions that dominate the outer limit, in particular, $\widehat{\theta}_{2,1} \sim \zeta_3$.

The significance of this is precisely its relation to the anomalously large value assumed by the individual wave components in the variational solution; what in the innermost layer is a subdominant solution becomes in the outer limit the dominant component for matching to the ζ_2 layer.

Appendix E. Numerical issues

E.1. *Spectral formulation*

Computation of the optimal solution is problematic with a Chebyshev matrix representation of D^4, which is unstable at moderate values of Ra. A set of orthogonal polynomials which are tailor-made for such a problem are Jacobi polynomials, for which the Galerkin projection of D^4 is an unconditionally stable matrix for all Ra.† The supplementary task of checking SC-stability was performed by an eigenvalue code solving system (3.9) for a broad sweep of wavenumbers.

We consider here only the solution of the 1-α optimal equations for simplicity of notation. The multi-α is an easy extension of this programme once equations (3.14) and (3.15) are included into the analysis.

If we denote by L the bi-Laplacian $(\mathrm{D}^2-\alpha^2)^2$ then optimal equations (3.3) and (3.4) can be rewritten as

$$q=-\lambda \mathrm{L}^{-1}(\widehat{\theta}\tau') \quad \text{and} \quad w=Ra\alpha^2\mathrm{L}^{-1}(\widehat{\theta}). \tag{E 1}$$

In this case, after some algebra, the non-scalar optimal equations (3.2), (3.3), (3.4) and (3.6) can be reduced to the single equation

$$2(\mathrm{D}^2-\alpha^2)\widehat{\theta}+2(\lambda+\langle w\widehat{\theta}\rangle)w-w^2\widehat{\theta}-Ra\alpha^2\mathrm{L}^{-1}(w\widehat{\theta}^2)=0, \tag{E 2}$$

where w depends linearly on $\widehat{\theta}$ by relation (E 1) and therefore its solution is contingent on pre-calculation of the inverse bi-Laplacian. Equation (3.7) for λ can be substituted explicitly into this equation. The system of optimal equations is then reduced to one spatial equation and one scalar equation, namely (E 2) and (3.14).

A strategy for inverting powers of the Laplacian using the spectral method with Jacobi polynomials and Galerkin projection was first presented in Ierley (1997). Application of the same program to horizontal convection at large Ra has since appeared in Siggers, Kerswell & Balmforth (2004).

We expand the temperature fluctuation field in the Jacobi polynomials $P_k^{(1,1)}$, namely

$$\widehat{\theta}(x)=(1-x^2)\sum_{k=0}^{K}\widehat{\theta}_k P_{2k}^{(1,1)}(x),$$

where $x=2z-1$ and we only select even polynomials because of the assumed symmetry in the optimal solution. The expansion of w (and similarly q) for no-slip boundaries is

$$w(x)=(1-x^2)^2\sum_{k=0}^{K}w_k P_{2k}^{(2,2)}(x),$$

and for free-slip boundaries

$$w(x)=(1-x^2)\sum_{k=0}^{K}(1-\gamma_{2k}\,x^2)w_k P_{2k}^{(1,1)}(x), \tag{E 3}$$

where

$$\gamma_j=\frac{j(j+3)+2}{j(j+3)+10}.$$

† In the case presented here, the formulation reduces to Legendre polynomials following the use of various standard identities. But the same idea applies to more general operators and then such a reduction does not generally obtain.

These representations for w and $\widehat{\theta}$ have the boundary conditions built in. The form in (E 3) is a special case. For the more general boundary condition introduced in (7.18), γ takes the form

$$\gamma_j = \frac{(1-\beta)(j^2+3j)+2}{(1-\beta)(j^2+3j+8)+2}. \tag{E 4}$$

Equation (E 2) is posed as a finite-dimensional approximation by taking Galerkin projections of the derivative operators, using LU decomposition to invert L, and tensor contractions to form the cubic terms. The derivative matrices are symmetric and sparse. For example, the bi-Laplacian L is a penta-diagonal matrix. The most expensive operations are calculating the cubic nonlinearity in equation (E 2), such as $w^2\widehat{\theta}$, since the Galerkin projection would seem to require a fourth-order contraction with a tensor having elements defined (for no-slip boundaries) by

$$c_{ijkl} = \int_{-1}^{1} \mathrm{d}x\,(1-x^2)^6 P_i^{(2,2)}(x)\,P_j^{(2,2)}(x)\,P_k^{(1,1)}(x)\,P_l^{(1,1)}(x).$$

Given that the basis sets have, for some extreme cases, included even polynomials to degree $m = 1800$, this approach is not remotely feasible, even with some reductions based on symmetries and other selection rules.

This difficulty can be partly overcome by performing sequential contractions with two third-rank tensors but the overhead for the initial computation of tensor elements with Gaussian quadrature of order $3m/2$ is still burdensome, and storage scales as $O(m^3)$.

It is preferable here simply to revert to a pseudospectral treatment of cubic nonlinearities since the operations count and storage requirements are both $O(m^2)$, a small fraction of the $O(m^3)$ requirements for matrix inversion at each step of Newton's method.† We elected to use a conventional forward transform. There is a potential gain by switching to the $O(m(\log m)^2)$ (Driscoll & Healy 1994) fast Legendre transform but the net speedup would be slight. For accuracy and consistency of the inverse transform, it is important to use a kernel consisting of $(1-x^2)P_j^{(1,1)}(x)$ even though this means the coefficients in the resulting expansion then require inversion of a (symmetric) tridiagonal form. (The basis set for $\widehat{\theta}$ diagonalizes the second derivative operator, not the unit operator.)

In developing a continuation code for this problem, the analytic Jacobian for the optimal equations was derived and used in the multi-dimensional Newton iteration scheme. This saved a good deal of CPU time over the alternative of finite-difference approximation of the Jacobian matrix. While computing the Jacobian matrix is a particularly laborious exercise in tensor manipulations, the algebra can be checked against a finite-difference approximation. The α-derivative of L^{-1} for instance, is

$$\frac{\mathrm{d}}{\mathrm{d}\alpha}(\mathrm{D}^4 - 2\alpha^2\mathrm{D}^2 + \alpha^4 I)^{-1} = \mathrm{L}^{-1}(-4\alpha\mathrm{D}^2 + 4\alpha^3 I)\mathrm{L}^{-1},$$

where the D^4 and D^2 here represent derivative matrices and I is defined by

$$I_{ij} = \int_{-1}^{1} \mathrm{d}x\,(1-x^2)^4 P_i^{(2,2)}(x) P_j^{(2,2)}(x).$$

† In principle the rank one updates of quasi-Newton methods can reduce the latter overhead but our experience of these with spectral methods has not proved encouraging.

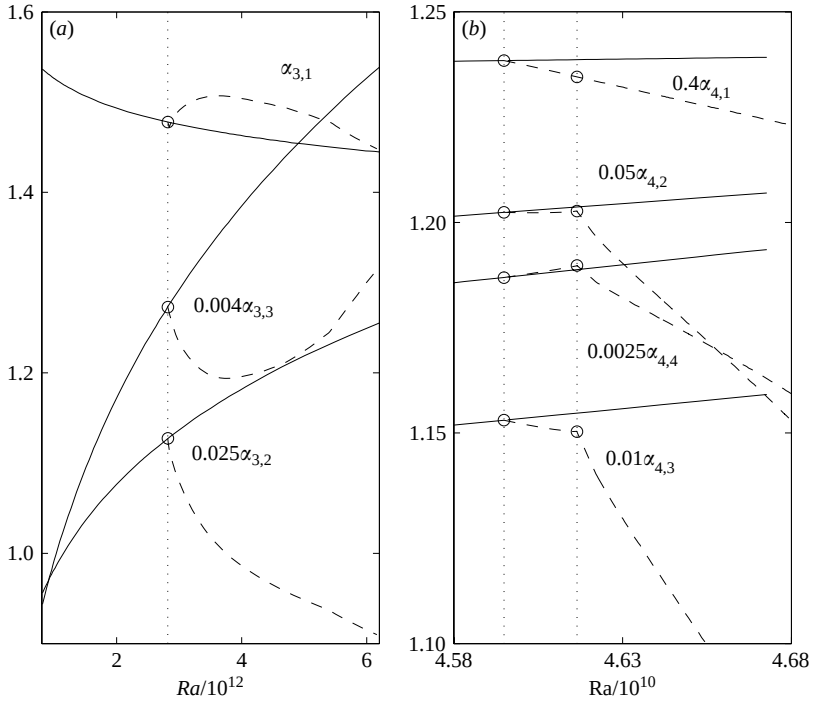

FIGURE 30. An indication of unanticipated structure in the variational solution: (*a*) free-slip, (*b*) no-slip.

E.2. *Secondary bifurcations*

In closing we remark that there is an unanticipated feature of the variational problem seen for the 3-α free-slip and 4-α no-slip branches. This is the existence of secondary bifurcations within the same k-α solution space, as illustrated in figure 30 by dashed lines. For graphical clarity, wavenumbers have been rescaled as labelled. Values of Nu are systematically less on the side branches, so the overall picture presented in this section remains intact, but this is yet another indication of the possible complications that can ensue with computed variational solutions for upper bound problems. In particular, without manual intervention, the dashed line was the realized numerical solution in both cases. We have examined the neutral eigenfunction for each bifurcation but in neither case is the structure revealing. It is important to bear in mind that the observed subsidiary bifurcations are here a nuisance only insofar as one is pursuing an asymptotic characterization of the given solution branch; the primary bifurcation to the next SC-neutral branch has already taken place, although it does not seem possible rigorously to preclude that an exchange of SC-neutrality within a given k-α solution space might in principle occur via such a bifurcation.

REFERENCES

BAKER, G. A. 1975 *Essentials of Padé Approximants*. Academic.

BUSSE, F. H. 1969*a* Bounds on the transport of mass and momentum by turbulent flow. *Z. Angew. Math. Phys.* **20**, 1–14.

BUSSE, F. H. 1969*b* On Howard's upper bound for heat transport by turbulent convection. *J. Fluid Mech.* **37**, 457–477.

Busse, F. H. 1970 Bounds for turbulent shear flow. *J. Fluid Mech.* **41**, 219–240.

Chan, S. K. 1970 Upper bound on turbulent heat convection for infinite Prandtl number. PhD thesis, Massachusetts Institute of Technology.

Chan, S. K. 1971 Infinite Prandtl number turbulent convection. *Stud. Appl. Maths* **50**, 13–49.

Constantin, P. & Doering, C. R. 1995 Variational bounds on energy-dissipation in incompressible flows: II. Channel flow. *Phys. Rev.* E **51**, 3192–3198.

Constantin, P. & Doering, C. R. 1999 Infinite Prandtl number convection. *J. Statist. Phys.* **94**, 159–172.

Courant, R. & Hilbert, D. 1953 *Methods of Mathematical Physics*. Interscience.

Doering, C. R. & Constantin, P. 1992 Energy dissipation in shear driven turbulence. *Phys. Rev. Lett.* **69**, 1648–1651.

Doering, C. R. & Constantin, P. 1994 Variational bounds on energy dissipation in incompressible flows: Shear flow. *Phys. Rev.* E **49**, 4087–4099.

Doering, C. R. & Constantin, P. 1996 Variational bounds on energy dissipation in incompressible flows: III. Convection. *Phys. Rev.* E **53**, 5957–5981.

Doering, C. R., Otto, F. & Reznikoff, M. G. 2005 Bounds on vertical heat transport for infinite-Prandtl-number Rayleigh–Bénard convection. *J. Fluid Mech.* **560**, 229–241.

Driscoll, J. R. & Healy, D. M. 1994 Computing Fourier transforms and convolutions on the 2-sphere. *Adv. Appl. Maths* **15**, 202–250.

Hopf, E. 1941 Ein allgemeiner endlichkeitssatz der hydrodynamik. *Mathematische Annalen* **117**, 764–775.

Howard, L. N. 1963 Heat transport by turbulent convection. *J. Fluid Mech.* **17**, 405–432.

Howard, L. N. 1972 Bounds on flow quantities. *Annu. Rev. Fluid Mech.* **4**, 473–494.

Ichinobe, K. 2001 The Borel sum of a divergent Barnes hypergeometric series and its application to a partial differential equation. *Publ. Res. Inst. Math. Sci.* **37** (1), 91–117.

Ierley, G. R. 1997 A class of sparse spectral operators for inversion of powers of the Laplacian in N dimensions. *J. Sci. Comput.* **12** (1), 57–63.

Ierley, G. R. & Ruehr, O. G. 1986 Analytical and numerical solutions of a nonlinear boundary layer problem. *Stud. Appl. Maths* **75**, 1–36.

Ierley, G. R. & Worthing, R. A. 2001 Bound to improve: a variational approach to convective heat transport. *J. Fluid Mech.* **441**, 223–253.

Jimenez, J. & Zufiria, J. A. 1987 A boundary-layer analysis of Rayleigh–Bénard convection at large Rayleigh number. *J. Fluid Mech.* **178**, 53–71.

Kerswell, R. R. 1996 Upper bounds on the energy dissipation in turbulent precession. *J. Fluid Mech.* **321**, 335–370.

Kerswell, R. R. 1997 Variational bounds on shear-driven turbulence and turbulent Boussinesq convection. *Physica* D **100**, 355–376.

Kerswell, R. R. 2001 New results in the variational approach to turbulent Boussinesq convection. *Phys. Fluids* **13**, 192–209.

Kerswell, R. R. 2002 Upper bounds on general dissipation functionals in turbulent shear flows: revisiting the 'Efficiency' functional. *J. Fluid Mech.* **461**, 239–275.

Kerswell, R. R. & Soward, A. M. 1996 Upper bounds for turbulent Couette flow incorporating the poloidal power constraint. *J. Fluid Mech.* **328**, 161–176.

Luke, Y. 1969 *The Special Functions and their Approximations, Vol. 1*, 1st edn. Academic.

Malkus, W. V. R. 1954*a* Discrete transitions in turbulent convection. *Proc. R. Soc. Lond.* A **225**, 185–195.

Malkus, W. V. R. 1954*b* The heat transport and spectrum of thermal turbulence. *Proc. R. Soc. Lond.* A **225**, 196–212.

Malkus, W. V. R. 1956 Outline of a theory for turbulent shear flow. *J. Fluid Mech.* **1**, 521–539.

Nicodemus, R., Grossmann, S. & Holthaus, M. 1997*a* Improved variational principle for bounds on energy dissipation in turbulent shear flow. *Physica* D **101**, 178–190.

Nicodemus, R., Grossmann, S. & Holthaus, M. 1997*b* Variational bound on energy dissipation in plane Couette flow. *Phys. Rev.* E **56**, 6774–6786.

Otero, J. 2002 Bounds for the heat transport in turbulent convection. PhD thesis, University of Michigan.

PLASTING, S. C. 2004 Turbulence has its limits: *a priori* estimates of transport properties in turbulent fluid flows. PhD thesis, University of Bristol.

PLASTING, S. C. & IERLEY, G. R. 2005 Estimates of heat transport in infinite Prandtl number convection. Part 1. Conservative bounds. *J. Fluid Mech.* **542**, 343–363.

PLASTING, S. C. & KERSWELL, R. R. 2003 Improved upper bound on the energy dissipation rate in plane couette flow: the full solutions to Busse's problem and the Constantin–Doering–Hopf problem with one-dimensional background field. *J. Fluid Mech.* **477**, 363–379.

SIGGERS, J. H., KERSWELL, R. R. & BALMFORTH, N. J. 2004 Bounds on horizontal convection. *J. Fluid Mech.* **517**, 55–70.

STEWARTSON, K. 1966 Appendix: Asymptotic Theory in the Limit $R \rightarrow \infty$. In *Non-Equilibrium Thermodynamics Variational Techniques and Stability* (ed. R. J. Donnelly, R. Herman & I. Prigogine), pp. 158–162. University of Chicago Press.

STRAUS, J. M. 1976*a* A note on the multi-α solutions of the upper bounding problem for thermal convection. *Dyn. Atmos. Oceans* **1**, 71–76.

STRAUS, J. M. 1976*b* On the upper bounding approach to thermal convection at moderate Rayleigh numbers, II. Rigid boundaries. *Dyn. Atmos. Oceans* **1**, 77–90.

VITANOV, N. K. 1998 Upper bound on the heat transport in a horizontal fluid layer of infinite Prandtl number. *Phys. Lett.* A **248**, 338–346.

VITANOV, N. K. 2000*a* Convective heat transport in a fluid layer of infinite Prandtl number: upper bounds for the case of rigid lower boundary and stress-free upper boundary. *Eur. Phys. J.* B **15**, 349–355.

VITANOV, N. K. 2000*b* Upper bounds on the heat transport in a fluid layer of infinite Prandtl number, rigid lower boundary and stress-free upper boundary. *Phys. Rev.* E **61**, 956–959.

VITANOV, N. K. & BUSSE, F. H. 1997 Bounds on the heat transport in a horizontal fluid layer with stress-free boundaries. *Z. Angew. Math. Phys.* **48**, 310–324.

WANG, X. M. 2004 Infinite Prandtl number limit of Rayleigh-Bénard convection. *Commun. Pure Appl. Maths* **57**, 1265–1282.

YAN, X. D. 2004 On limits to convective heat transport at infinite Prandtl number with or without rotation. *J. Math. Phys.* **45**, 2718–2743.